On the Role of SSM/I Derived Precipitable Water over the Globe and Tropical Pacific

by
Darren L. Jackson and Graeme L. Stephens

Department of Atmospheric Science
Colorado State University
Fort Collins, Colorado

Research Supported by NASA grants NAG8-876 and NAG5-112 and NOAA grant NA90AA-D-AC022

Colorado State University

Department of Atmospheric Science

Paper No. 507

ON THE ROLE OF SSM/I DERIVED PRECIPITABLE WATER OVER THE GLOBE AND TROPICAL PACIFIC

Darren L. Jackson and Graeme L. Stephens

Research supported by NASA grants NAG8-876 and NAG 5-112 and NOAA grant NA90AA-D-AC022

Principal Investigator: Graeme L. Stephens

Department of Atmospheric Science

Colorado State University

Fort Collins, CO 80523

August 1992

Atmospheric Science Paper No. 507

ABSTRACT

Understanding the distribution and movement of water vapor around the globe and tropical atmosphere is vital for understanding problems concerning climate change and tropical convection. Analysis of the global distribution of precipitable water content (PWC), the interannual vapor variability of PWC, and the relationship of PWC with tropical convection was investigated using data from the Special Sensor Microwave/Imager (SSM/I). Daily and monthly mean 1 degree resolution global data sets of PWC were produced over a $3\frac{1}{2}$ year time period beginning in August of 1987. Several different PWC retrieval methods were compared through validation with two different radiosonde data sets. Statistically based retrieval methods were generally found to have less bias and variance than the physical methods; however, the statistical methods showed a climatological bias which produced a smoothing of the daily variations in the PWC observed in the tropical western Pacific. Further comparisons of the zonally averaged and global mean PWC for 1989 showed the physical methods produced a broader distribution from pole to pole which resulted in an overestimation of PWC in the higher latitudes. Daily PWC variations over a month period were found to be greatest in convective regions and were largest for the physical retrieval method found in Tjemkes *et al.* (1991).

The relationship between PWC and sea surface temperature (SST) was investigated over a 3 year period beginning February 1988. A Clausius-Clapeyron relationship was found between PWC and SST similar to the relationship found in Stephens (1990). The 3 year southern and northern hemispheric mean SST and PWC time series showed a strong relationship while the global mean time series showed less correlation. Differences between this study and Stephens (1990) were primarily due to the increased resolution the present data sets and improved accuracy of their retrieval methods. Analysis of the 1987 El Niño

and 1988 La Niña using PWC data showed the great influence large scale tropical motions have on the hydrologic cycle. PWC monthly anomalies as low as -13.05 kg m^{-2} occurred during the 1988 La Niña indicating a significant drying of the tropical atmosphere over the central and eastern Pacific. Higher frequency motions such as westerly wind bursts were also investigated and results suggest that moisture convergence occurred in the convective regions of these events. This study shows the effectiveness of the SSM/I data for both climate scale problems and localized case studies.

ACKNOWLEDGEMENTS

I would like to begin by thanking my advisor, Dr. Graeme Stephens, for his ideas and guidance towards this thesis over the past couple years. I would also like to thank Dr. Stephen Tjemkes at the Institute of Meteorology and Oceanography, State University of the Netherlands at Utrecht for helping me more fully understand the different satellite retrieval methods and for helping me get started with computing on the CRAY Y-MP8/864 at NCAR. I extend my gratitude to Dr. James Purdom and Dr. Thomas Vonder Haar for their efforts in obtaining the large SSM/I data needed to complete this study. Thanks are due to Dr. William Gray for his ideas on water vapor which have helped me focus on my future research. I also would like to extend a sincere thank you to Nan McClurg and Debra Lubick for their efforts in organizing and accessing the SSM/I data. I couldn't have finished this study without the help of Frank Evans, Tom Greenwald and Kelly Dean. They helped provide the necessary software, graphics, data, and insights needed to finish this study. I need to thank Sue Lini for taking care of the endless amounts of paper work required to achieve a Master's degree and for her efforts in producing the final manuscript. I would like to finish by sending a most sincere thank you to my fiance, Christy, for her love, encouragement, and support over the past three years.

CONTENTS

LIST OF FIGURES

Chapter 1

INTRODUCTION

Understanding the role water vapor has on the tropical atmosphere is essential for solving fundamental meteorological problems concerning tropical convective systems and the earth's climate. Diabatic and radiative processes caused by the transport and phase changes of H_2O play a key role in the dynamical flow fields of the tropical atmosphere. Therefore, diagnosing the distribution and convergence of water vapor in the tropical atmosphere through remote sensing methods can be a vital means of addressing the role water vapor plays in the tropical atmosphere. While current methods of retrieving water vapor are not perfect, the improved resolution and accuracy of SSM/I data can help atmospheric scientists gain great insight into water vapor's role in both low and high frequency motions in the tropics and over the entire globe.

1.1 PRECIPITABLE WATER RETRIEVAL

Through improved retrieval theory and radiometric technology, the ability to retrieve water vapor over the globe has improved substantially over the past few decades. Pioneering studies such as Benton and Estoque (1954) and Starr *et al.* (1969), prior to the satellite age, investigated the global distribution of water vapor using a global network of radiosondes. The recent development of satellites has begun the development of remote sensing techniques which give higher resolution measurements of the global distribution of water vapor.

Two primary regions of the electromagnetic spectrum used to retrieve water vapor from satellites are the infrared (IR) and microwave regions. Water vapor data derived from remote sensing in the IR spectrum has been primarily done by using data from the High Resolution Infrared Radiation Sounder (HIRS/2) instrument (Hillger and Vonder Haar,

1981). The TIROS Operational Vertical Sounder (TOVS), using the HIRS/2 instrument, was used to derive the TOVS global water vapor data sets which provide vertical distributions and complete global coverage of water vapor. However, the problem with the TOVS water vapor data is that the data can only be retrieved over clear sky areas since clouds strongly absorb and emit IR radiation. Therefore, passive microwave retrieval methods have become recognized as an alternative to IR retrieval methods because most clouds appear transparent to microwave radiation. This advantage is particularly important in water vapor studies because the convergence and divergence of water vapor most likely occurs in cloud regions. However, the disadvantages of microwave retrieval at the SSM/I frequencies are their inability to retrieve water vapor over land and retrieve vertical distributions of water vapor. Retrieval over land is complicated because generally land surfaces provide a "bright" background which hides the water vapor signal in the atmosphere, and the wide range of surface emissivities due to changing vegetation, even over one satellite footprint, is difficult to model. Vertical distributions are difficult to retrieve because of the uncertainties using weighting functions at the SSM/I frequencies.

Several retrieval methods have been recently introduced in the literature which use SSM/I data to retrieve PWC. The physical method of Tjemkes *et al.* (1991) used polarization changes of the brightness temperature at the 19 GHz frequency to extract the PWC. The statistical methods of Petty and Katsaros (1990) and Alishouse *et al.* (1990) developed regression formulas which related several SSM/I channel brightness temperatures to radiosonde data. Schluessel and Emery (1990) developed regression formulas between the brightness temperatures at the SSM/I frequencies and PWC by using a simple radiative transfer model to predict brightness temperatures at these frequencies using a set of representative atmospheric profiles. Since most of these retrieval methods have been developed recently (over the last 4 years), no studies have attempted to examine the differences between these methods for an extended time period over the entire oceanic globe.

The water vapor field has been found to be an integral part for many scales of motion in the tropical atmosphere. Stephens (1990) developed a correlation between SSTs and

PWC using a 52 month climatology of PWC and SST data. Using this climatology, he found anomalously high values of PWC in the eastern Pacific during the 1982/83 El Niño. The eastward movement of anomalously high PWC marked the shift of the ascending Walker cell from the western to eastern Pacific in association with rising SSTs in that region. Gill (1982) developed a model which hypothesized the role of water vapor in low frequency oscillations. Wiekmann and Khalsa (1990) showed the role water vapor convergence has on convection associated with the 30-60 day oscillation. Lau *et al.* (1989) hypothesized that low, intermediate and high frequency motions are coupled to each other in the tropical climate. Sui and Lau (1989) showed that the intraseasonal oscillation (30 to 60 day) is in phase with higher frequency motions especially in the warm pool region of the western Pacific. Their model showed that the ocean and atmosphere are coupled so that the signal in 30 to 60 day oscillation is most visible over warmer ocean waters, and the convection associated with the oscillation exhibits higher frequency features such as westerly wind bursts. These studies show significant sensitivity to the convergence of water vapor; therefore, stimulating the need to investigate water vapor distribution and low level convergence in the tropical atmosphere.

1.2 BACKGROUND ON TROPICAL MOTIONS

The tropical atmosphere contains various scales of motion which will be discussed in this study. The two scales of tropical motions which were analyzed in this study are the El Niño/La Niña events of 1987-88 and the westerly wind burst events during the fall of 1987. The following sections present background information concerning these motions.

1.2.1 El Niño

A large scale tropical feature commonly discussed in the literature is the El Niño phenomena. During this phenomena, a remarkable transformation occurs in the climatological tropical atmosphere where wind and precipitation patterns change dramatically in the tropics and weather patterns globally show anomalous changes. El Niño has been observed for several centuries as a warm ocean current along the South American coast

which generally appeared a few days after Christmas. The first scientific work concerning this oscillatory pattern was done by Walker (1923, 1924 and 1928). Walker first used the phrase 'Southern Oscillation' (SO) to describe the observed coherent sea level pressure changes between the eastern and western tropical Pacific. His work found a correlation between the SO and changes in precipitation and wind patterns. Reduced sea level pressure in the eastern Pacific was found well correlated to increased precipitation in the central and eastern Pacific.

These correlations went virtually unnoticed until the 1960's when the work of Bjerknes (1966, 1969) developed the first physical explanation for these correlations. He described the 'Walker Circulation' which is a thermally direct circulation where large scale subsidence dominates the eastern tropical Pacific and convection dominates the western Pacific thus inducing easterly flow at the surface and westerly flow aloft. During El Niño, however, a reversal of the the Walker Circulation was observed thus inducing increased convection and precipitation in the central and eastern Pacific. The 1960's also introduced studies by Berlage (1966) and Doberitz (1968) that found interannual changes in SST correlated well with the SO and El Niño.

Since Bjerknes work in the 1960's, many studies have been conducted to examine both the evolution and possible starting mechanisms by which El Niño occurs. A composite study of six El Niño events from 1949 through the 1970s by Rasmusson and Carpenter (1982) helped develop a climatology of these warm events using ship data to compile surface wind and SST data over the central and eastern Pacific. Zebiak and Cane (1987) developed a coupled ocean-atmospheric model which uses no anomalous external forcing for its resulting 3 to 4 year periodicity that resembles in a crude way the development and structure of El Niño. Barnett *et al.* (1991) used GCM calculations to hypothesize that the ocean forces an atmospheric response that produce the El Niño phenomena. Numerous other studies have been conducted during the past couple of decades which separately describe the evolution or onset of El Niño; however, a better understanding of this phenomenum could be achieved if a better description of the hydrologic cycle could be made. Satellite based retrieval methods can provide the high resolution water vapor data needed to explore this problem.

1.2.2 Westerly Wind Bursts

Westerly wind bursts have become a topic of great interest over the past decade because of their possible relationship to the onset of El Niño. Luther (1983) identified these highly energetic episodic bursts as synoptic scale features observed in the equatorial western Pacific between 5N and 5S which have a duration of 5 to 10 days. Chu *et al.* (1988) observed wind speeds as strong as 15 ms^{-1} during these bursts while wind speeds of 5 ms^{-1} were more commonly observed. Wiekmann and Khalsa (1990) and Chu (1988) and gave evidence that westerly bursts are typically associated with intense convection along the equator.

The origin of westerly wind bursts in the tropical western Pacific is still a topic of great debate in the atmospheric science community. One possible explanation is the westerly burst is a response to midlatitude forcing from cold air outbreaks from strong baroclinic development moving eastward from the Asian continent (Chu, 1988). This theory perhaps explains the existence of a small fraction of westerly bursts; however, westerly bursts occur most frequently in the northern hemisphere fall when such outbreaks are infrequent. Gill (1980) demonstrated how a simple tropical disturbance perturbed by a stationary heat source centered on the equator produced a dynamical response which produced strong westerly winds on the west side of the convective region. Lau *et al.* (1989) and Sui and Lau (1989) used mobile-wave CISK theory to couple the dynamics and thermodynamics and explained westerly wind bursts as a higher frequency event which is in phase with lower frequency phenomena such as the 30-60 day oscillation (Madden and Julian, 1973). All of these theories demonstrate that westerly wind bursts are an essential feature of the tropical atmosphere, so further work is needed to more fully understand the evolution of westerly bursts in the tropical atmosphere.

Westerly wind bursts have been suggested to be a precursor to El Niño. Harrison and Luther (1990) and Chu *et al.* (1991) showed that westerly wind bursts occur predominately during October, November and December which is roughly the same period shown in the composite study of Rasmusson and Carpenter (1982) when El Niño begins. Chu *et al.* (1991) showed that the frequency of westerly wind burst increased during the

El Niño years, and Murakami and Sumathipala (1989) showed the frequency maximum of the westerly bursts moved toward the central Pacific during the El Niño. However, Murakami and Sumathipala (1989) demonstrated that westerly bursts occurred more frequently during the mature stage of the 1982-83 El Niño rather than during the onset of the El Niño. Studies thus far have not conclusively demonstrated that westerly wind bursts are a necessary component for El Niño; however, strong evidence does exist that show a connection between the two events.

1.3 OBJECTIVES AND THESIS OUTLINE

There are five objectives this thesis attempts to achieve.

1. Validate five PWC retrieval methods derived from SSM/I data using selected radiosonde data. While all five retrieval methods have published results, no study has attempted to establish the relative differences each retrieval method has with the same set of radiosonde data.

2. Produce a three year climatology of PWC derived from SSM/I data using the retrieval method described in Tjemkes *et al.* (1991). Published work using SSM/I data has centered around the development of retrieval methods, and the data has only recently been made available for an extended time period; therefore, no climatological study has been performed using SSM/I until this study.

3. Determine the relationship between PWC and SST by using a simple Clausius-Clapeyron relationship discussed in Stephens (1990). The goal was to examine how well the PWC/SST relationship using these new independent data compare to the results found in Stephens (1990).

4. Compare the global distributions of PWC for the five retrieval methods over seasonal and daily time scales. Identifying the temporal and spatial variability of these methods over long and short time scales is important for establishing the relative differences between these methods and has not been performed in previous studies.

5. Use data from one of the retrieval methods to examine the convergence and divergence of PWC for both large and small scale motions in the tropical Pacific. This study presents a unique look at the different time and space scales SSM/I data can be used to analyze tropical disturbances. By examining the PWC at these different scales, the role of water vapor in tropical convection can be established.

This study begins in Chapter 2 by describing in detail the several data sets used in this thesis. Chapter 3 describes the theory of the physical and statistical retrieval methods used to produce the PWC data sets. Chapter 4 uses radiosonde data to test the validity of the retrieval methods. Results show the physical method of Tjemkes *et al.* (1991) captures the daily variability of water vapor in the moist western Pacific very well, but generally overestimates the PWC in the higher latitudes. The statistical methods show generally good agreement with the global radiosonde data with slightly less scatter than Tjemkes' method; however, one method shows a weakness of statistically based retrievals by its inability to represent the daily variability of PWC in the tropical western Pacific. Chapter 5 analyzes the global distributions of the five retrieval methods and the global relationship between SST and PWC. Results show the SST/PWC relationship is approximated well with the Clausius-Clapeyron relationship described in Stephens (1990), but time series of the global mean PWC and SST show significant differences between the results from this study and the results from Stephens (1990). Comparison study of the five retrievals identifies significant differences in the daily variability of PWC; however, seasonal changes of the global PWC show remarkable similarities. Chapter 6 uses PWC data to analyze the interaction of PWC with large and small scale tropical disturbances. Results show water vapor convergence in regions of greater convective activity both for low frequency motions such as El Niño and high frequency motions such as westerly wind bursts. Chapter 7 presents the conclusions to this study.

Chapter 2

DATA

A culmination of several data sets were needed to accomplish the goals for this thesis. A brief description of all the data sets along with their pertinent references are provided in this chapter. The data sets examined in this study are listed as follows:

1. European Centre for Medium Range Weather Forecasts (ECMWF) wind analysis data,
2. National Oceanic and Atmospheric Administration (NOAA) outgoing longwave radiation (OLR) data,
3. Reynolds' sea surface temperature data,
4. Special Sensor Microwave/Imager data,
5. National Meteorological Center (NMC) Global Upper Air radiosonde data, and
6. Bismarck Air-Sea Interaction and Circulation Study (BASICS) radiosonde data

The following sections provide background information for each of these data sets.

2.1 ECMWF WIND ANALYSIS DATA

The ECMWF wind analysis has been widely regarded as the highest quality global wind analysis available for research. In particular, a study using the ECMWF wind analysis in the tropics (Murakami and Sumathipala, 1989) demonstrated the validity of this analysis by comparing the 850 mb wind field with Comprehensive Oceanic Atmospheric Data Set (COADS) data. Programs such as the Tropical Ocean Global Atmosphere Program (TOGA) will hopefully introduce a larger array of wind observations which can

be compared rigorously with both the NMC and ECMWF wind analysis since a lack of quality observations of high spatial resolution exist in the oceanic regions.

The u and v component wind fields were accessed from the World Meteorological Organization Archive made available at the National Center for Atmospheric Research (NCAR). The analysis used to produce the ECMWF initialization fields is a multi-step process involving assimilation of observational data from radiosonde data, ship and aircraft reports, and satellite data along with the previous 6 hour forecast made by the model.

The procedure for assimilating the data fields first finds the errors in the 6 hour forecast by constraining the fields to geostrophic balance. Errors between observational data and the 6 hour forecast are analyzed and used to normalize the first guess field. The multivariate optimal interpolation scheme presented in Lorenc (1981) is used in interpolate the fields accounting for errors in each field, and a nonlinear normal mode initialization is used to eliminate the amplification of high frequency gravity waves.

2.2 NOAA OLR DATA

From June 1974 to January 1989, the NOAA polar orbiting satellites were used to collect OLR data globally. Currently, the Climate Analysis Center has archived these data on 9 track tapes. Two similar but separate data sets from the Climate Analysis Center were used to analyze the variability of OLR on pentad, monthly and yearly time scales. Gruber and Winston (1978) and Gruber and Krueger (1984) discuss the overall features of the data along with the limitations and biases of these data sets.

The NOAA polar orbiting satellites used a scanning radiometer which measured radiation intensity at two portions of the energy spectrum: the visible portion (0.5-0.7 μm) and the infrared portion (10.5-12.5 μm). The OLR flux was derived using radiance measurements from the infrared measurements and a regression model which used 99 different atmospheres covering a broad range of atmospheric conditions. The spatial resolution of the radiometer was $\sim$4 km for the visible and $\sim$8 km for the infrared. The satellites were sun synchronous and orbited the earth at $\sim$1500 km with a period of 117 min. Each satellite had a different equatorial crossing time which caused some diurnal biases in the data (Gruber and Krueger, 1984).

Two separate data sets were used in the OLR data analysis. The data set used for the pentad analysis consisted of daily average OLR data gridded on a 2.5 x 2.5 degree grid from 40N to 40S. Quality control checks were needed to remove spurious errors found in the gridded data. The monthly mean and annual mean global OLR was obtained from a separate data set which had quality control checks already applied to the data.

2.3 REYNOLDS SST DATA

The 2 x 2 degree globally gridded sea surface temperature data set of Reynolds (1988) was established by the WMO and the United States National Weather Service in support of the TOGA Coupled Ocean-Atmosphere Response Experiment (TOGA COARE). The Climate Analysis Center was made responsible for the technical guidance while the Ocean Analysis Center was made responsible for the operations. This data set blends ground based observational data (such as ships and unmoored buoys) and satellite data through a sophisticated method which performs quality control on both data sets and merges them through a technique which satisfies Poisson's equation (Oort and Rasmusson, 1971).

The observational data consists of ship and buoy data from NMC using the Global Telecommunication System. A nonlinear filter based on medians was used to remove extreme values instead of the more traditional technique of applying weighting functions to all the data points. Satellite data provide complete global coverage of the oceans; therefore, large oceanic regions with little *in situ* data such as the southeastern Pacific were weighted more heavily with the satellite data. The satellite data were derived from the multichannel sea surface temperature technique developed by McClain *et al.* (1985) using radiances from the advanced very high resolution radiometer (AVHRR) on the NOAA orbiting satellites. Again, extreme values and unrealistic gradients were removed from the data to ensure a more realistic representation of the sea surface temperatures.

The blended analysis generally uses the *in situ* data in regions of dense observations such as ship routes and coastal regions. The satellite data is primarily weighted in the areas with very few *in situ* observations. Biases in the SST satellite data were recognized by Reynolds (1988); for example, aerosols from El Chichon caused a reduction in the

globally averaged SSTs for a 2 year period during the mid 1980's. The blending procedure removes these effects so that these biases were not a factor in the research reported here.

2.4 SSM/I DATA

The SSM/I instrument was placed aboard the Defense Meteorological Satellite Program (DMSP) Block 5D-2 Spacecraft F8. The SSM/I instrument measures microwave radiation at several frequencies from which information about several atmospheric parameters including precipitable water can be retrieved. Since analysis of the data collected from the SSM/I constitutes the major component of this thesis, a description of the instrument and data retrieval procedure are now described.

2.4.1 The SSM/I Instrument

The SSM/I instrument is a passive microwave radiometer which measures microwave emission from earth and its atmosphere at four different frequencies. Horizontal and vertical polarization measurements are taken at 19.35, 37.0 and 85.6 GHz while the 22.235 GHz channel measures only the vertical polarization. The retrieval scheme primarily used in this thesis uses the dual polarization of the 19.35 GHz channel which has a spatial resolution of 69 km along the track and 43 km across the track within the 3-dB footprint size. Table 2.1 from Wentz (1988) provides information about spatial and temporal resolution at each frequency.

The orbit of the DMSP satellite is a sun synchronous, near-polar orbit at an altitude of approximately 860 km. Each orbit is 102 minutes, and the orbit almost completely covers the earth except for two circles of 2.4 degrees centered on each pole. The SSM/I orbit almost gives complete global coverage in one day except for diamond shaped regions in the subtropics. These regions move from orbit to orbit such that complete global coverage is achieved in 2 to 3 days. Figure 2.1 illustrates the geometry of the SSM/I instrument scan. The swath width measures approximately 1400 km, and the view angle of the satellite from the vertical is approximately 53.1 degrees. This angle is advantageous because it allows each footprint for a particular scan to be approximately the same size, and this angle provides a larger percentage of polarized radiation emitted from the ocean surface.

The A scan involves measurements at the lowest 3 frequencies while the B scan takes the higher resolution measurements for the 85 GHz channel.

Table 2.1: Temporal and Spatial Resolution of SSM/I Channels (from Wentz, 1988).

Frequency (GHz)	Polarization	Integration Period	3 dB Footprint Size Along-track	Cross-track
19.35	vertical	7.95 ms	69 km	43 km
19.35	horizontal	7.95 ms	69 km	43 km
22.235	vertical	7.95 ms	50 km	40 km
37.0	vertical	7.95 ms	37 km	28 km
37.0	horizontal	7.95 ms	37 km	29 km
85.5	vertical	3.89 ms	15 km	13 km
85.5	horizontal	3.89 ms	15 km	13 km

The improved design of the SSM/I instrument has significantly reduced the errors obtained during data processing. The SSM/I instrument exhibits on board calibration which enables the calculation of the antenna temperatures to be calibrated upon each scan. Calibration includes effects from radiation absorption of the feedhorn, isolator, and front end waveguide components. The calibration system is far simpler and more accurate than the Scanning Multichannel Microwave Radiometers (SMMR) which were flown on SeaSat and Nimbus-7. Wentz (1988) describes in greater detail the calibration advantages of the SSM/I instrument.

A second important advantage of SSM/I is that its parabolic reflector and feedhorn rotate as a one unit. SMMR, on the other hand, exhibited a fixed feedhorn with a scanning parabolic reflector; therefore, each scan involved a mixture of horizontal and vertical polarized radiation which varied throughout the scan. Data processing of the raw data from SMMR involved complicated conversion equations which extracted the two polarized radiation fields as a function of scan position. SSM/I eliminated this problem resulting in a more efficient and accurate processing of the data.

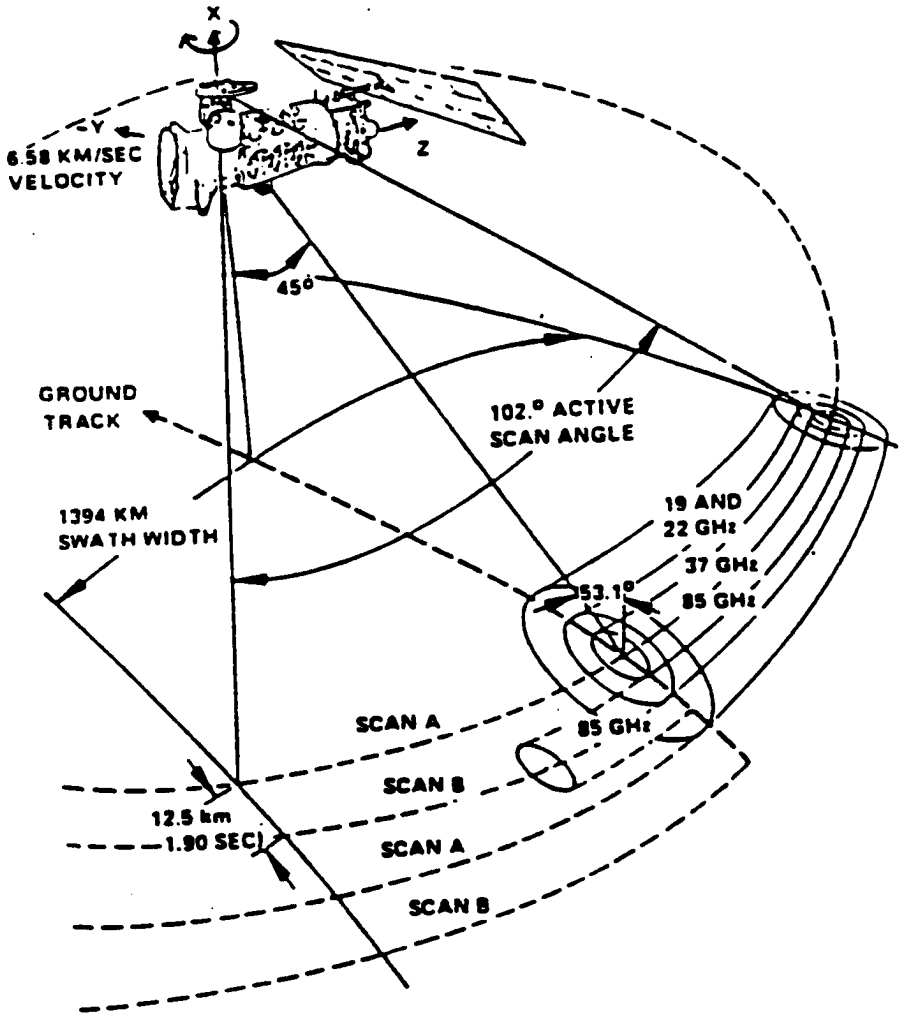

Figure 2.1: SSM/I orbit and scan geometry (from Hollinger *et al.*, 1987).

2.4.2 SSM/I Data Processing

A brief discussion of the retrieval scheme procedure is given to explain more comprehensively the details of producing global data sets of PWC. The discussion of the procedure begins with the raw antenna temperature data from the SSM/I data tapes provided by the National Environmental Satellite, Data, and Information Service (NESDIS) and ends with a 1 degree gridded global data set of PWC over the oceanic regions.

The procedure begins by extracting the antenna temperature data from the SSM/I data tapes. The antenna temperature is a measure of the radiation power entering the feedhorn port of the SSM/I instrument. The primary component of the radiation enters the feedhorn from the parabolic reflector; however, considerations for the feedhorn spillover were made so that the small amount of radiation entering the feedhorn from space could be removed. The procedure used to extract these data from tape is discussed in greater detail in Wentz (1988) and Hollinger *et al.* (1987).

Conversion of the antenna temperatures into brightness temperatures was done using a straight forward technique provided in Wentz (1988). The procedure in this study eliminated the brightness temperatures at the 85 GHz channel because the retrieval schemes used in this thesis did not require information at this channel. Errors in the brightness temperatures were cited in Wentz (1988) as being less than 0.1 K for a range of antenna temperatures from 176 to 270 K.

After calculation of the brightness temperatures, various retrieval schemes were executed to produce global PWC data sets at the pixel level. These schemes are discussed and compared in the next chapter. A crude quality control was used to eliminate erroneous brightness temperature data. All data mislocated with an erroneous time tag and all data with unreasonable antenna temperature values were removed by using information provided by Wentz. All land areas were removed using a 1.0 degree resolution land mask data set provided in the Reynolds' data sets at NCAR. Coastal regions within 1 degree of land were also removed due to the high sensitivity of the Tjemkes *et al.* (1991) retrieval scheme to land regions. The Reynolds' SST blended analysis (Reynolds, 1988) was used in the retrieval scheme for surface temperature data.

The final step required binning the pixel data into a 1×1 degree grid. Each grid point represented the center of a 1.0 degree grid box where the grid point value is the average of all the pixels within the grid box. A basic assumption made during this procedure was that the variations within each grid box were not considered significant; therefore, no attempts were made to apply weighting functions which would weight the pixels closest to the center of the grid box more heavily. This assumption was considered valid for the 5 day and monthly averaged PWC data used in this study. While grid spacing of 1.0 degree was picked arbitrarily, it does match requirements stated for other programs such as the Tropical Rainfall Measurement Mission (TRMM) program of NASA. It should be noted that finer resolution can be achieved using SSM/I data.

2.5 RADIOSONDE DATA

Two sets of radiosonde data were used to validate the PWC data. The first data set was the NMC radiosonde data which provided an extensive set of observations for the subtropical and midlatitude regions. Tropical data from this data set was generally removed because most observations were located over continents or large islands. Since this thesis carefully examines PWC variability in the tropics, a second set of data using data acquired from the Bismarck Air-Sea Interaction and Circulation Study (BASICS) was used to verify the retrieved PWC in a tropical regions.

2.5.1 NMC Radiosonde data

NMC radiosonde data is a global data set of ship and land based radiosonde collected daily by NMC where quality control checks are made to ensure hydrostatic balance and reasonable sounding data. The data are available at NCAR where they have been reformatted and archived on their mass storage system.

The data were filtered by removing all land based stations using the 1×1 degree land mask data provided from the Reynolds' data sets. However, 1.0 degree resolution was found to be too course for particular stations located at small islands where the land mask did not capture the small island. In these instances, the retrieval method of Tjemkes *et al.* (1991) which is sensitive to the land emissivity was found to overestimate the radiosonde

data significantly. Therefore, quality control checks were made to remove stations located on islands that produced a bias when comparing radiosonde data with retrieved data.

2.5.2 BASICS Radiosonde Data

A need for a more comprehensive radiosonde data set for the tropical regions forced an examination of radiosonde data not available in the NMC data set. Radiosonde data from an experiment using a research ship were made available for the research described here. BASICS was a study conducted by the Division of Oceanography, Hobart; the Centre for Environmental Mechanics, Canberra; and the Division of Atmospheric Science, Melbourne. This study acquired radiosonde data from a research vessel located in the Bismarck Sea north of New Guinea (4S,149E) from September 9, 1990 to September 24, 1990.

The BASICS radiosonde data was post processed to account for errors in the calibration of the humidity sensor during each flight of a radiosonde balloon. The data contained the time, pressure, height, temperature, dew point, relative humidity and water vapor pressure for a high density of levels in the vertical. Cloud cover information from visual observations were also provided for each launch.

Chapter 3

RETRIEVAL METHODS FOR PRECIPITABLE WATER

The retrieval of global precipitable water has been a topic of great interest for several decades. Before the age of satellites and microwave radiometers, global retrieval of precipitable water was accomplished by collecting radiosonde data from around the world. Starr *et al.* (1969) and later Piexoto and Oort (1983) and Rosen (1979) estimated the globally averaged precipitable water using conventional radiosonde data and described the water vapor transport by the general circulation.

With the introduction of microwave radiometers aboard satellites over the past decade, it became possible to develop algorithms to determine precipitable water over the previously unsampled global oceans. The advantage of remotely sensing precipitable water is clearly due to the far greater spatial coverage and resolution given by polar orbiting satellites in comparison to the current global radiosonde network. This chapter outlines the physical retrieval schemes of Tjemkes *et al.* (1991) and Chang and Wilheit (1979) and provides the equations for the statistical schemes of Alishouse (1990), Petty and Katsaros (1990), and Schluessel and Emery (1990). A discussion regarding the basic similarities and differences between these five retrieval methods will given in this chapter.

3.1 PWC RETRIEVAL SCHEMES

Two different types of retrieval schemes have been used over the past decade to derive precipitable water. The first type which will be discussed at some length are the physically-based retrieval schemes of Tjemkes *et al.* (1991) and Chang and Wilheit (1979). These schemes use the radiative transfer equation and make some simplified assumptions (which will be explained later) to formulate an equation for the retrieval of precipitable water. The second type involves statistically based retrieval methods (ie. Alishouse *et al.* (1990),

Petty and Katsaros (1990), and Schluessel and Emery (1990)) which develop statistical relationships between the derived brightness temperatures at selected microwave channels and ground based PWC radiosonde measurements. This thesis will make comparisons between these two different types of schemes in order to investigate their similarities and differences.

Chang and Wilheit (1979) and Prabhakara *et al.* (1983) developed retrieval methods for the Scanning Multichannel Microwave Radiometers (SMMR) data set that used the brightness temperature difference between the 18 and 21 GHz channels. The advantage of using these multichannel methods was that these methods removed the surface emissivity dependence by assuming the surface emission to be nearly identical at close frequencies. Therefore, these methods removed any need to parameterize surface winds and foam fractions which are needed to calculate the surface emission.

A significant problem occurs when considering using these retrieval schemes for SSM/I data because the microwave channel frequencies were changed to 19 and 22.235 GHz. Since the 22.235 GHz channel lies at the center of a water vapor absorption line, saturation effects occur when using both channels in regions of high precipitable water. Tjemkes *et al.* (1991) compared the brightness temperature differences between the channels used by SMMR and SSM/I. They clearly showed how the brightness temperature difference for the SSM/I channels at 19 and 22.235 GHZ saturates for regions of precipitable water exceeding 35 kg m^{-2}. This saturation effect does not represent complete saturation at the 22.235 GHz channel, but shows a nonlinear response at that channel particular in moist regions.

In light of the change in measured frequencies between the SMMR and SSM/I instruments and the lack of sensitivity of frequency differences formed from SSM/I observations, Tjemkes *et al.* (1991) introduced a retrieval scheme based on the brightness temperature difference between the horizontal and vertical polarized 19 GHz channel. The premise of this retrieval scheme is that absorbing constituents, such as water vapor and cloud droplets, depolarize the the radiation at this frequency; therefore, the change in the polarization difference at 19 GHz can be used to measure the amount of water vapor within a

particular column of air. The advantage of Tjemkes' scheme is that it removes the saturation problem encountered when using the Chang and Wilheit (1979) retrieval scheme with SSM/I data (discussed in Tjemkes *et al.*, 1991); therefore, Tjemkes' scheme is more sensitive to water vapor variability in moist tropical regions. The disadvantages of Tjemkes' scheme are its sensitivity to the surface emission, precipitation, and cloud liquid water although the latter can be retrieved when other channel information is included in the retrieval (Greenwald *et al.*, 1992). The details of these disadvantages will be discussed later.

Statistical methods have been developed to retrieve precipitable water using simpler algorithms than physical routines which are based on relationships developed between selected radiosonde derived precipitable water and SSM/I brightness temperatures. The first operational algorithm was the Hughes algorithms (Hollinger, 1987); however, these algorithms were later found to fail performance criteria necessary to use operationally. Therefore, Alishouse *et al.* (1990) improved these algorithms by developing similar linear and nonlinear algorithms which better represented the PWC field. Petty and Katsaros (1990) found errors in the Alishouse algorithm especially at low (< 10 kg m^{-2}) and high (> 55 kg m^{-2}) precipitable water amounts. They concluded that the Alishouse *et al.* (1990) showed a correlation between high cloud water and high precipitable water which contaminated the results significantly in cloud regions. Therefore, a modified method was developed which removed the higher frequency channel at 37 GHz from the Alishouse *et al.* (1990) scheme. This channel is more sensitive to cloud liquid water and precipitation, so its removal placed a quality control check for precipitating clouds.

A problem which is inherent with all statistical retrieval methods is the unexplained physics hidden within the empirically derived coefficients and the apparent arbitrariness in the selection of these coefficients. Unlike physical retrieval methods where the tunable parameters are physically meaningful (such as the water vapor absorption coefficient), statistical methods have empirically calculated coefficients which have little physical basis. The coefficients from a statistical routine are generated from a set of globally representative radiosonde data which are intended to represent all aspects of the earth's climate. The

danger of using these routines is that the radiosonde subset often does not represent the wide range of conditions experienced around the globe. Furthermore, the empirical parameters do not represent any state different from those defined by the radiosonde data and thus are difficult to apply to climate change.

3.2 PHYSICAL RETRIEVAL METHODS

The physical retrieval schemes of Chang and Wilheit (1979) and Tjemkes *et al.* (1991) will be developed to show the similarities and differences between the retrieval methods. An outline of Chang and Wilheit's retrieval scheme has been presented merely for the purposes of illustration. It should be kept in mind that the original scheme of Chang and Wilheit was designed for SMMR channels and has not been optimally tuned to the SSM/I channels in this thesis. This discussion will begin with the generalized radiative transfer equation for an absorbing and emitting atmosphere and be followed by the derivations of both retrieval methods.

The generalized radiative transfer equation including both the effects of absorption and emission of energy can be expressed as

$$dI = -k_\nu [I - B] ds \tag{3.1}$$

where I is the intensity, k_ν is the volume absorption coefficient, and B is the emission represented by Planck's function. Brightness temperature measured by the satellite can be derived from (3.1) if we consider only the upwelling radiation, convert from a slanted optical path to optical depth, and use the Rayleigh-Jeans approximation.

The radiation received by a satellite can be expressed in terms of brightness temperature by

$$T_b = T_b(z_o)\tau(z_o, z_t) + \int_{z'=z_o}^{z_t} T(z') \frac{\partial \tau(z', z_t)}{\partial z'} dz' \tag{3.2}$$

where

$$T_b(z_o) = T_s e_s + (1 - e_s) \int_{z'=z_t}^{z_o} T(z') \frac{d\tau(z_o, z')}{dz'} dz' \tag{3.3}$$

and

$$\tau(z_o, z_t) = \tau_{o\alpha}\tau_{h_2o} = \exp\left[- \int_{z_o}^{z_t} (k_{h_2o}\rho_{h_2o} + k_{o\alpha}\rho_{o\alpha}) dz \right]. \tag{3.4}$$

T_b is the brightness temperature for the horizontal or vertical polarizations, z_o and z_t is the bottom and top of the atmosphere respectively, $\tau(z_o, z_t)$ is the total transmission function, k_{h_2o} and k_{ox} is the mass absorption coefficient for water vapor and oxygen respectively, and ρ_{h_2o} and ρ_{ox} is the density of water vapor and oxygen respectively. The first term on the right hand side of (3.2) represents the total microwave energy from the lower boundary while the second term represents the microwave emission from the atmosphere. Equation (3.3) shows that the energy from the surface is composed of both the surface emission of microwave radiation and the reflection of microwave radiation from the atmosphere which are functions of surface wind speed and SST. The sea surface acts as a specular reflector under calm conditions while high wind conditions tend to produce Lambertian reflection (Prabhakara *et al.*, 1982). Under normal conditions with an average wind speed of 5-10 ms^{-1}, the sea surface creates an atmospheric emission over a spectrum of angles which peaks in the specular direction (Rosenkrantz *et al.*, 1978).

If we assume that temperature varies linearly with height then (3.2) can be integrated to the form

$$T_b(z_t) = T_s[1 - (1 - e_s)\tau^2] + \gamma[z^+ + (1 - e_s)z^-\tau] \tag{3.5}$$

where,

$$z^+ = \int_{z'=z_o}^{z_t} z' \frac{\partial \tau(z', z_t)}{\partial z'} dz' \tag{3.6}$$

and

$$z^- = \int_{z'=z_t}^{z_o} z' \frac{\partial \tau(z', z_t)}{\partial z'} dz' \tag{3.7}$$

The retrieval scheme used by Tjemkes *et al.* (1991) approximated z^+ and z^- by performing a Taylor expansion about τ_{h_2o} and assuming τ_{ox} to be a constant. After considerable manipulation, the following expression for brightness temperature at the top of the atmosphere can be expressed as

$$T_b(z_t) = T_s[1 - (1 - e_s)\tau^2] + \gamma z_\rho (1 - \tau_{h_2o})[\tau_{ox} + (1 - e_s)\tau^2] \tag{3.8}$$

where T_s is the surface temperature, e_s is the surface emissivity, and z_ρ is the e-folding height for water vapor. The first term represents the surface emission and reflection of

radiation and the second term represents the atmospheric emission of microwave radiation. If the limiting cases of $\tau = 1$ and $\tau = 0$ are considered, Tjemkes *et al.* (1991) point out that the lower boundary plays the most significant role in influencing T_b. Both cases show that the atmospheric influence is small in comparison to the lower boundary.

3.2.1 Chang and Wilheit Retrieval Method

Equation (3.8) marks the point where the Chang and Wilheit (1979) method and Tjemkes *et al.* (1991) method diverge. Chang and Wilheit (1979) assumes the atmospheric term in (3.8) is small by assuming an isothermal atmosphere ($\gamma = 0$) or that the atmosphere is transparent to water vapor and oxygen ($\tau = 1$). Given this approximation, we can rewrite (3.8) to be

$$T_b \approx T_s[1 - \tau^2(1 - e_s)]. \tag{3.9}$$

Chang and Wilheit (1979) defined a ratio based on (3.9) that eliminates the surface emissivity dependence by assuming that the surface emissivity changes very little between nearby frequencies. Therefore, the transmission functions at 22 and 19 GHz can be related by using (3.9) so that

$$\frac{\tau_{22v}^2}{\tau_{19v}^2} = \frac{T_b^{22} - T_s}{T_b^{19} - T_s}. \tag{3.10}$$

If we use the definition of the transmission function given in (3.4), then we can rewrite (3.10) to be

$$w_{cw} = \frac{1}{2(k_{19} - k_{22})} \ln\left[\frac{T_b^{22v} - T_s}{T_b^{19v} - T_s}\right], \tag{3.11}$$

where w_{cw} is the precipitable water retrieved from Chang and Wilheit (1979).

3.2.2 Tjemkes Retrieval Method

If the difference in the horizontal and vertical temperatures at 19 GHz is taken then

$$\Delta = T_b^h - T_b^v = \frac{\gamma z_\rho}{\tau_{o2}} r^v \left(1 - \frac{r^h}{r^v}\right) \tau^3 + (T_s - \gamma z_\rho) r^v \left(1 - \frac{r^h}{r^v}\right) \tau^2 \tag{3.12}$$

where the surface reflectivity and the surface emissivity are related by

$$r^{v,h} = 1 - e^{v,h}. \tag{3.13}$$

Therefore, using (3.13) we can rewrite (3.12) to be

$$\Delta = [T_s - \gamma z_\rho (1 - \tau_{h_2o})](r^v - r^h)\tau^2. \tag{3.14}$$

If the assumption that

$$T_c \approx T_s - \gamma z_\rho (1 - \tau_{h_2o}) \tag{3.15}$$

is used where T_c is the monthly mean SST, then (3.14) can be rewritten to be

$$\Delta = T_c(r^v - r^h)\tau^2. \tag{3.16}$$

The simplification of (3.14) by using the sea surface temperature assumes the second term on the right hand side of (3.15) is much smaller than sea surface temperature. The second term has a negligible effect in all regions except possibly in the tropics where τ_{h_2o} reaches it minimum value and z_ρ reaches its maximum value. For this study, the second term was neglected. Therefore, using (3.4) and (3.16), the expression for the precipitable water can be written as

$$w_{tj} = -ln\left(\frac{\sqrt{\Delta/T_c r^v(1 - r^h/r^v))}}{\tau_{ox}}\right)/\kappa_{h_2o}\sec\theta. \tag{3.17}$$

It should be noted that this derivation differs slightly from the results presented in Tjemkes *et al.* (1991). Tjemkes' paper incorrectly wrote (3.14) which resulted in a slightly different expression for (3.15). Equation (3.15) was defined in that paper as the "reduced" temperature which may be misleading since this expression always has a slightly larger temperature than the surface temperature.

A parameterization of the surface emissivity was used to determine r^v at 19 GHz. First, the ratio of the reflectivities at the different polarizations was calculated using (3.8) such that

$$F = \frac{r_h}{r_v} = \frac{T_b^h - T_o}{T_b^v - T_o} \tag{3.18}$$

where

$$T_o = T_s + \gamma z_\rho (1 - \tau_{h_2o})\tau_{ox}. \tag{3.19}$$

T_o is approximated by the monthly mean SST for the same reason given for the approximation of (3.15).

Using a linear approximation for the surface wind speed described in Wilheit (1979) ($F = g_0 + g_1 V$), then (3.18) can be used to relate the reflectivity of the horizontal and vertical components of the incident radiation to the surface wind speed. g_0 is a constant determined by the Fresnel equations, and g_1 is constant determined from a surface emissivity model described in Padey and Kakar (1982). From (3.18), we can determine the surface wind speed V which is used to determine the foam fraction of the ocean surface. Calculation of the foam emissivity at the satellite view angle and the wind induced emissivity at that angle allows for the determination of the surface emissivity in the vertical polarization at 19 GHz. Sensitivity studies from Tjemkes *et al.* (1991) show that the near surface wind speed when varied over a range of values expected over much of the oceans only produces 3 percent variations in the precipitable water field.

3.2.3 The Absorption Coefficient

One of the major problems influencing the results of the Tjemkes' method is the sensitivity of the method to the water vapor absorption coefficient (k_{h_2o}) at 19 GHz. The problem with this absorption coefficient is that its value is poorly known, and the values derived from various detailed radiative transfer models are model dependent and sensitive to the spectroscopic data upon which the models are based. Also, determining this coefficient by fitting satellite observations to radiosonde observations introduces the same class of problem as those encountered in deriving coefficients in statistical schemes. This study will consider two different values of this coefficient, one value from Tjemkes' results and the other from Greenwald (personal communication), and the effects of the differences in this coefficient on the PWC are evaluated.

The absorption coefficient at 19 GHz is related to the transmission function for water vapor in Tjemkes' retrieval method by

$$\tau_{h_2o} = \exp\left[k_{h_2o}\sec\theta\left(\frac{\mathrm{T_o}}{\mathrm{T_s}}\right)^{\mathrm{n}}\right] \tag{3.20}$$

where T_o is some reference temperature (300°K in this retrieval scheme) and T_s is the surface temperature. $\left(\frac{T_o}{T_s}\right)^n$ represents the temperature dependence of the water vapor line strength at 19 GHz. Tjemkes' method found $n = 0.47733$ which shows very little

temperature dependence of PWC while Greenwald's coefficient assumes a stronger temperature dependence implied by $n = 0.8$ which was derived by fitting coincident clear sky radiosonde observations to satellite observations.

In Tjemkes et al. (1991), k_{h_2o} was determined using a radiative transfer model based on Ulaby *et al.*(1982) and derived k_{h_2o} by finding the slope of the logarithm of the transmission function for 19 and 22.235 GHz (see Tjemkes *et al.* (1991), Fig. 4). They found $k_{h_2o}\sec\theta$ to be 4.4516×10^{-3} m^2 kg^{-1} from this model. While this value was found to produce reasonable values for the PWC global mean, it will be shown that this value results in PWC values too low in the tropical regions.

It has been demonstrated in this study by using a radiative transfer model based on Liebe (1981) that the value of k_{h_2o} at 19 GHz (from Greenwald, personal communication) significantly improves the PWC values in the tropical regions but significantly overestimates PWC at higher latitudes. The high values in the upper latitudes are a culmination of cloud liquid water effects and a possible poor assumption made in the retrieval method. The improved results in the tropics is because $k_{h_2o}\sec\theta$ was found to be 3.937×10^{-3} m^2 kg^{-1} which is a 14% decrease from the value found in Tjemkes *et al.* (1991).

Cloud water contamination causes erroneous results especially in regions where cloud water is high. Alishouse *et al.* (1990) developed a global liquid water retrieval method which unrealistically mimics the water vapor field. Work by Petty and Katsaros (1990) appears to represent the distribution of cloud liquid water in a more realistic way; however, its effectiveness outside of the statocumulus regions for which it was tuned is at best questionable. A retrieval scheme which retrieves cloud liquid water and PWC is currently under development by Tom Greenwald and Graeme Stephens at Colorodo State University. Preliminary results show that the monthly averaged PWC could be significantly different in persistent cloud regions in the higher latitudes. However, until more ground truth measurements of cloud liquid water are taken in different climatic regions particularly in the tropics, the validity of the liquid water retrieval methods will be questioned.

3.3 STATISTICAL RETRIEVAL METHODS

Three statistical retrieval methods (Alishouse (1990), Schluessel and Emery (1990), and Petty and Katsaros (1990)) were used in the present study to compare with the physical retrieval methods described in the last section. The Alishouse *et al.* (1990) nonlinear global algorithm is based on 19 selected NMC radiosonde data stations spanning over a wide range of climatological zones on the globe. The equation derived in Alishouse *et al.* (1990) which was used in this thesis is

$$w_{al} = a_0 + a_1 T_b^{19v} + a_2 T_b^{22v} + a_3 T_b^{37v} + a_4 (T_b^{22v})^2. \tag{3.21}$$

where a_0, a_1, a_2, a_3 and a_4 are predetermined empirical constants. The nonlinear equation was found to be better than the linear equation algorithm used in Hollinger *et al.* (1987) because it could better represent the precipitable water variations between latitude zones. Both algorithms separated the globe into latitude belts and developed the statistical regression around the grouped radiosonde data for each band. A disadvantage to the nonlinear routine is its greater sensitivity to cloud water and rain sensitivity; however, comparisons between the two algorithms and radiosonde data show the results are better from the nonlinear routine.

The Petty and Katsaros (1990) method is slightly more sophisticated than Alishouse *et al.* (1990) which attempted to eliminate those pixels which were also contaminated by rain. The same radiosonde data used in Alishouse *et al.* (1990) were also used to ensure consistency between the two retrieval methods. Furthermore, they constructed their retrieval around the two lowest frequency channels (T_b^{19v}, T_b^{19h} and T_b^{22v}) in order to minimize the sensitivity of the retrieval to clouds and precipitation which occurs at the higher frequency channels of 37 and 85 GHz. They also constructed their retrieval method around the logarithmic function $\ln(280 - T_b)$ since experience with the data indicated that this function is more linear with precipitable water than a direct relationship with brightness temperature. The algorithm used in this thesis from Petty and Katsaros (1990) is

$$w_{pk} = 11.98 \ln(280 - T_b^{19v}) + 42.06 \ln(280 - T_b^{19h}) - 54.36 \ln(280 - T_b^{22v}) - 20.5. \tag{3.22}$$

The final retrieval method used in this comparison study was developed in Schluessel and Emery (1990). This retrieval method used a simple radiative transfer model to predict the correlation between the brightness temperature at several frequencies and the water vapor field. Their model considered a large variation of meteorological conditions which attempt to represent the wide variability of weather over the global oceans. The model considered only cloud free areas and makes no considerations for scattering in the atmosphere; therefore, limitations of this method over climatologically high cloud regions was expected. Their results showed the best correlation between between T_b^{22v} and w while higher frequencies show much greater scatter due to their far greater sensitivity to liquid water and clouds. The algorithm from their study used in this thesis is

$$w_{se} = 23.82 - 4.059 \ln(280 - T_b^{22v}) + .02451[\ln(280 - T_b^{22v}) - T_b^{37v}]. \tag{3.23}$$

With these five retrieval methods, a comparison study was conducted to examine their major differences and similarities. Chapter 4 will use radiosonde observations to measure the validity of each retrieval method while Chapter 5 will examine the products of each retrieval method on a global scale for various time periods.

Chapter 4

RADIOSONDE VALIDATION

Radiosonde observations of water vapor represent the most common data form used to validate satellite retrieved data. Typically in the literature, PWC derived from the SSM/I data is validated through scatter plot comparisons with a selected subset of global radiosonde data (ie. Alishouse *et al.* (1990), Tjemkes *et al.* (1991), and Petty and Katsaros (1990)). This chapter will also use a global radiosonde data set which was compiled by NMC and archived by NCAR and a radiosonde data set from the BASICS experiment to evaluate the five retrieval methods outlined in Chapter 3. Through these comparisons, the accuracy of the PWC over the oceanic regions of the globe and the accuracy of the temporal variability of PWC in the western Pacific will be assessed.

Obvious pitfalls occur when comparing radiosonde data to satellite observations. These pitfalls undermine the ability to compare radiosonde observations to satellite observations. The following is a list of four difficulties in comparing these data.

1. Comparisons between a point observation (radiosonde data) and an area observation (satellite data) can be imprecise due to spatial variations in PWC.

2. Time coherence is not exact.

3. Both radiosonde and satellite measurements have a particular amount of uncertainty.

4. Local environmental effects can substantially contaminate results of the different measurements in different ways.

These problems generally occur in all techniques used to validate satellite retrieval products with ground observations. Throughout this chapter, these problems will be discussed in greater detail.

4.1 TECHNIQUE

The technique used to derive PWC from radiosonde data is based on Teten's formula (Teten, 1930) which has been widely used in the literature. This method uses the Clausius-Clapeyron equation to predict the saturation vapor pressure which allows calculation of the mixing ratio and ultimately the precipitable water.

Given the dew point temperature T_d in Kelvin, the saturation vapor pressure was calculated using the Clausius-Clapeyron equation

$$e_s = e_s^{\circ}\exp[17.27(\mathrm{T_d} - 273.15)/(\mathrm{T_d} - 35.86)] \tag{4.1}$$

where e_s is the surface vapor pressure and e_s° is the surface vapor pressure at standard temperature and pressure. The mixing ratio can be calculated by transforming the equation of state to

$$r \approx \epsilon \frac{e_s}{p} \tag{4.2}$$

where ϵ is the ratio of the gas constant for dry air over the gas constant for water vapor. The total precipitable water can now be calculated by integrating the mixing ratio along a vertical path. Introducing the hydrostatic equation in this integral leads to

$$w = \frac{1}{g}\int_0^{p_o} r(p)dp. \tag{4.3}$$

where p_o is the surface pressure and g is gravity. Using the trapezoidal approximation, we can derive PWC numerically using radiosonde data as

$$w = \frac{1}{2g}\sum_i (r_{i-1} + r_i)(p_{i-1} - p_i) \tag{4.4}$$

where i is an index which increases as the level of the sounding increases. This technique is the most common method of retrieving PWC from radiosonde data.

Spatial coincidence between the radiosonde and satellite data is generally a problem in validation because radiosonde observations are point observations while satellite observations are averaged over a specific area. Spatial averaging was handled the same way for both radiosonde data sets. All pixels of the satellite data within 0.5 degree of the

radiosonde location were averaged and compared with the radiosonde data. This technique assumes small variations in the PWC field over a 1.0 degree grid box. Later results will show that variations within this box are generally small except in thick cloud regions where variations seen in several retrieval methods can be significant.

Time coincidence is considered a serious problem given the lack of knowledge about the diurnal variability of PWC. A fairly strict test was imposed on the BASICS data where only satellite overpasses within 2 hours of the radiosonde observations were considered. A lesser restriction was used with the NMC data. All NMC radiosonde data for a particular day were compared with the daily 1 degree resolution PWC data which are composed of 6:00 am and/or 6:00 pm local time satellite overpasses from the DMSP satellite. Therefore, much of the scatter found in the data for the NMC data can be attributed to the lack of time coincidence between the two data sets. However, for the purpose of measuring the validity of the retrieval methods over the globe, the time coincident problem with the NMC data is considered minimal.

All scatter plots were filtered by removing points two standard deviations from the mean retrieval value for a 5 kg m^{-2} radiosonde interval. Only about 5 percent of the data points were generally removed from the scatter plots in this manner. Further quality control removed all points greater located north of 70N or south of 70S because of potential ocean ice contamination of the satellite data. Removal of unrealistic PWC values exceeding 100 kg m^{-2} from both the radiosonde and satellite data was also performed.

4.2 RESULTS

Several different time periods of SSM/I derived PWC data were compared to NMC and BASICS radiosonde data. The time periods used in the NMC comparison were January 1989 and July 1989 while the time period of the BASICS experiment was from September 9, 1990 to September 24, 1990. All time periods were tested to compare results among from several different PWC retrieval methods. The BASICS data were introduced to examine a time series of PWC in the west Pacific basin using all the retrieval methods since the NMC data did not provide a good coverage for this region of interest.

4.2.1 NMC Radiosonde Data

A comparison study was made to evaluate the performance of the physical and the statistical retrieval schemes. Since the Alishouse and Petty and Katsaros retrieval methods used the NMC radiosonde data to develop their regression coefficients, biases were expected which would make these retrieval methods appear more accurate than the PWC data derived from other retrieval methods.

Figures 4.1 and 4.2 show scatter plots of radiosonde data versus the retrieved SSM/I PWC of Tjemkes *et al.* (1991) and Chang and Wilheit (1979) methods respectively for January and July of 1990. Tjemkes' method shows more scatter particularly where the radiosonde PWC exceeds 30 kg m^{-2} and a slight positive bias in the drier regions. Possible reasons for this bias will be explained later. The saturation effect can be detected in the Chang and Wilheit method for regions wetter than 40 kg m^{-2} where this method underestimates the PWC. These results support the conclusion found in Tjemkes *et al.* (1991) which showed the saturation effect at PWC values exceeding 40 kg m^{-2} using data from the fall of 1987.

Figures 4.3, 4.4 and 4.5 are similar scatter plots of the statistical routines. Both Schluessel and Emery's method and Petty and Katsaros' method overestimate the PWC in regions where the radiosonde PWC exceeds 45 kg m^{-2}. All three methods give good results where the radiosonde PWC is less than 30 kg m^{-2} and generally less scatter is found in these methods than what was found in Tjemkes' method. Alishouse's retrieval shows the least amount of scatter which was surprising since Petty and Katsaros' method was intended to be an improved modification of Alishouse's method particularly in the moist regions.

Table 4.1 gives the root mean square (RMS), correlation (COR) and bias (BIS) for all five retrieval methods for January and July of 1989. Differences between January and July are small with the largest changes occurring with Chang and Wilheit and Schluessel and Emery's retrieval. Tjemkes' retrieval scheme has approximately 1-2 kg m^{-2} higher RMS values then the statistical routines for both months. The correlation is also about .02 to .04 less than those retrieval methods. The major reason for the larger RMS errors stem from

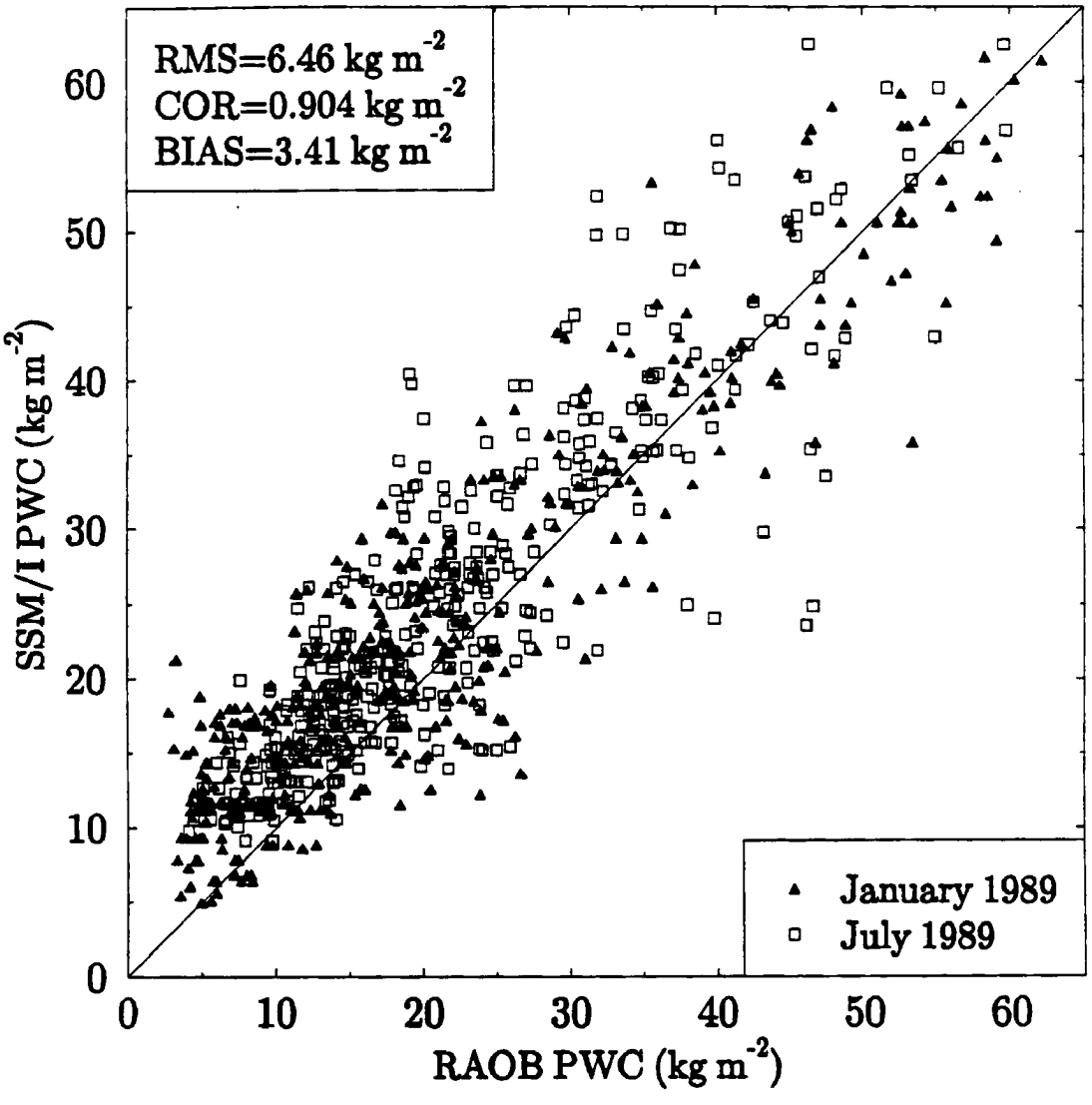

Figure 4.1: Comparison of precipitable water derived over global oceans for January 1989 using Tjemkes *et al.* (1991) retrieval method and precipitable water derived from NMC radiosonde data.

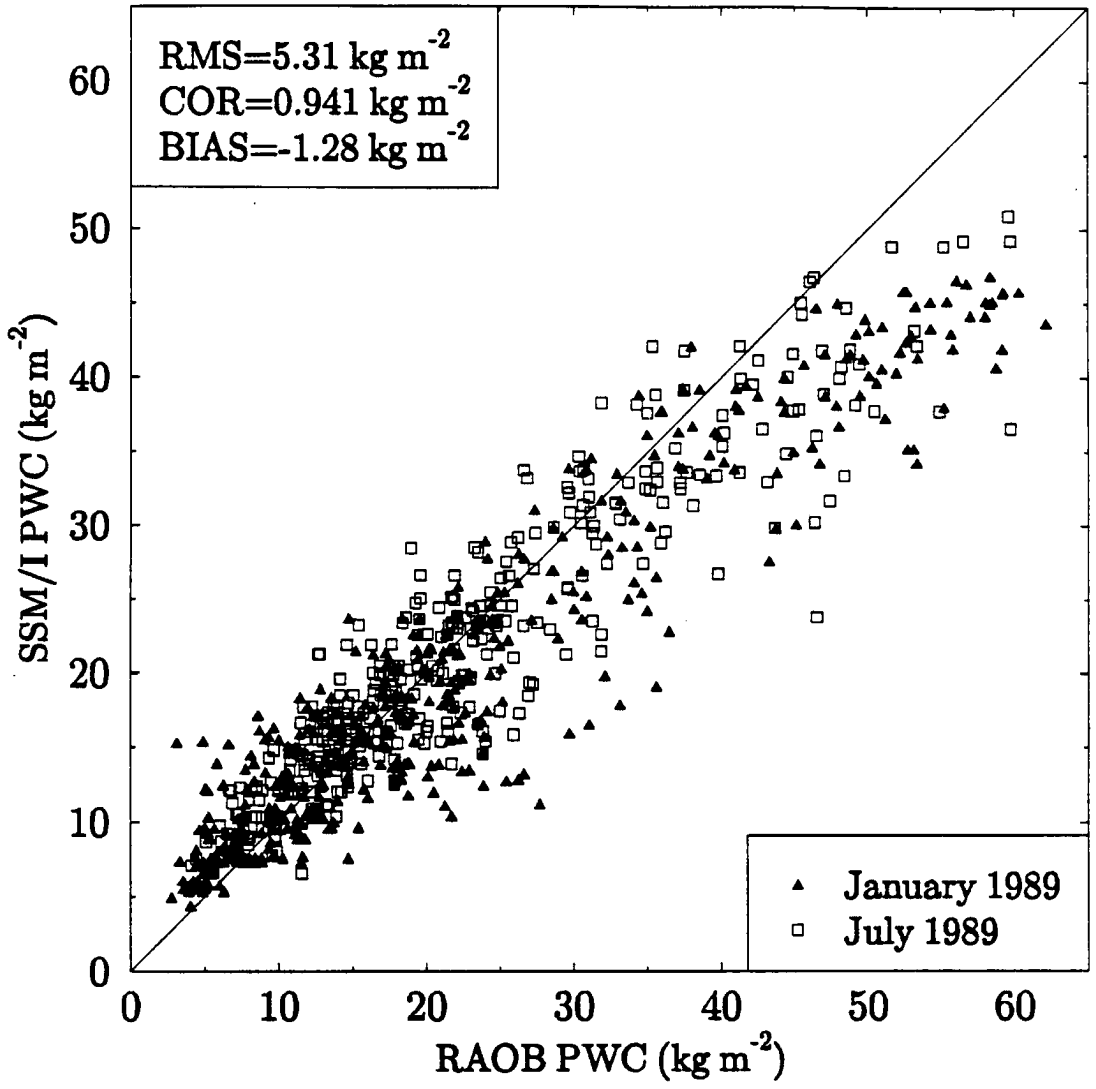

Figure 4.2: The same as Figure 4.1 except using the retrieval method of Chang and Wilheit (1979).

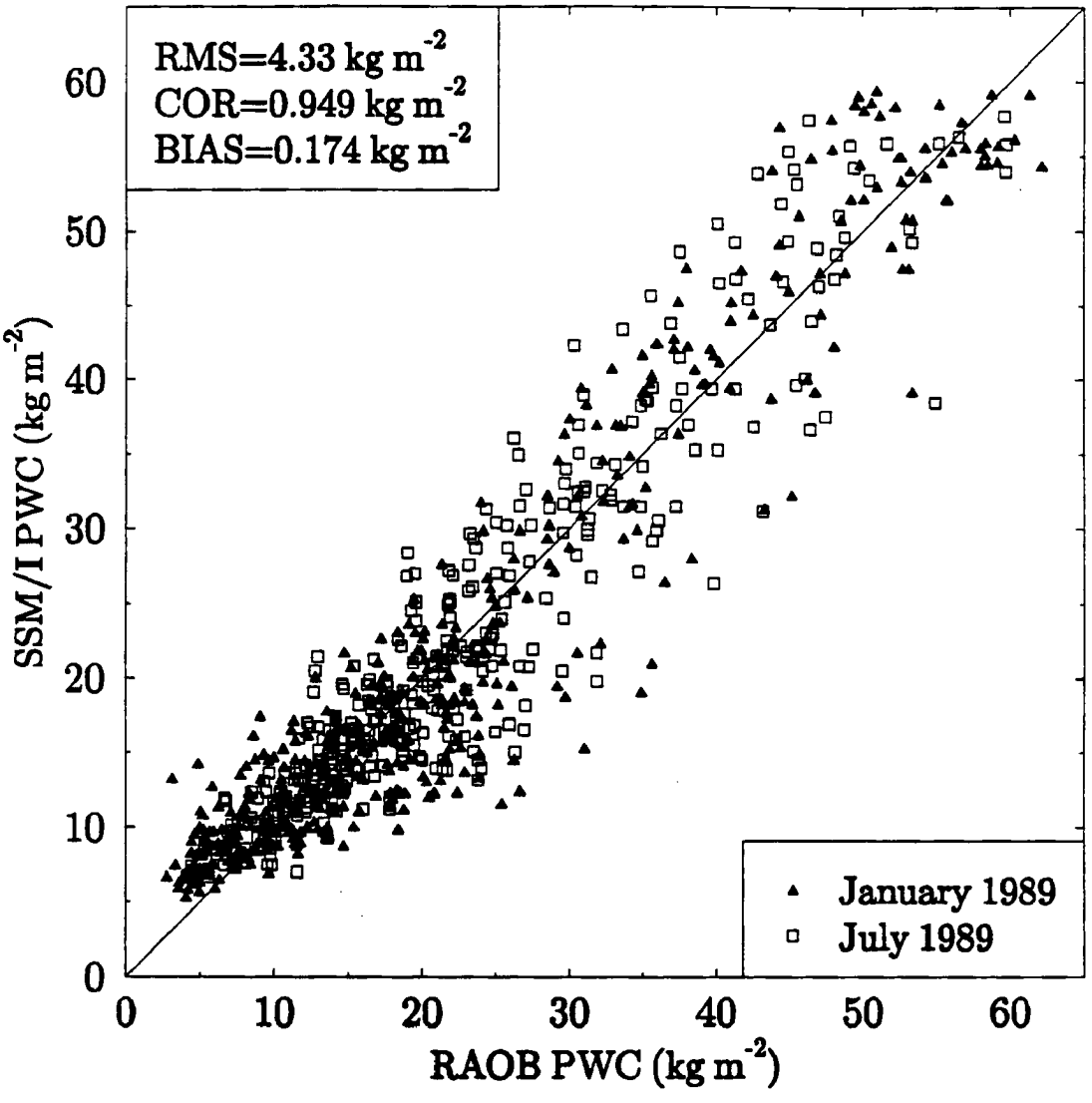

Figure 4.3: The same as Figure 4.1 except using the retrieval method of Alishouse (1990).

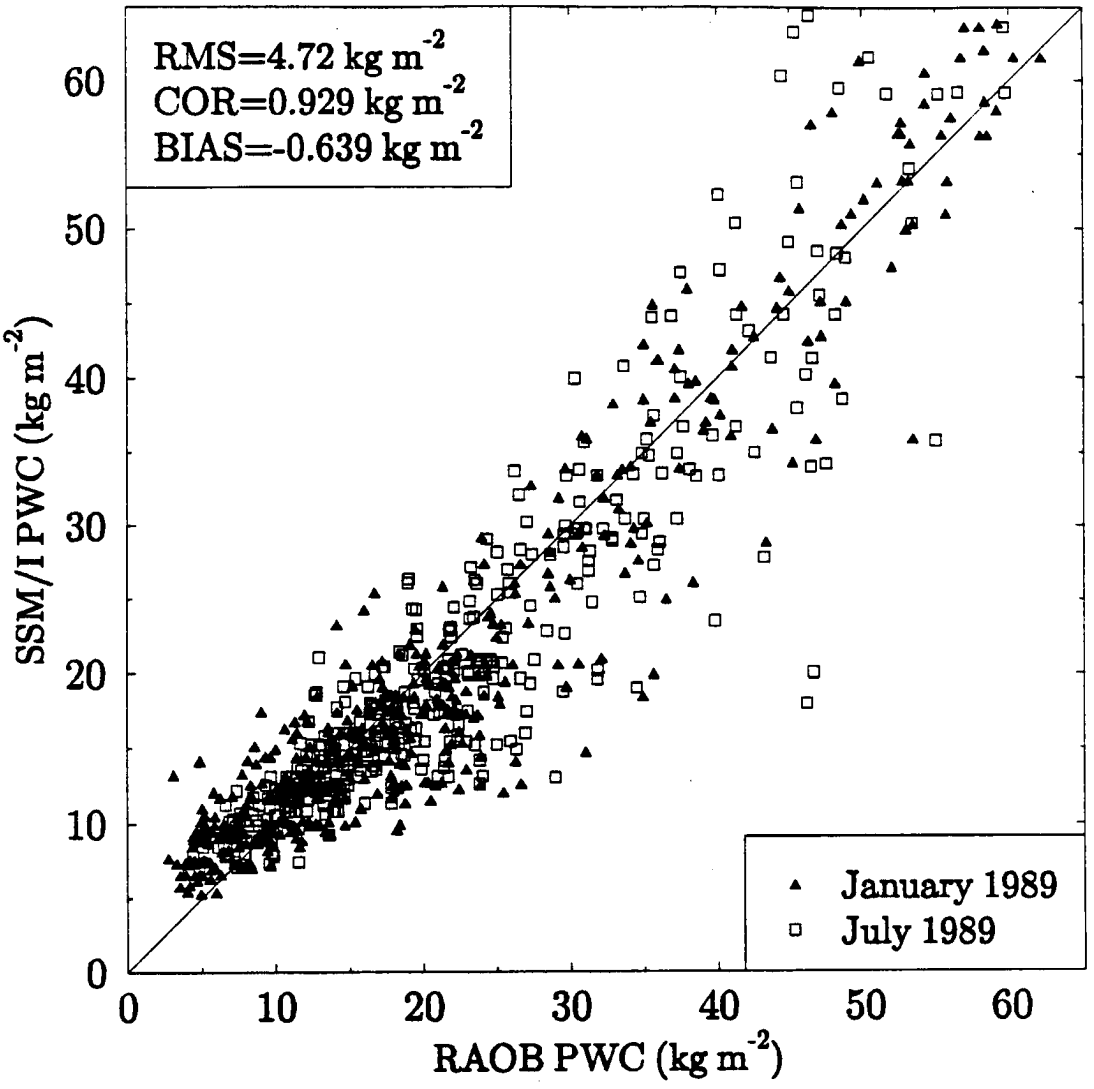

Figure 4.4: The same as Figure 4.1 except using the retrieval method of Schluessel and Emery (1990).

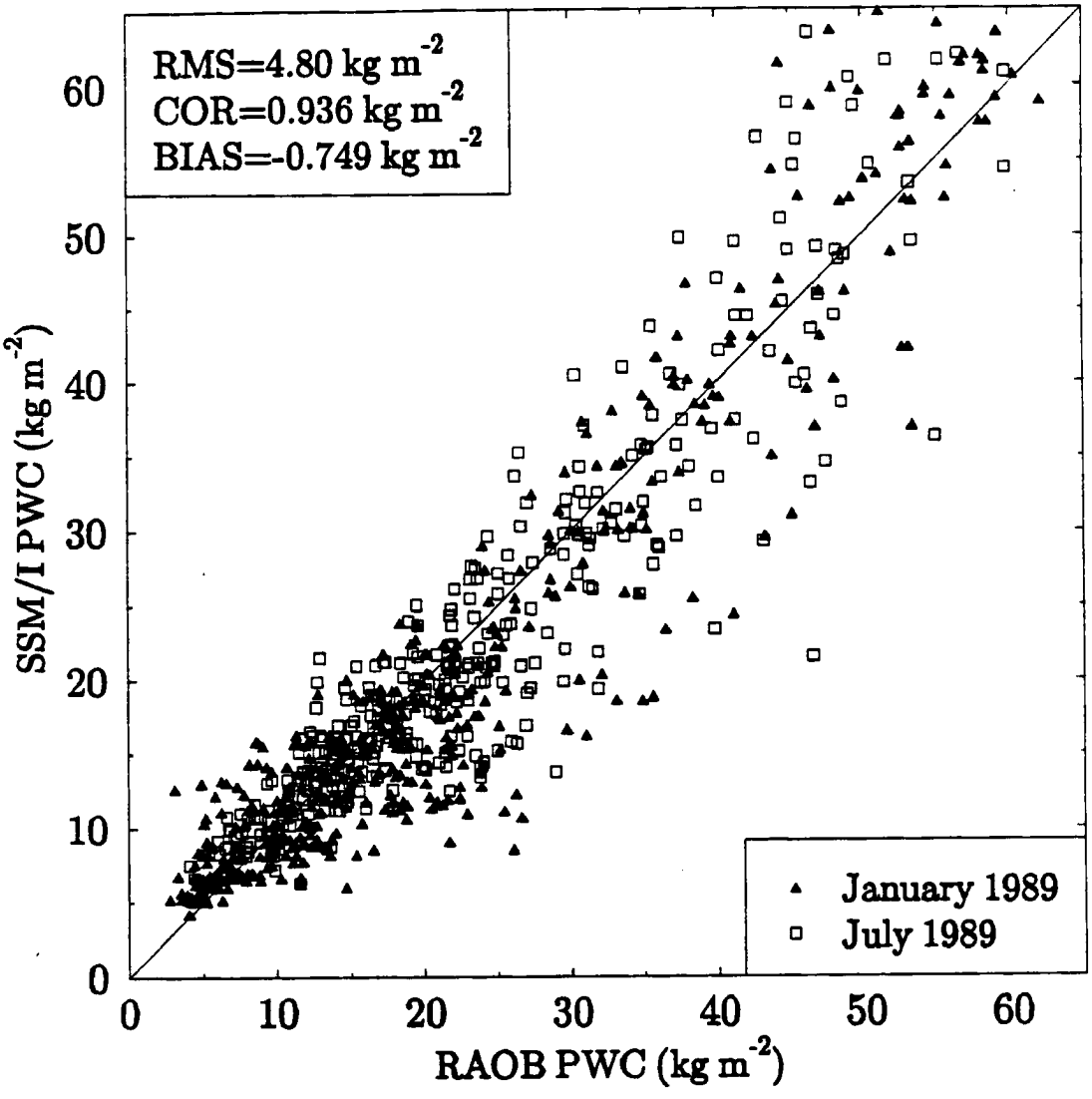

Figure 4.5: The same as Figure 4.1 except using the retrieval method of Petty and Katsaros (1990).

the sensitivity of the Tjemkes' retrieval method to cloud liquid water and precipitation along with the positive bias found in the PWC values in the higher latitudes. This bias is partly caused by cloud water contamination since a significant percentage of the radiosonde observations were located in persistent cloud regions in the north Atlantic and Pacific. It should also be noted that this bias could also be the result of the assumptions built into the retrieval. These assumptions include a constant lapse rate and scale height for water vapor which are weak functions of SST. However, Tjemkes' errors are not large enough to dismiss the his retrieval method especially when studying mean fields of PWC.

Table 4.1: Root mean square (RMS), correlation (COR) and bias (BIS) of PWC data (in kg m^{-2}) for the retrieval methods of Tjemkes *et al.* (TJ), Chang and Wilheit (CW), Alishouse *et al.* (AL), Schluessel and Emery (SE), and Petty and Katsaros (PK).

NMC Radiosonde Statistics					
JANUARY 1989					
	TJ	CW	AL	SE	PK
RMS	6.25	5.85	4.41	4.52	4.96
COR	.925	.949	.956	.947	.944
BIS	3.21	-1.90	.18	-.31	-.94
JULY 1989					
	TJ	CW	AL	SE	PK
RMS	6.70	4.68	4.24	4.96	4.61
COR	.879	.932	.940	.909	.927
BIS	3.63	-.55	.16	-1.01	-.53

4.2.2 BASICS Radiosonde Data

BASICS experiment introduced an independent, quality controlled data set which was used to test all five retrieval methods against radiosonde data obtained from the warm pool region of the western Pacific. The goal for using these data was to test more rigorously the ability of these retrieval methods to measure daily changes of PWC in a region where water vapor content is large and its temporal variability is significant.

Figure 4.6 shows a time series of the radiosonde data along with the retrieved products from the three statistical methods. The radiosonde data shows a gradual decline in PWC

from 60 kg m^{-2} to 45 kg m^{-2} over the first week and then a rapid increase up to 62 kg m^{-2} during the second week. Alishouse's retrieval scheme shows the worst day-to-day sensitivity especially from day 19 through 24 where the Alishouse PWC is nearly invariant. Petty and Katsaros' method appears to be too wet throughout the time period except the last two days while Schluessel and Emery's method most closely represents the magnitude of the PWC from BASICS radiosonde data. Standard deviations from the mean were generally less than 2 kg m^{-2} except during precipitation periods when Schluessel and Emery along with Petty and Katsaros' methods had significantly greater deviations.

Figures 4.7a and 4.7b show BASICS PWC time series compared with the Tjemkes' retrieval method using the two different absorption coefficients described in Chapter 3. Both Tjemkes' time series show the standard deviation of all the observations within 0.5 degrees of a radiosonde observation. These results show that the absorption coefficient used in Tjemkes *et al.* (1991) (Figure 4.7a) produces a PWC time series which is significantly less than observed in western Pacific while the Greenwald's absorption coefficient produces results which correspond very well with the radiosonde time series. These results also show that Tjemkes' retrieval method captures the overall trend of the radiosonde data fairly well; however, precipitation contamination was found to be significant in this retrieval method. Day 21 was not plotted because heavy precipitation caused the PWC to exceeded 65 kg m^{-2} and produced a large standard deviation. However, Tjemkes' method generally does a very good job in capturing the day to day variability of the PWC in the tropics.

Figure 4.8 shows the serious problems Chang and Wilheit's method has in the tropics. The time series does not capture the shape of the PWC, and this method produces results that are too dry. Adjustment of the absorption coefficient at 19 or 22.235 GHz could improve the magnitude of the PWC values; however, the temporal variation of Chang and Wilheit's PWC is far too flat to accurately represent the daily variability of PWC. This result further supports the assertion of Tjemkes *et al.* (1991) that the brightness temperature difference between 22.235 and 19 GHz losses sensitivity to PWC values in excess of 40 kg m^{-2}. Obviously, the Tjemkes' physical retrieval method better represents PWC variability in moist regions of the oceanic globe.

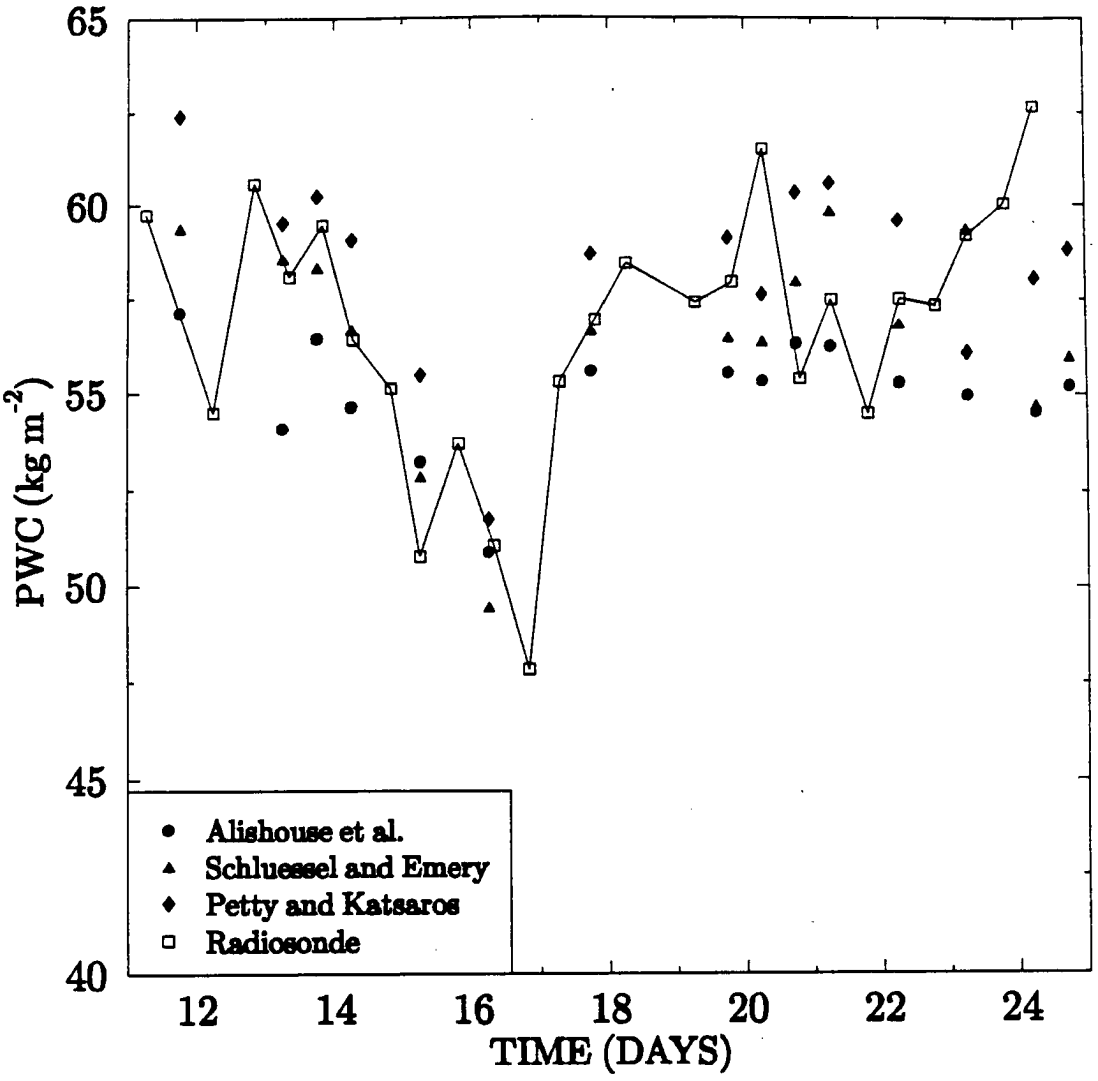

Figure 4.6: Time series of precipitable water from the Bismarck radiosonde data at 149E 9S from September 11-24, 1990 compared with three statistical retrieval methods.

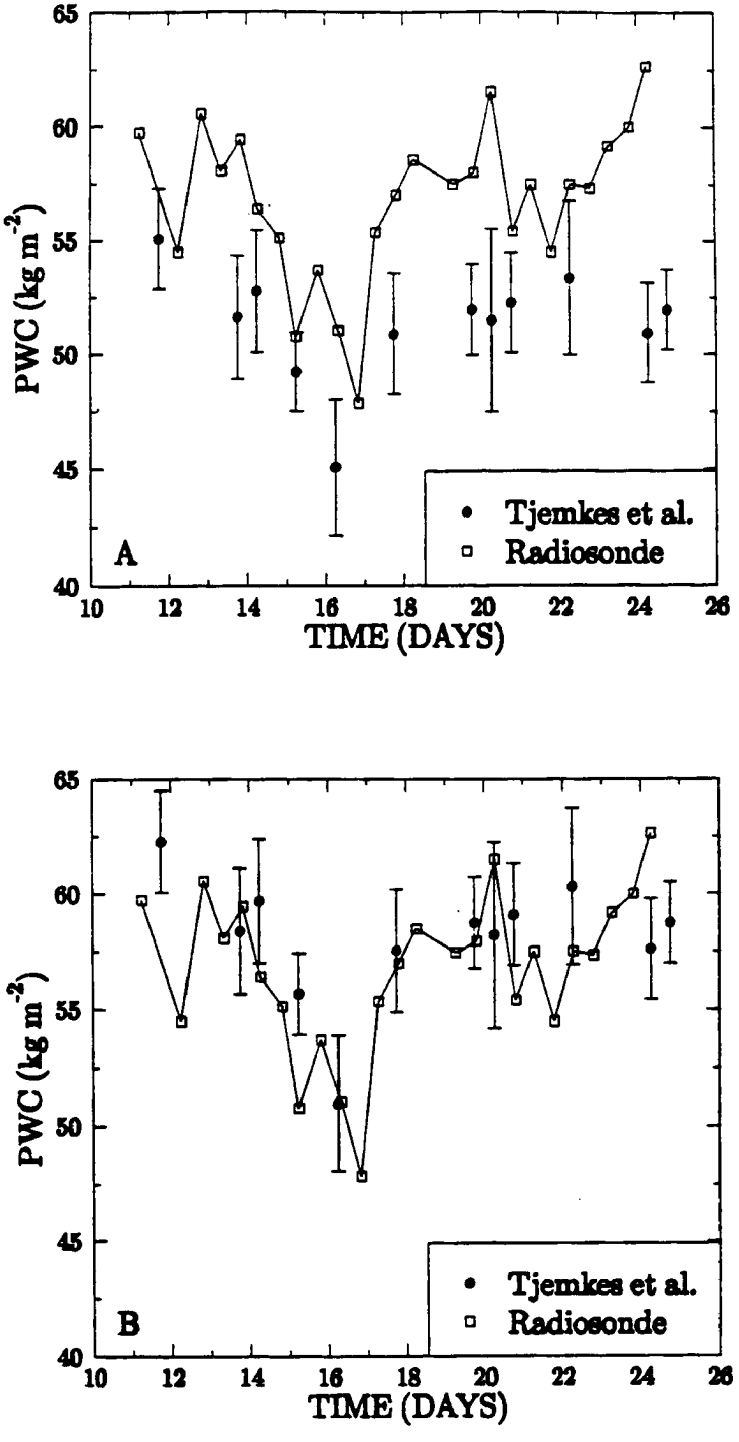

Figure 4.7: Time series of precipitable water from the Bismarck radiosonde data compared with Tjemkes *et al.* (1991) method. Error bars indicate one standard deviation of all observations within 0.5 degrees of the radiosonde location. (A) uses $k_{h_2o} = 4.4516 \times 10^{-3}$ m^2 kg^{-1}, and (B) uses $k_{h_2o} = 3.937 \times 10^{-3}$ m^2 kg^{-1}.

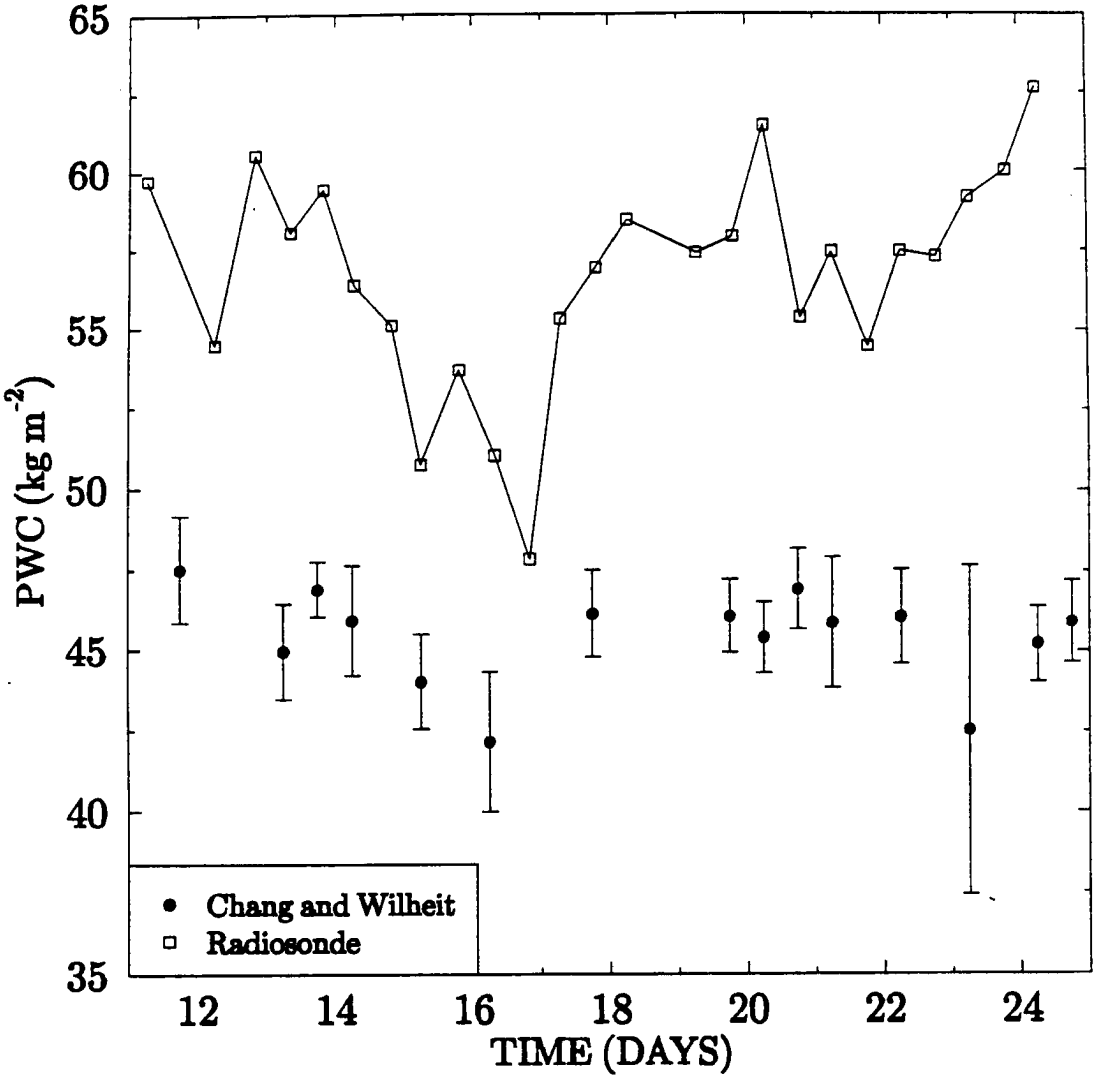

Figure 4.8: Same as Figure 4.7b except for the retrieval method is from Chang and Wilheit (1979).

Chapter 5

GLOBAL ANALYSIS OF PRECIPITABLE WATER

While documenting the global distribution and transport of water vapor has been an issue of interest for several decades, only recently has the atmospheric community been able to establish the more quantitative aspects of these topics. After World War II, a newly devised global network of radiosondes allowed for quantitative studies to be conducted which enabled scientists to understand the water vapor distribution and variations in a very gross manner. Papers such as Benton and Estoque (1954) and Sellers (1965) summarize the early work concerning water vapor distribution and transport (see Wittmeyer (1991) for further details and references). The major problem with these studies was that they were naturally restricted to land masses; therefore, the lack water vapor measurements in the data sparse regions of the ocean significantly hampered the results of these studies.

The introduction of satellites in the 1960's created a new platform by which water vapor could be monitored. While many papers concerning the retrieval theory of satellite-based methods for the calculation of PWC, very few studies have made efforts to use these type of water vapor data to describe the variability of the water vapor field. In Stephens (1990), a global analysis of water vapor was conducted using SMMR data, and many features of the general circulation were extracted including interannual variations of PWC in different climate regions and their relationship to El Niño. A simple relationship reminiscent of the Clausius-Clapeyron relationship was found between PWC and SST, and this relationship was used to explain large scale changes in the PWC. For example, Stephens (1990) showed a reduction of PWC in the tropical west Pacific and anomalously high PWC in the central and eastern Pacific during the El Niño event of 1982. The large scale convergence and divergence of water vapor was also identified in many regions of the globe in this study.

This chapter presents analysis of the climatology of PWC and its relationship to SST by using the SSM/I derived PWC data and Reynolds' SST data which are the most current data sets of their kind available. Analysis of 1 × 1 degree daily global PWC data was made for the five retrieval methods described in Chapter 4 for the year of 1989 and global comparisons between these retrieval methods were made over annual, seasonal and monthly time scales. Intrannual and interannual variations in the PWC were analyzed, and large scale PWC changes during the 1988 La Niña were made evident.

5.1 A BULK RELATIONSHIP BETWEEN PWC AND SST

The relationship between PWC and SST was examined over a three year time period using Tjemkes' retrieval method and Reynolds' SST data and comparisons were made between these results and the results found using SMMR derived PWC and NMC blended SST data discussed in Stephens (1990). The relationship derived in Stephens (1990) assumed the specific humidity vertical profile had the form

$$q = q_o \left(\frac{p}{p_o}\right)^{\gamma}. \tag{5.1}$$

where q is the specific humidity, p is pressure, q_o and p_o are the respective surface values, and γ describes the scale height of water vapor. Integration over p from the top to bottom of atmosphere and incorporation of the Clausius-Clapeyron equation results in the following relationship between PWC and SST,

$$w = 10.82 \left(\frac{r}{1+\gamma}\right) \exp[a(T_s - 288)] \tag{5.2}$$

where a=0.0686 K^{-1}, T_s is the SST in Kelvin and r is the relative humidity. This equation was used to fit the data used in Stephens (1990) and in this study by a least squares method which solved for the factor $r/(1+\gamma)$.

Figure 5.1 shows a scatter plot of PWC against SST with the error bars represent one standard deviation from the mean PWC. Regions with SST > 15°C match very well with the exponential relationship described in Stephens (1990) equation (5). He found the factor $r/(1+\gamma) = 0.162$ with standard error of 4.8% while the present results show

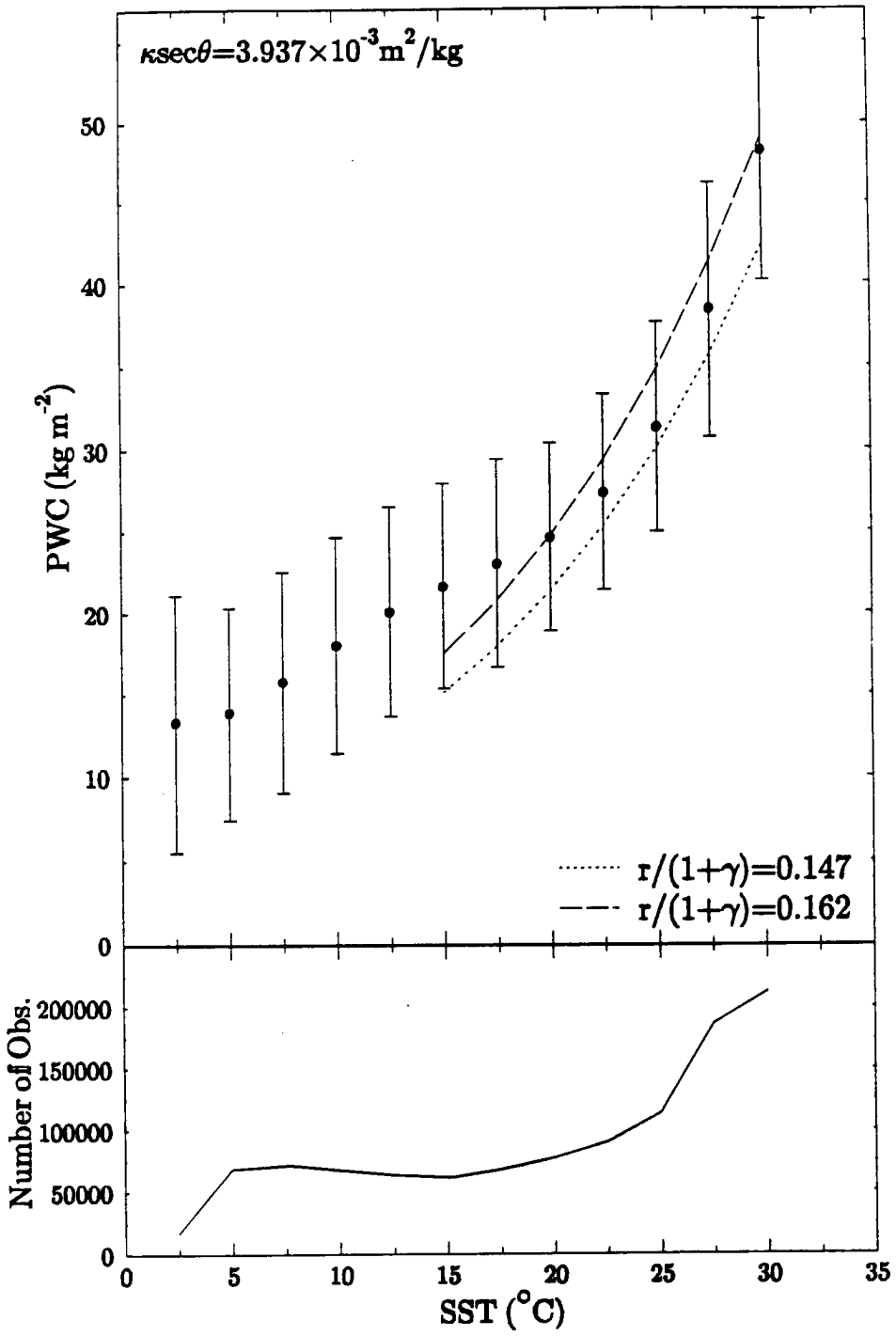

Figure 5.1: The relationship between PWC and SST over a three year period from February 1988 to January 1991. Error bars represent one standard deviation from the mean PWC averaged over a bin of corresponding SST values spanning 2.5°C either side of the plotted SST value.

$r/(1+\gamma) = 0.158$ with standard error of 4.9%. These results also show the difference the value of the absorption coefficient produces in the PWC distribution. With $\kappa \sec\theta = 4.4516 \times 10^{-3}$ $m^2 kg^{-1}$ as it was reported in Tjemkes *et al.* (1991), the least squares fit results in $r/(1+\gamma) = 0.147$ which produces PWC values that are too low in the tropics (as was shown in Figures 4.7a and 4.7b). The greatest differences between the present results and the SMMR results occur in coldest waters where the SSM/I derived results show significantly larger PWC than the SMMR results. Radiosonde observations, shown in Chapter 4, suggest that the SSM/I results used in this research do in fact overestimate the PWC at the higher latitudes.

The seasonal variability of the PWC-SST relationship is shown in Figure 5.2. This figure indicates that the greatest seasonal variability of the global relationship between PWC and SST occurs in regions where SSTs are less than 20°C. The seasonal variability can be attributed to the large seasonal changes in this relationship in the northern hemisphere. Figure 5.3 shows the relationship between PWC and SST changes dramatically from February 1989 to July 1989 particularly where SSTs are less than 20°C. July 1989 shows higher PWC at all SSTs than February 1989, and the exponential shape of the relationship flattens in July for SSTs less than 20°C. Figure 5.4 shows the corresponding changes in the southern hemisphere to be far less dramatic, and the exponential shape of the PWC-SST relationship is preserved for both months. This result suggests that the error bars in Figure 5.1 are not solely errors in the retrieval method, but these deviations represent physical changes in the hydrology of the atmosphere.

The large seasonal variability in the northern hemisphere can be largely attributed to the dramatic changes in the SST-PWC relationship in the northern Pacific. The divergence and convergence of water vapor over the globe for February and July 1989 were calculated in Figures 5.5 and 5.6 using the 3 year PWC-SST relationship found in Figure 5.1. The standard deviations in Figure 5.1 represent physical changes in the hydrologic cycle where points above the mean value represent a state where the atmosphere has greater quantities of water vapor than normal. Therefore, positive values in Figures 5.5 and 5.6 represent water vapor convergence while negative values represent water vapor

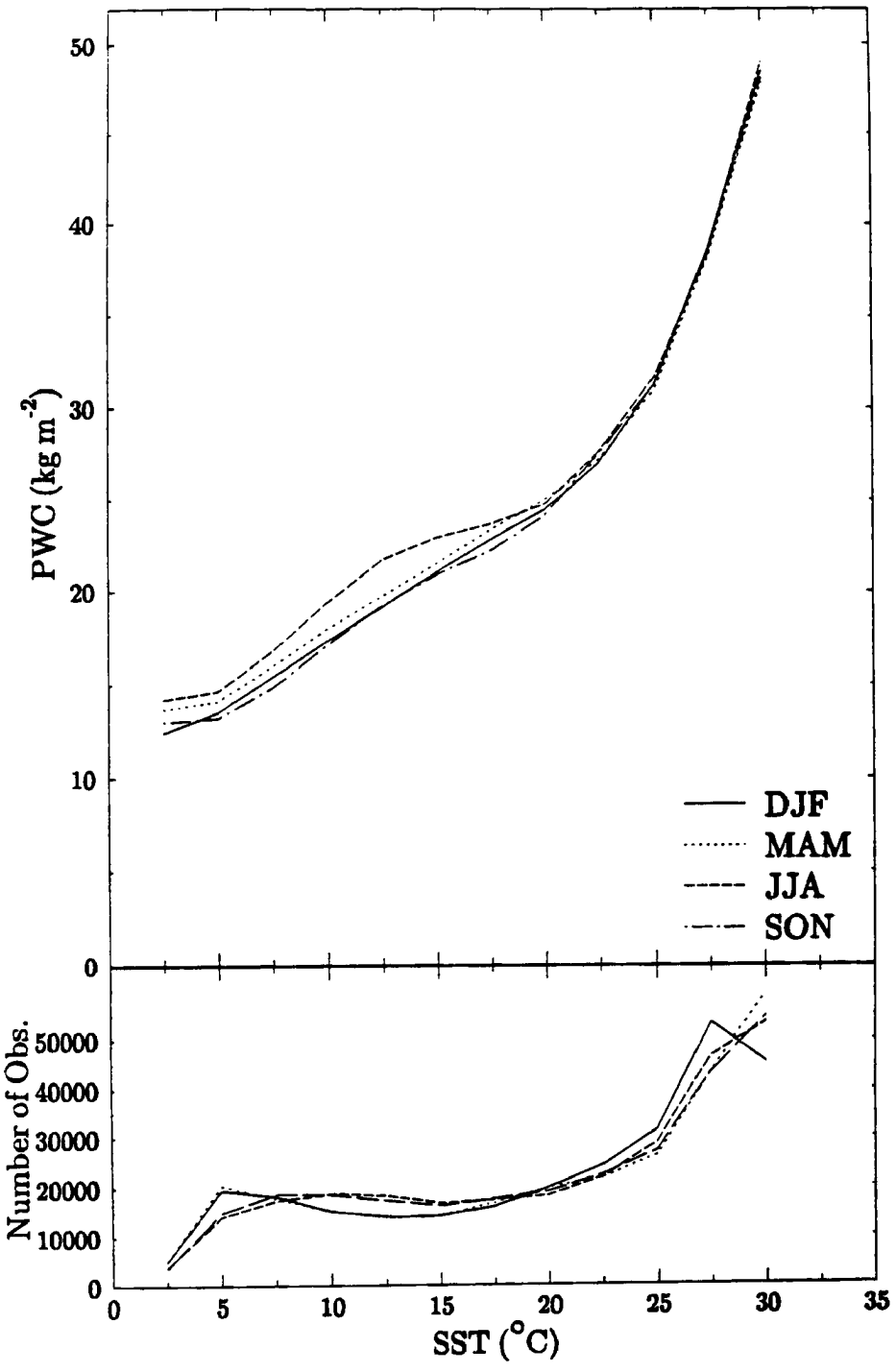

Figure 5.2: The relationship between PWC and SST over four seasons during the three year period from February 1988 to January 1991.

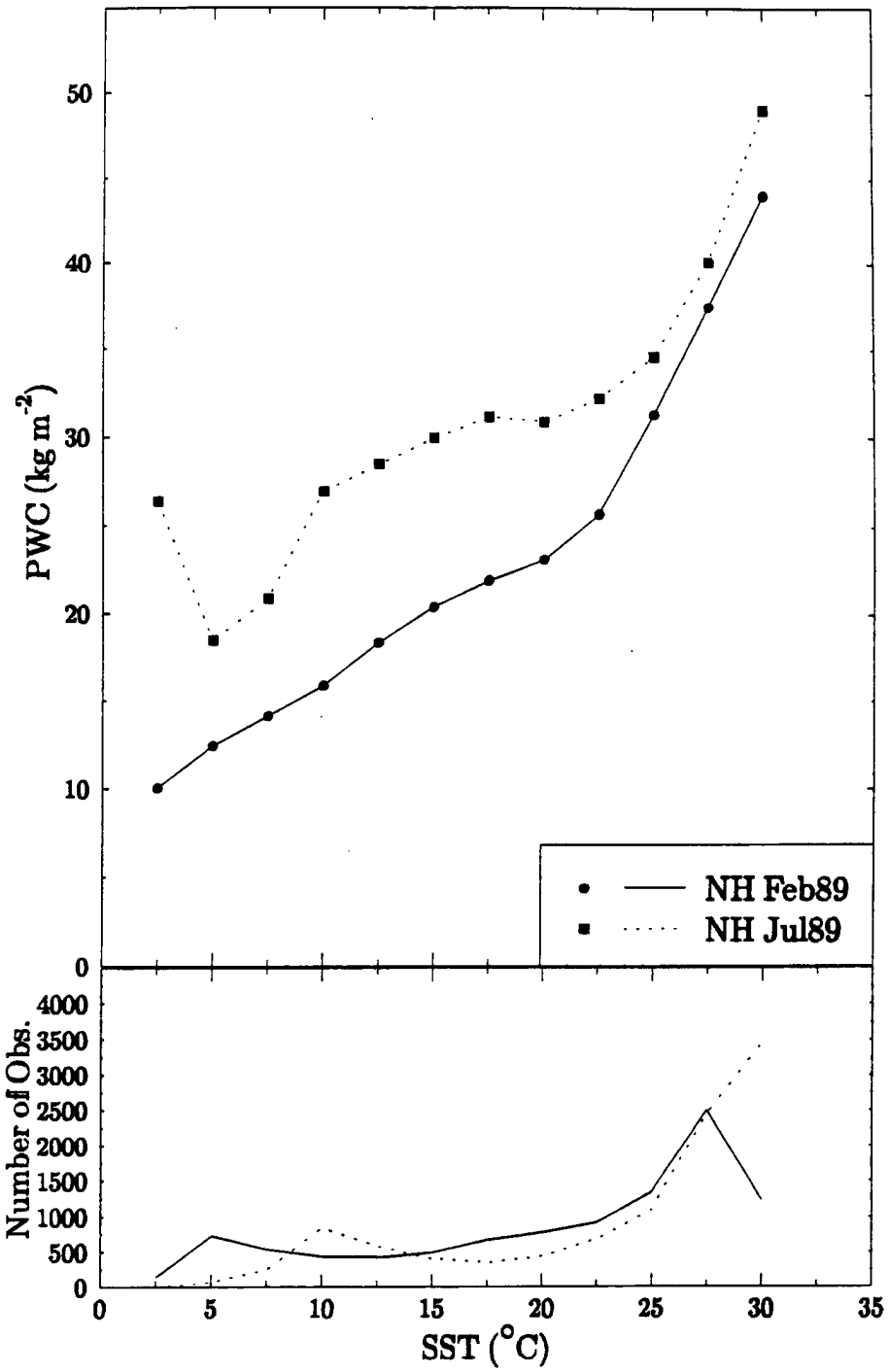

Figure 5.3: The relationship between PWC and SST for the northern hemisphere for February and July 1989.

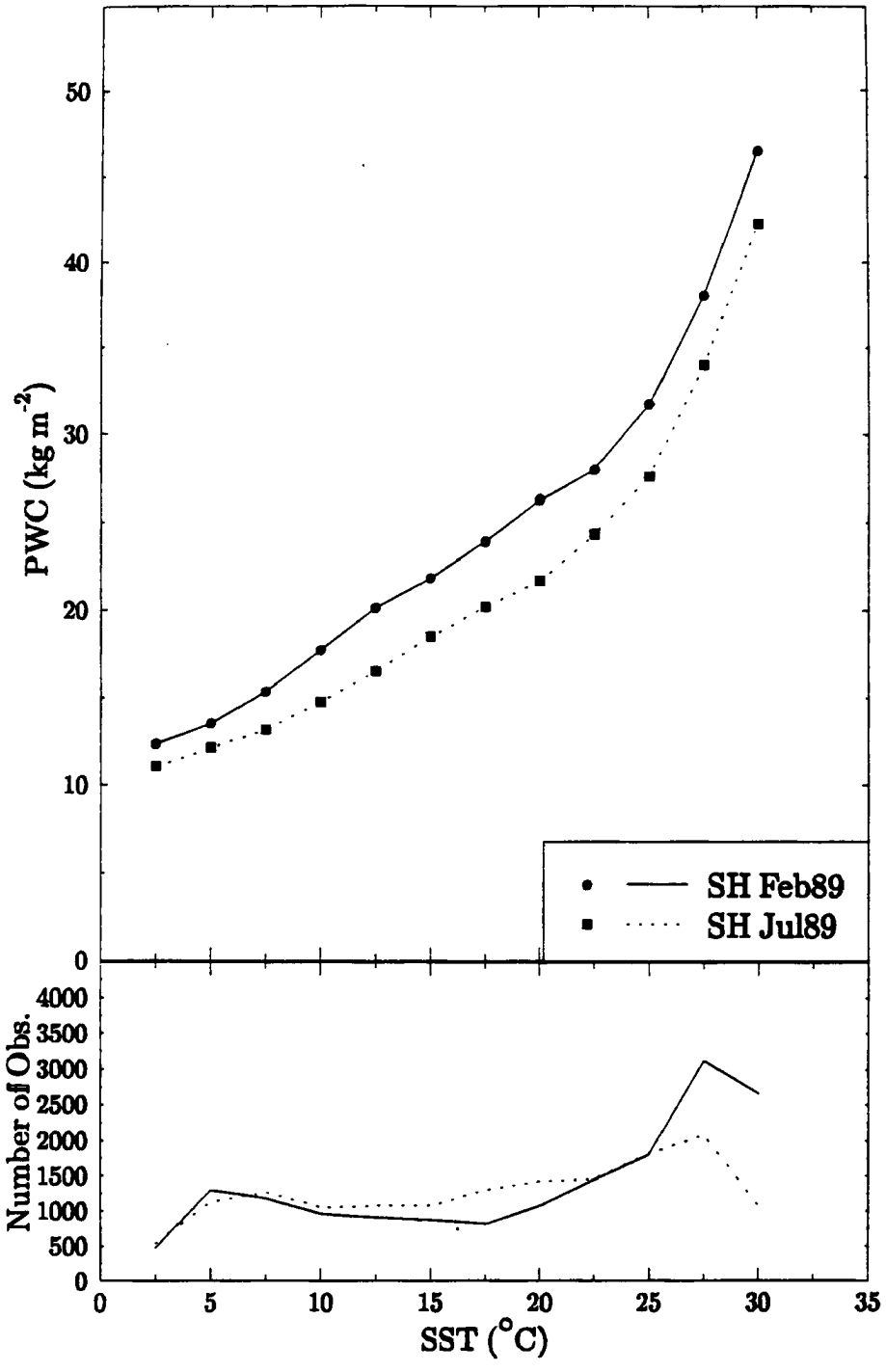

Figure 5.4: The relationship between PWC and SST for the southern hemisphere for February and July 1989.

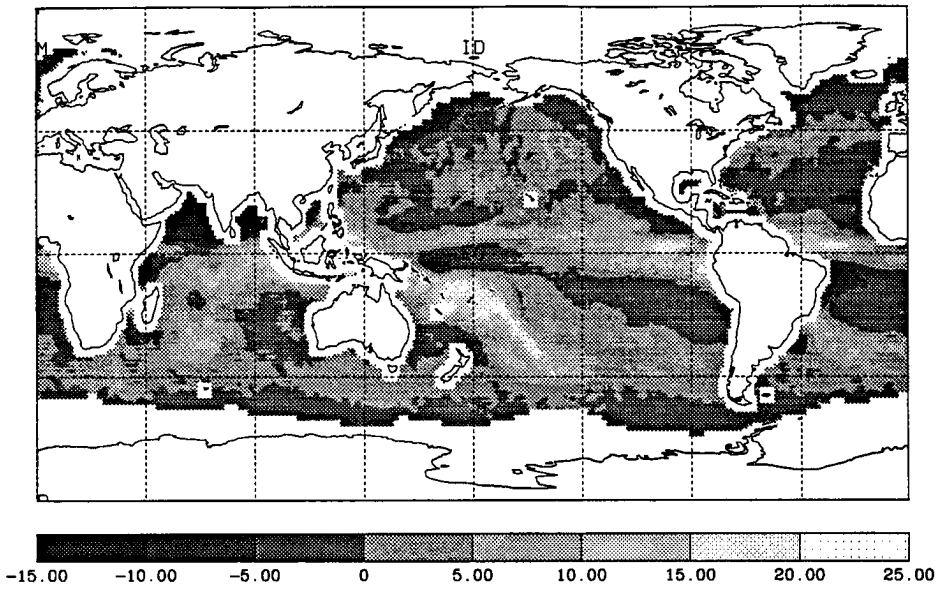

Figure 5.5: The difference (in kg m^{-2}) between the February 1989 monthly mean PWC and the predicted PWC using February SST means along with an exponential fit to Figure 5.1 (PWC(mm)-PWC(fit)). Positive regions indicate regions of PWC convergence while negative regions indicate PWC divergence.

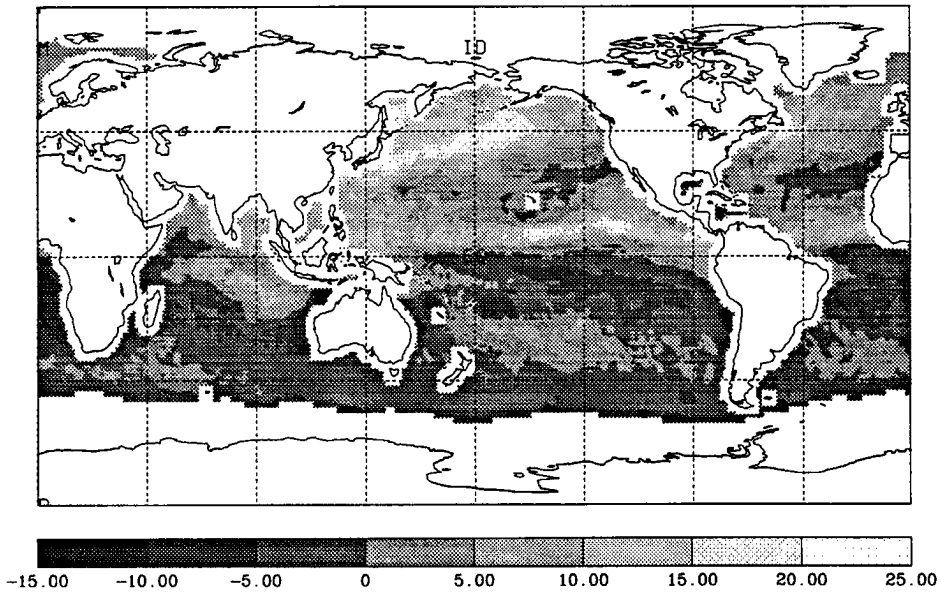

Figure 5.6: Same as Figure 5.5 except for July 1989.

divergence. Positive values in the northern Pacific in July 1989 are as large as 25 kg m^{-2} which indicates significant water vapor convergence in this region, while February 1989 shows water vapor divergence in the northern Pacific. This large region of water vapor convergence corresponds quite well with the results in Greenwald and Stephens (1991) and Greenwald *et al.* (1992). Greenwald and Stephens (1991) found a large region of shortwave cloud forcing which produced net radiation budgets of less than -100 W m^{-2} in the northern Pacific during the boreal summer. Little is known about the cloud types in this region; however, persistent highly reflective clouds in this region was attributed for the large negative radiative forcing. Greenwald *et al.* (1992) showed a broad region of significantly high amounts of cloud liquid water associated with these clouds in August 1987. The results of this study show a corresponding broad region of water vapor convergence in this region during the boreal summer which presumeably provides water for cloud development.

Other regions in Figures 5.5 and 5.6 show less dramatic changes in the seasonal relationship between PWC and SST. Generally, these maps show convergence regions in the summer hemispheres with the exception of the subtropical high regions. The Intertropical Convergence Zone (ITCZ) shows convergence during both the winter and summer; however, the convergence line shows the highest positive differences near 10N in the boreal summer and near the equator during the boreal winter. This shift correlates well with the observed seasonal movement of the ITCZ. The South Pacific Convective Zone (SPCZ) shows a broad region of convergence in February 1989 near the International Date line with positive values near 25 kg m^{-2}. Increased convection in the SPCZ generally occurs during the boreal winter, and these observations indicate significant water vapor convergence in this region. The broad regions of subsidence in the subtropical high regions of the eastern Pacific and Atlantic show greater divergence during the winter. Both the amplitude and the spatial area of the divergence is larger during the winter in the subtropics because the descending branch of the Hadley cell is strongest in the winter hemisphere, therefore providing greater subsident drying in the subtropics and greater transport of water vapor to the tropics.

The global relationship between PWC and SST can also be illustrated by considering the difference between a seasonal average of each field during an El Niño year and an average year. Figures 5.7 and 5.8 show the difference between the El Niño year of 1987 and the average year of 1989 during the boreal fall season for both the PWC and SST data. Warmer than average SST temperatures during El Niño are evident in the central and eastern Pacific, and the magnitude of the change is near 2.0°C which is a comparable in magnitude to the SST variations given in Rasmusson and Carpenter (1982). The western Pacific and the SPCZ shows cooler than average SST during the El Niño; however, the magnitude of that change is smaller. This result is consistent with past work which has shown smaller amplitude changes in the western Pacific. The PWC field shows large negative changes in the central and eastern Pacific especially near the ITCZ and SPCZ since the ITCZ tends to move farther south and the SPCZ moves northeast during a typical El Niño. The PWC field reflects the movement of convection in these regions during this El Niño.

5.2 THE ANNUAL CYCLE

Monitoring the annual cycle of water vapor and its interannual variability plays a key role in understanding the general circulation. The interannual changes in the global distribution of water vapor can quite possibly indicate large scale phenomena such as El Niño where the role the hydrologic cycle has in enhancing convection in the central and eastern Pacific is certainly important. This section will first investigate the global and hemispheric interannual and seasonal variability of PWC derived from Tjemkes' retrieval method and its relationship with Reynolds' SST by analyzing a three year time period. Following the PWC/SST analysis, a comparison between the five retrieval methods over a one year period will be made to investigate their similarities and differences.

5.2.1 Global and Hemispheric Analysis

Global and hemispheric averages of PWC and SST for each month from February 1988 to January 1991 were calculated and compared to the results found in Stephens (1990).

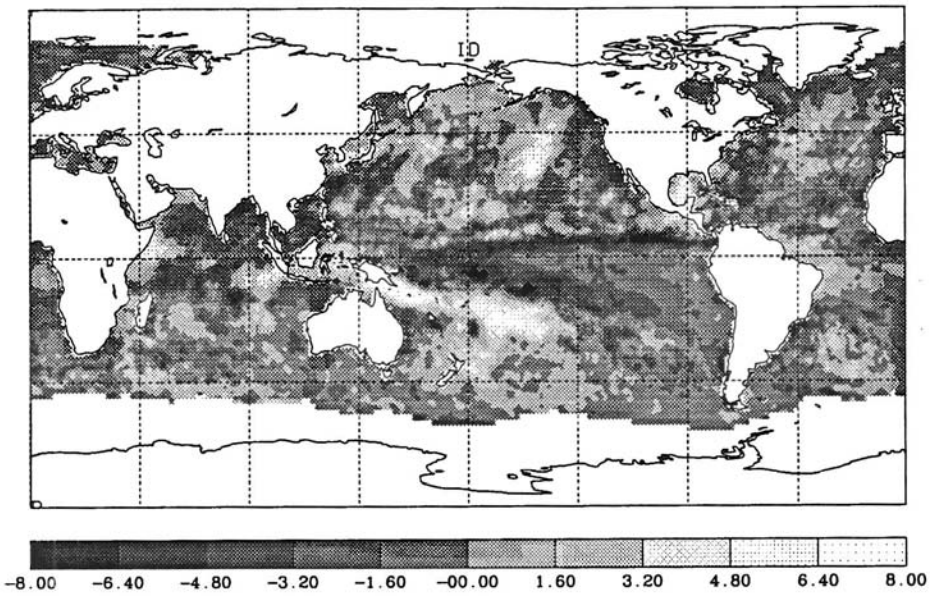

Figure 5.7: PWC difference (in kg m^{-2}) between SON 1989 and SON 1987. Positive regions indicate larger PWC values in 1989.

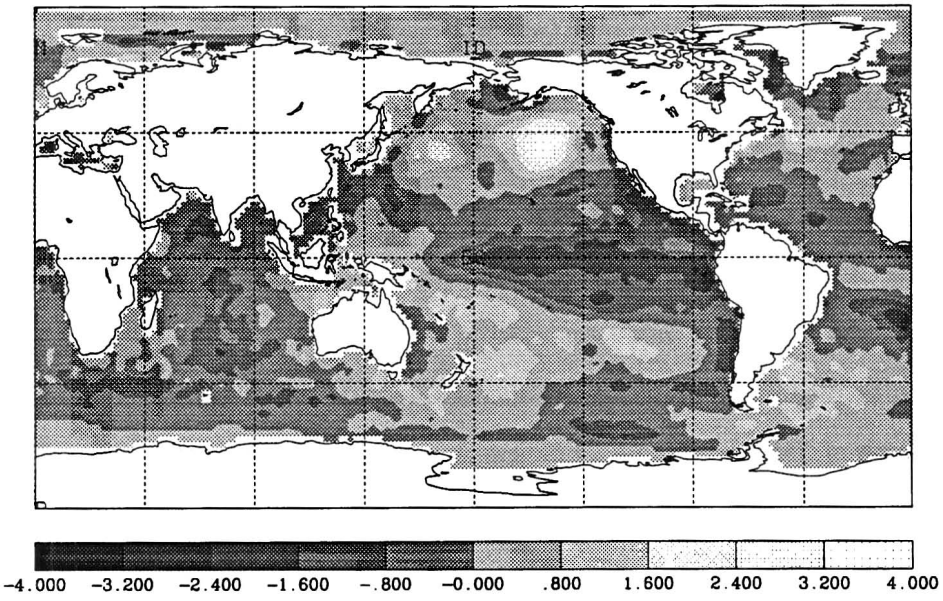

Figure 5.8: SST difference in Celsius between SON 1989 and SON 1987. Positive values indicate larger SST values in 1989.

Global and hemispheric averages were area weighted in each latitude band by using $\sin\phi_2$-$\sin\phi_1$ where ϕ_1 and ϕ_2 define the boundaries of a latitude belt. The percentage of land mass within a 1.0 degree latitude band was weighted for both the global and hemispheric averages by calculating the percentage of oceanic surface area for that latitude band to the total global or hemispheric oceanic surface area.

Figure 5.9 displays a time series of the hemispheric and globally averaged PWC and SSTs from Tjemkes' method for a 3 year period. The correlation between SST and PWC in the hemispheric averages is quite good. The amplitude of the annual oscillation of SST and PWC is slightly larger in the northern hemispheric means than in the southern hemispheric means. Since the sun supplies approximately the same amount of energy to both hemispheres during the annual cycle, the greater surface area of the southern hemisphere ocean reduces the SST fluctuation significantly. The magnitude of the SST and PWC reach higher values in the northern hemisphere for also the same reasons.

Global averages in Figure 5.9 show good agreement between the changes in PWC and SST during the last six months of each year. The globally averaged SST shows two maxima during each year corresponding to the maximum southern and northern hemisphere SSTs in April and August respectively. The SST results deviate from the results presented in Stephens (1990) and Shea *et al.* (1990). Stephens (1990) using the NMC blended satellite and *in situ* data set showed the global mean SST was dominated by the southern hemispheric SST mean. On the other hand, Shea *et al.* (1990) showed using the COADS that the northern hemispheric SST mean dominated the global average; therefore, the maximum value occurred in August. Shea *et al.* (1990) argued that the northern hemisphere dominates the average because there are larger annual changes in SSTs north of 25N than south of 25S, and more importantly, the average SST north of 25N is greater than south of 25S almost every month except during February and March. The current results show a combination of these two effects with the higher of the two maxima occurring during March when the larger oceanic basin of the southern hemisphere dominates the global average after its peak heating. The boreal summer peak shows the effect the northern hemisphere ocean has on the global average due to significant heating in the higher latitudes.

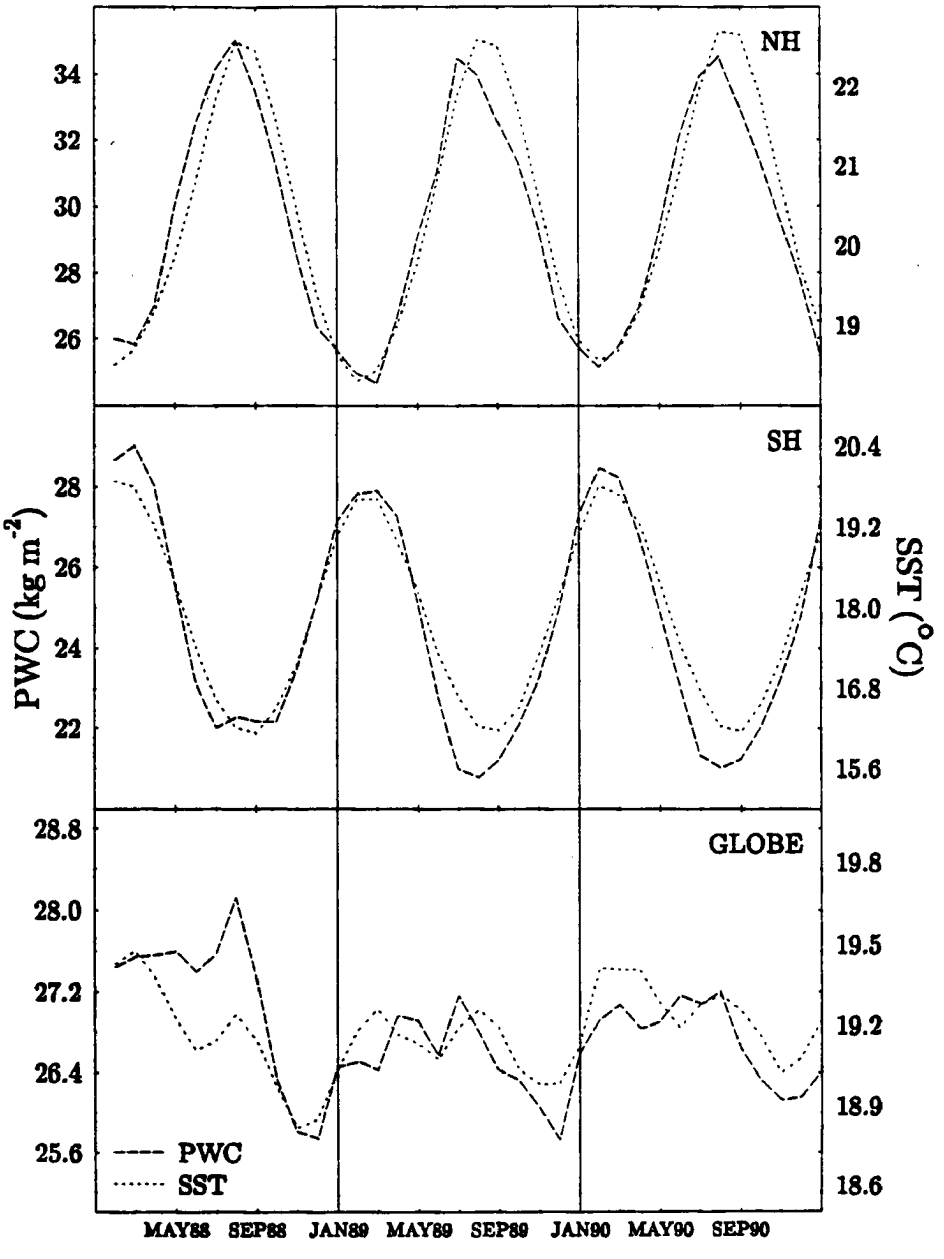

Figure 5.9: Time series of the hemispheric and globally averaged PWC and SST derived from the Tjemkes' retrieval scheme and Reynolds' data respectively from February 1988 through January 1991.

The global mean PWC time series has a less distinctive double annual maximum, but it does crudely correspond with the SST time series in 1989 and 1990. The global average PWC using $k_{h_2o} = 4.4516 \times 10^{-3} \mathrm{m^2 kg^{-1}}$ found for this 3 year period was 26.78 kg $\mathrm{m^{-2}}$. This result was slightly higher than the results of 25.3, 25.7 and 25.8 kg $\mathrm{m^{-2}}$ found in Rosen *et al.* (1979), Piexoto and Oort (1983) and Stephens (1990) respectively. Results from using $k_{h_2o} = 3.937 \times 10^{-3}$ $\mathrm{m^2 kg^{-1}}$ found the global mean to be 30.5 kg $\mathrm{m^{-2}}$ which is substantially higher than past results. Tjemkes' absorption coefficient can be seen as compromise which crudely attempts to incorporate liquid water contamination while Greenwald's absorption coefficient more accurately describes the PWC in clear sky conditions and in the tropics.

The results presented in Figure 5.9 show both similarities and differences from the results presented in Figure 8 in Stephens (1990). Both results show a one month lag of the SST mean to the PWC mean in the hemispheric averages. This result physically represents the atmosphere's ability to store and remove energy faster than the ocean; therefore, the temperature of the atmosphere reduces after the summer solstice faster than the ocean which results in a smaller capacity to hold water vapor. And finally, the SST global mean value in Stephens (1990) was found to be 15 to 16°C while the Reynolds' SST data in this study and the COADS data in Shea *et al.* (1990) found a global average from 19 to 19.5 °C respectively. While the corresponding annual cycles of PWC and SST were very similar between Stephens (1990) and the present results, it should be noted that the SST means shown in Stephens (1990) appear to be too low.

5.2.2 Global PWC Retrieval Method Comparison

A comparison of the five retrieval methods during 1989 was conducted in order to demonstrate similarities and differences between the retrieval methods. Time series of the globally averaged monthly mean PWC and zonal averages were constructed for this period. Figure 5.10 indicates a seasonal cycle in PWC for all five retrieval methods with the highest global values in PWC in July and the lowest values in January. Monthly variations in the global PWC show large variations particularly in March and June when the PWC drops 0.4 to 0.5 kg $\mathrm{m^{-2}}$ in all the retrieval methods. Generally, the PWC

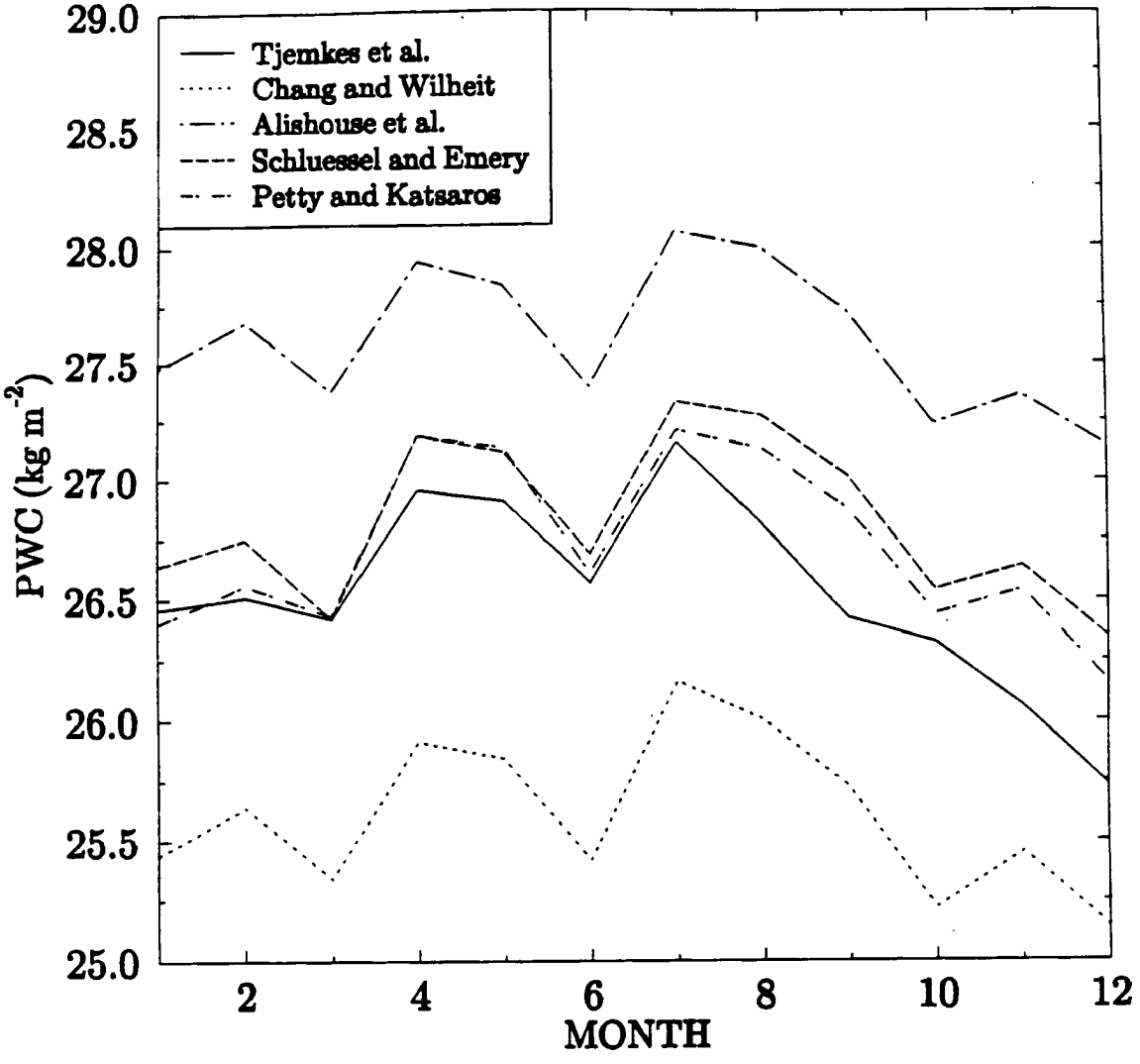

Figure 5.10: Time series of globally averaged PWC for 1989 for all five retrieval methods.

increases to its peak value in July for all retrieval methods and begins a steady decrease as the global average SST begins to cool following the summer solstice (see Figure 5.9). All five retrieval methods show basically the same monthly trends and differ primarily by a bias.

The annual PWC averages for 1989 were 27.60, 26.83, 26.72, 26.53 and 25.61 kg m^{-2} for the Alishouse, Schluessel and Emery, Petty and Katsaros, Tjemkes, and Chang and Wilheit respectively. These values were generally higher than the results from Rosen *et al.* (1979) and Piexoto and Oort (1983) which were discussed in the previous section. The most striking feature of the annual averages were the biases found between these retrieval methods. Alishouse showed the overall highest value while the Petty and Katsaros, Schluessel and Emery, and Tjemkes' retrievals gave similar values over the 12 month period. Chang and Wilheit's values were significantly less than the other retrievals; however, it compared the best to the results of Rosen *et al.* (1979), Piexoto and Oort (1983), and Stephens (1990). Since the first two studies consisted of observations over land, their global means were expected to be less than the oceanic averages. Stephens (1990) results were derived from the SMMR data set whose courser resolution and calibration difficulties made the data set suspect to significant errors.

Latitudinal averages were performed on the annually averaged data in order to investigate latitudinal differences between the five retrieval methods. The method averaged 5 degree latitude bands from the south pole to the north pole. Figure 5.11 shows a basic difference between the statistical and physical retrieval methods. The physical methods tend to produce more PWC in the upper latitudes. The slopes of the PWC distributions on either side of the equator for both the Tjemkes and Chang and Wilheit methods are nearly the same and both exceed the PWC values retrieved by the statistical methods. The tropics show good agreement between the all the methods except Chang and Wilheit's method which underestimates the PWC significantly.

An interesting feature found in the Tjemkes' retrieval is the larger PWC values found in the northern hemisphere north of 40 degrees. Cloud contamination could, in part, be responsible for these larger values; however, its persistence throughout the 1989 annual

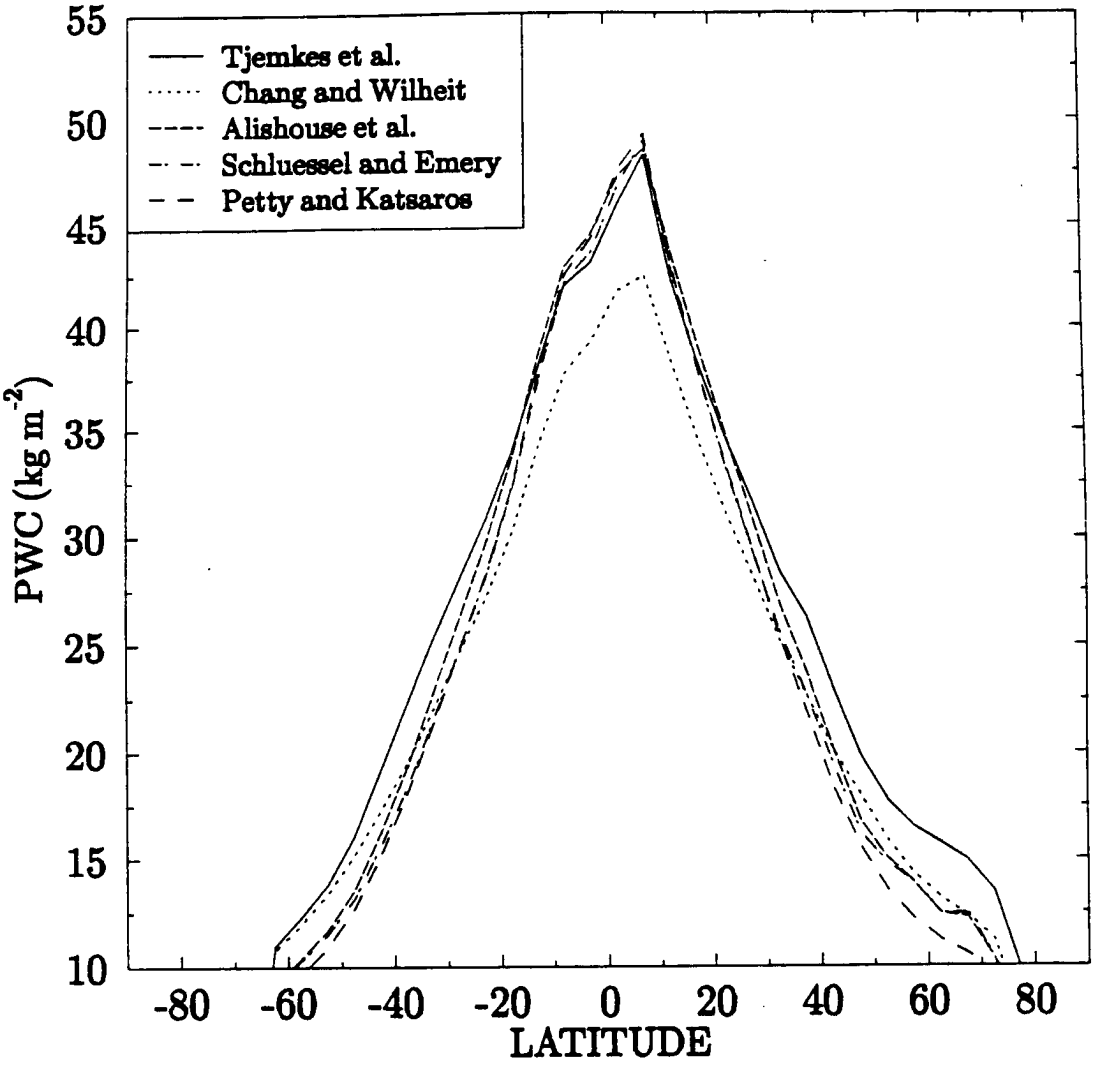

Figure 5.11: Zonal distribution of annually averaged PWC for 1989 for all five retrieval methods.

cycle along with no evidence of this feature in the southern hemisphere tends to refute this idea. The presence of cloud liquid water in this region is quite high (Greenwald *et al.*, 1992) due primarily to high moisture convergence within the strong baroclinic systems which exists in that region.

Variations in the zonally averaged, monthly averaged PWC give evidence of the seasonal movement of water vapor. Figure 5.12 displays the movement of water vapor for 4 months in 1989 where each month is in a different season. A seasonal cycle for PWC is evident between the northern and southern hemisphere. The summer hemispheres show greater PWC amounts over the oceanic regions. This result was expected since the summer hemispheres have warmer atmospheres and oceans, thus enabling them to hold greater amounts of water vapor.

A closer look at the monthly changes in PWC in the tropics indicates shifts in the convective patterns of the ITCZ. February shows a double peak in the PWC field in the tropics with one peak near 10S and a second peak at 2N. This feature is associated with a double ITCZ feature commonly seen in the cloud field in the tropical Pacific (Saha (1973) and Kornfield and Hasler (1969)) during the late winter and early spring of the northern hemisphere. By May, the tropical water vapor has progressed northward where a maximum value occurs near 8N. Also, the PWC maximum in the tropics has increased nearly 5 kg m^{-2} from February to May. August shows the same peak, however, the higher latitudes show a significant increase in the PWC. By November, the water vapor field shows the same maximum peak, and the water vapor field looks strikingly similar to the May average except for generally drier values in the equatorial regions.

5.3 RETRIEVAL COMPARISON OF PWC MONTHLY MEANS AND DAILY VARIATIONS

Monthly mean and standard deviations of 1 × 1 gridded PWC were investigated over the entire globe for all five retrieval methods in order to compare similarities and differences between the five retrieval methods. Figures 5.13 and 5.14 give the global PWC distribution and daily standard deviation from the monthly mean for the Petty and Katsaros retrieval method. The southern monsoon is at its strongest during this period and is evident by

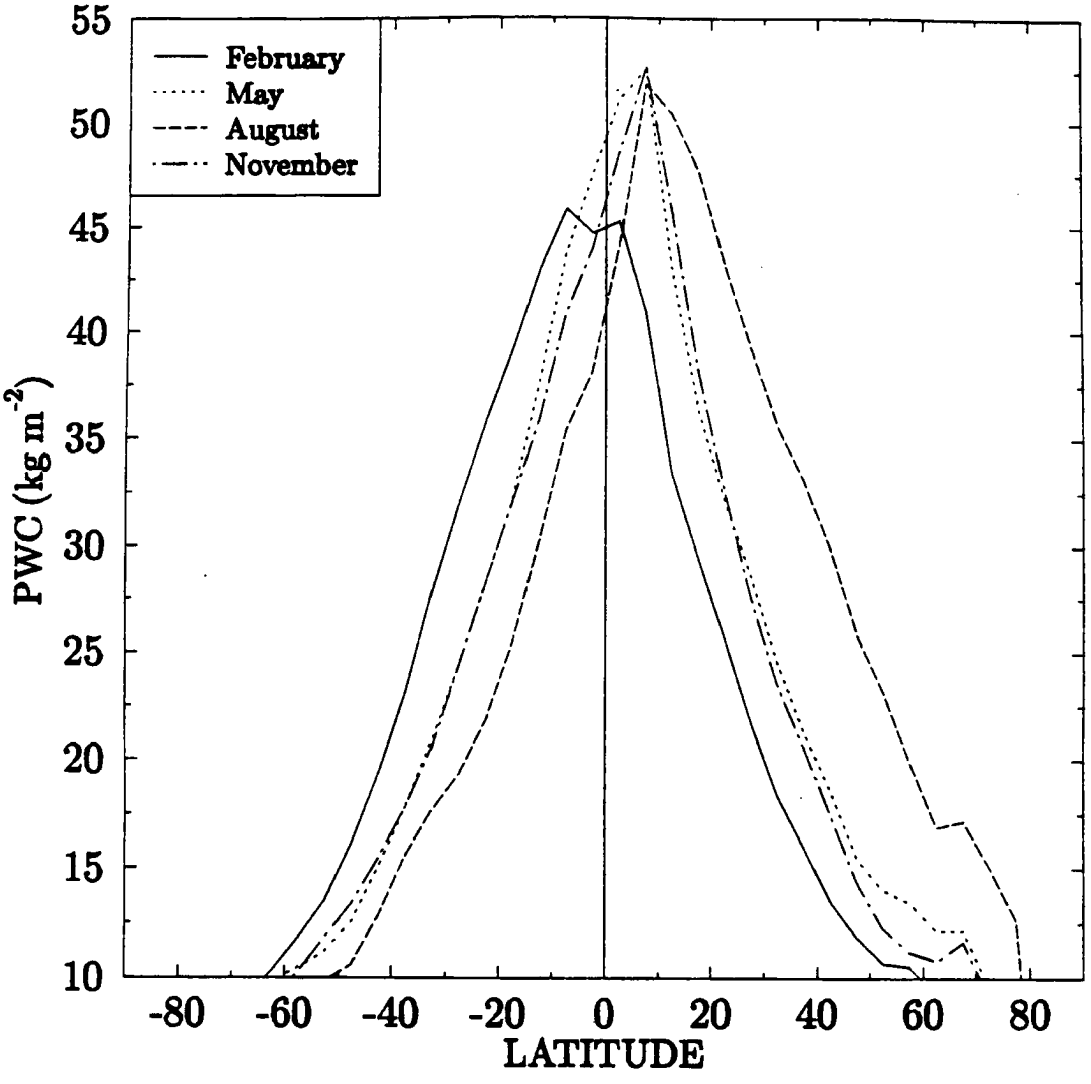

Figure 5.12: Zonal distribution of monthly average PWC for 1989 of four months from four different seasons. These results are from Schluessel and Emery (1990) and are representative of all five retrieval methods.

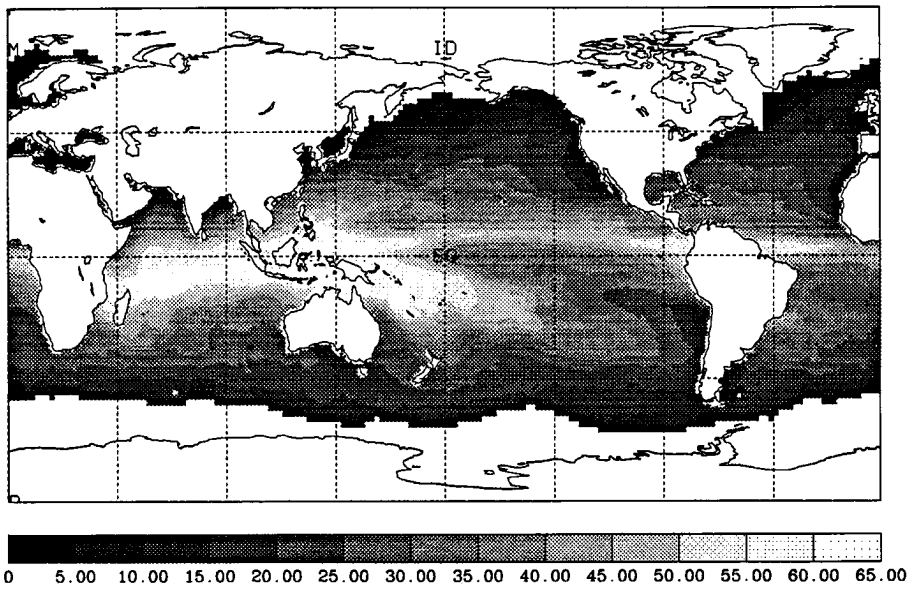

Figure 5.13: Monthly mean precipitable water (kg m^{-2}) for January 1989 using the statistical retrieval of Petty and Katsaros (1990).

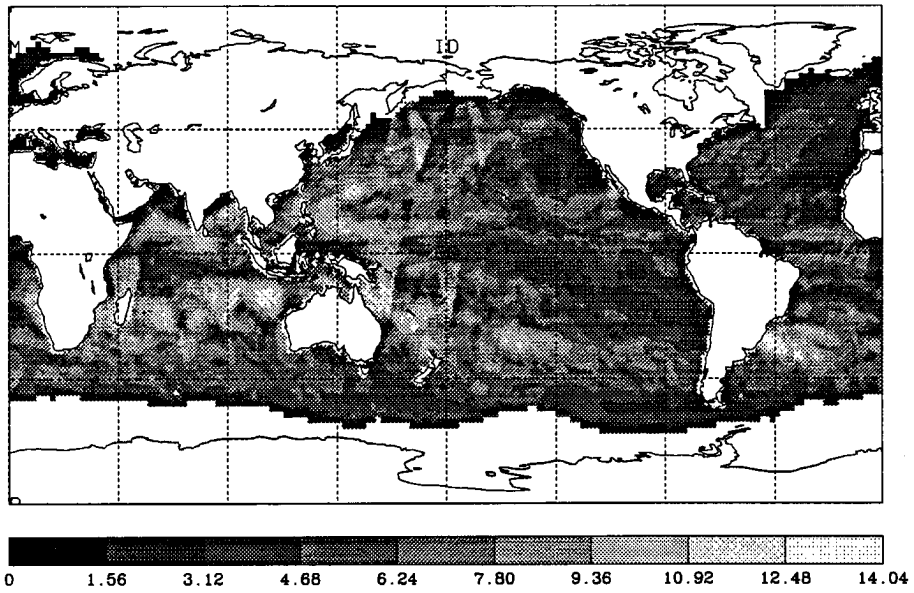

Figure 5.14: Standard deviation of precipitable water (kg m^{-2}) for January 1989 using the statistical retrieval of Petty and Katsaros (1990).

the PWC values greater than 52 kg m^{-2} off the northern coast of Australia and in regions south of the equator in the Indian Ocean. The SPCZ is shown to be quite broad and extends deep into the southeast Pacific. The ITCZ is marked by a thin strip of PWC exceeding the 50 kg m^{-2} circling the globe. Subtropical high regions off the west coasts of the North and South America show dry regions where subsidence and cold SSTs force low PWC values below 20 kg m^{-2}. The standard deviation map in Figure 5.13 shows greater variability in the midlatitudes, in particular, in the storm track regions of the northern hemisphere where cyclogenesis is strongest in the winter. The southern hemisphere also shows significant PWC variability in the midlatitudes where storms persist year round. Small temporal changes in PWC can be seen in the subtropical high regions where storm development has been suppressed from the subsiding air. A broad region along the coast of Europe and northern Africa shows low PWC variability.

Figures 5.15 and 5.16 give the results from the Alishouse retrieval method. The monthly mean structure of the PWC is very similar to Petty and Katsaros; however, the standard deviation field is significantly flatter in the tropical regions of the west and central Pacific. The flattened deviation field of Alishouse is most likely due to the nature of his retrieval method. It was discussed in Chapter 3 that the Alishouse method promotes a water vapor distribution and temporal change which resembles climatology. Evidence of that fact is found in deviation field particularly in the tropics.

Figures 5.17 and 5.18 give the results from the Schluessel and Emery retrieval method. Again the monthly mean data is very similar to those of the previously discussed retrievals; however, the standard deviation field shows far greater daily variability in the PWC field than the previously discussed retrievals. The largest differences occur in the typical convection zones of the western Pacific and storm track regions of the northern hemisphere. This result exemplifies the problems clouds can create in certain retrieval methods. Schluessel and Emery (1990) state that cloud contamination could be a significant problem in their retrieval method and Figure 5.18 gives evidence to that fact.

Figures 5.19 and 5.20 give the results from the physical retrieval Tjemkes' method. Tjemkes' method gives finer structure in the monthly mean fields in comparison to the past

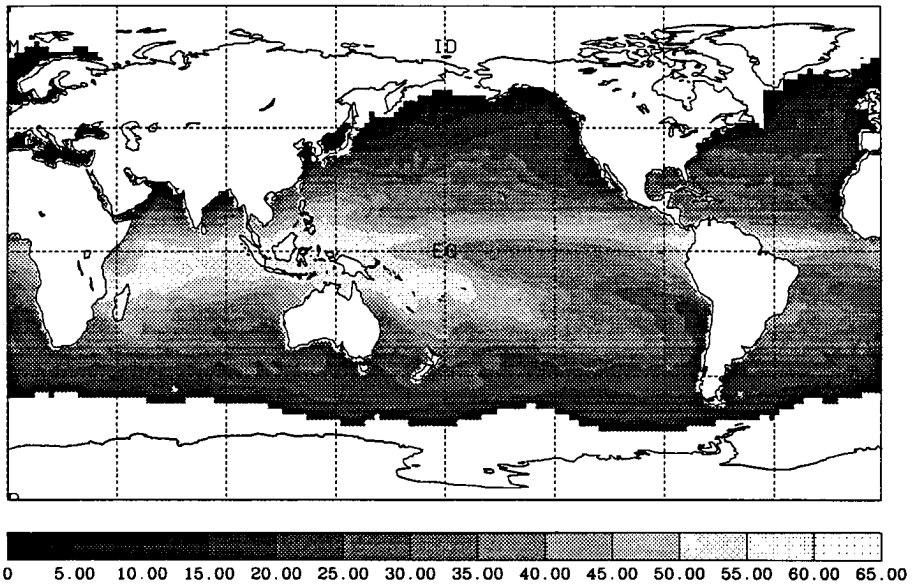

Figure 5.15: Same as Figure 5.13 except using the Alishouse *et al.* (1990) retrieval method.

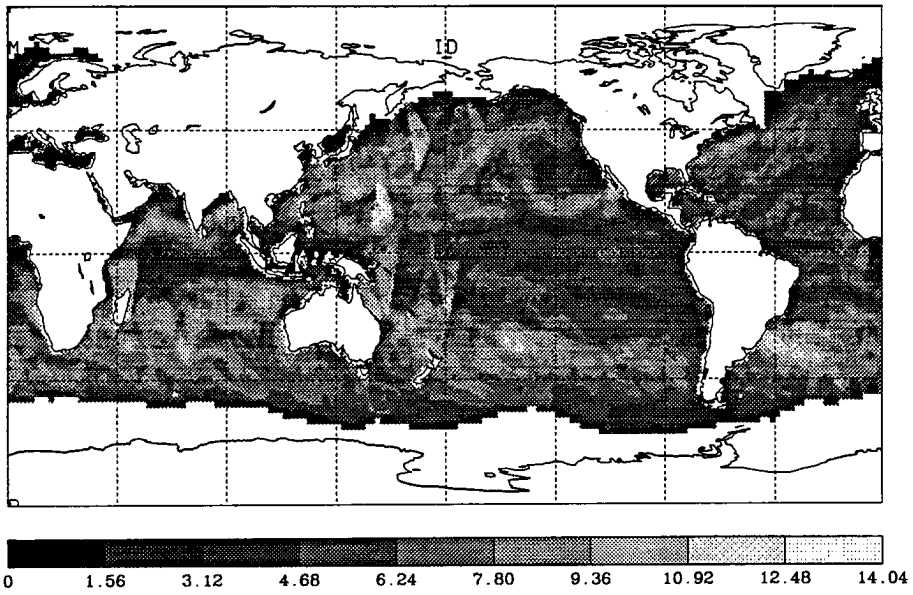

Figure 5.16: Same as Figure 5.14 except using the Alishouse *et al.* (1990) retrieval method.

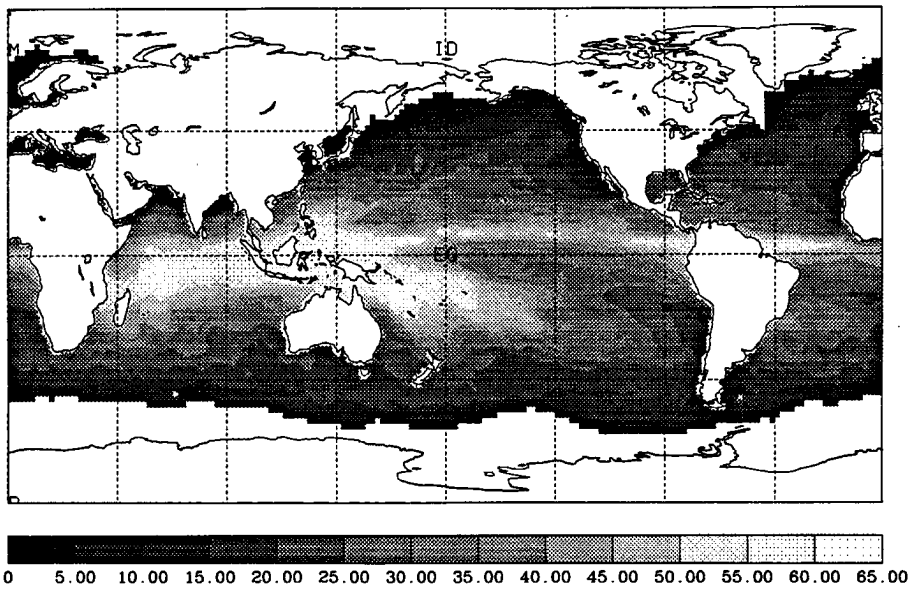

Figure 5.17: Same as Figure 5.13 except using the Schluessel and Emery (1990) retrieval method.

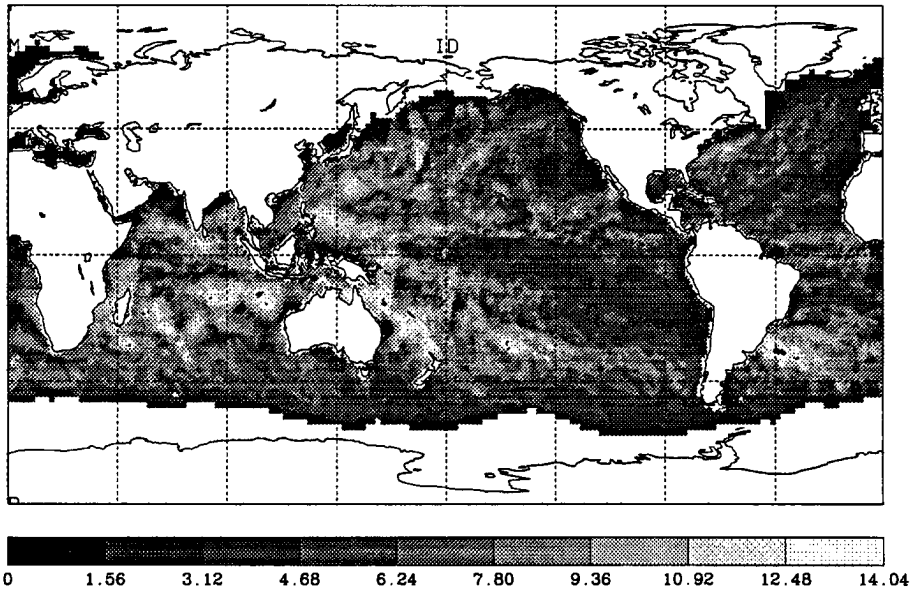

Figure 5.18: Same as Figure 5.14 except using the Schluessel and Emery (1990) retrieval method.

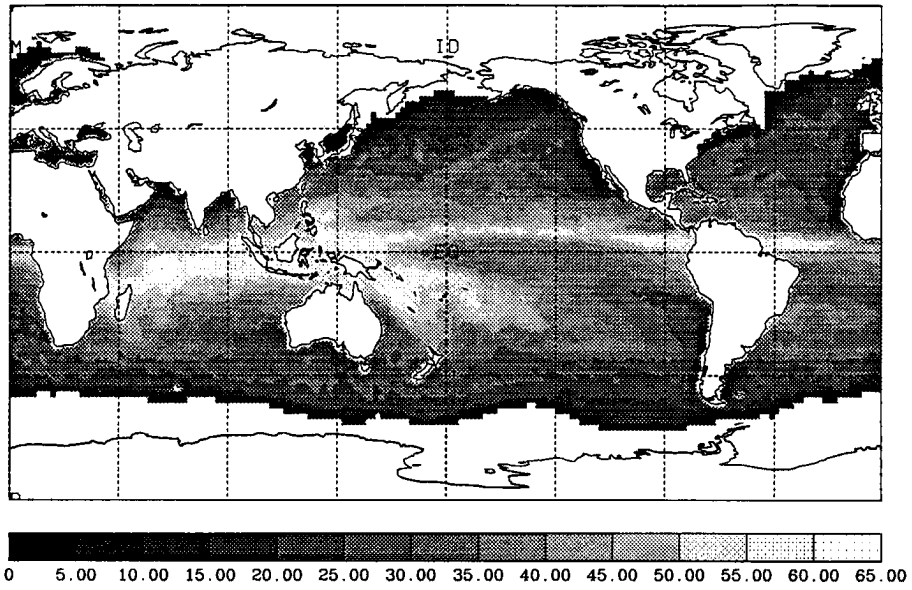

Figure 5.19: Same as Figure 5.13 except using the Tjemkes *et al.* (1991) retrieval method.

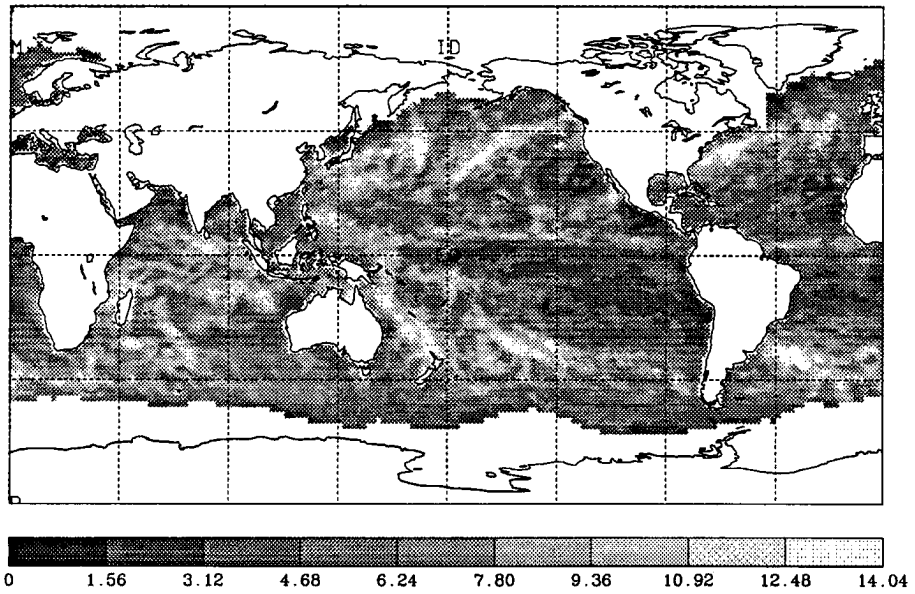

Figure 5.20: Same as Figure 5.14 except using the Tjemkes *et al.* (1991) retrieval method.

three retrieval methods which is evident in the midlatitude PWC fields. The PWC is larger in the higher latitudes for this method in comparison to the statistical methods which was expected from the results of the radiosonde comparison found in chapter 4. Temporal variability shows significant changes in the PWC field in the tropical cloud regions and storm track regions. Part of the variability is real where moisture convergence in cloudy air contributes to the variability while the other part may be artificial and associated with cloud contamination due to large cloud droplets and precipitation.

Figure 5.21 and 5.22 give the results from Chang and Wilheit's retrieval method. The monthly mean fields are much smoother than Tjemkes' retrieval and the PWC is underestimated in the tropical regions. The standard deviation field shows small daily variability in the tropics where saturation effects of the 22.235 GHz channel are the greatest (Tjemkes *et al.*, 1991).

The zonally averaged daily PWC deviations were calculated to more easily compare the daily variability of all five retrieval methods. Figures 5.23a and 5.23b show the deviations for January and July of 1989. Clearly evident is the large deviations in Tjemkes' method with maxima at approximately 40N, 40S and 8N for both time periods. These deviations are a reflection of this retrieval methods greater variability in persistent cloud regions. The tropical regions show significant differences between the methods. Chang and Wilheit and Alishouse show the least amount of temporal variability which is consistent with results from the BASICS data discussed in Chapter 4. July data shows opposite changes in the deviation field between Tjemkes' and Schluessel and Emery's methods and the rest of the retrievals with maxima occurring at 8N for the prior methods and minima occurring for the latter methods. Alishouse's method shows the same magnitude of variability as Chang and Wilheit's method in the tropics. Since Chang and Wilheit's method is known to have saturation effects in the tropics, this result further demonstates the problem the Alishouse method has with representing the daily variability of PWC in the tropics. Considering that the ITCZ typically has significant cloud and water vapor variability in both time and in space, a minimum PWC daily deviation in the ITCZ shows the limitation of statistical methods and Chang and Wilheit's physical retrieval.

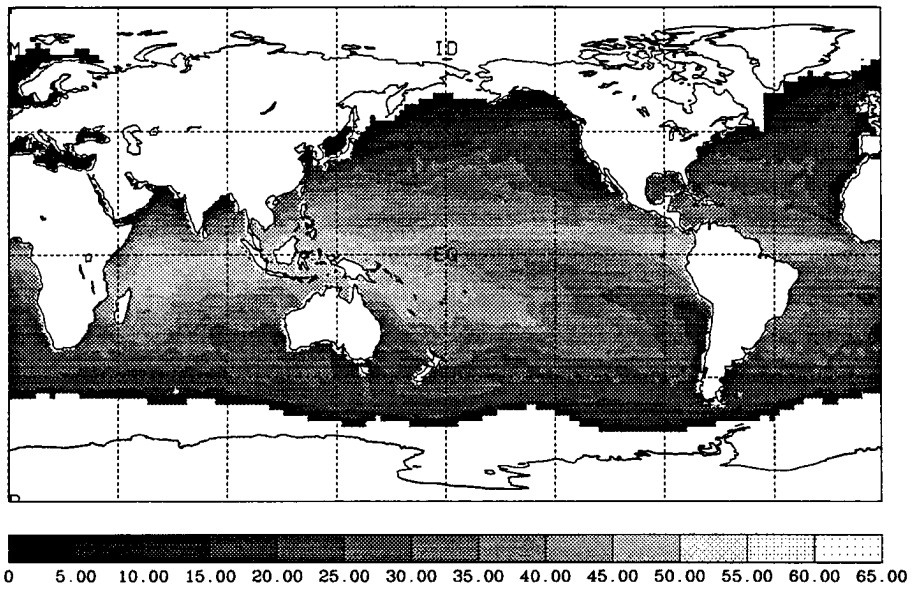

Figure 5.21: Same as Figure 5.21 except using the Chang and Wilheit (1979) retrieval method.

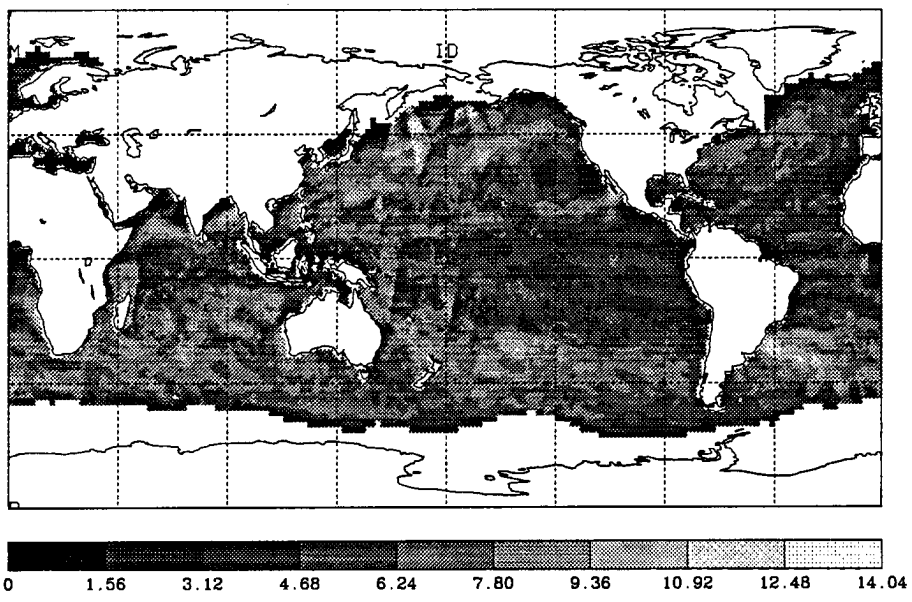

Figure 5.22: Same as Figure 5.22 except using the Chang and Wilheit (1979) retrieval method.

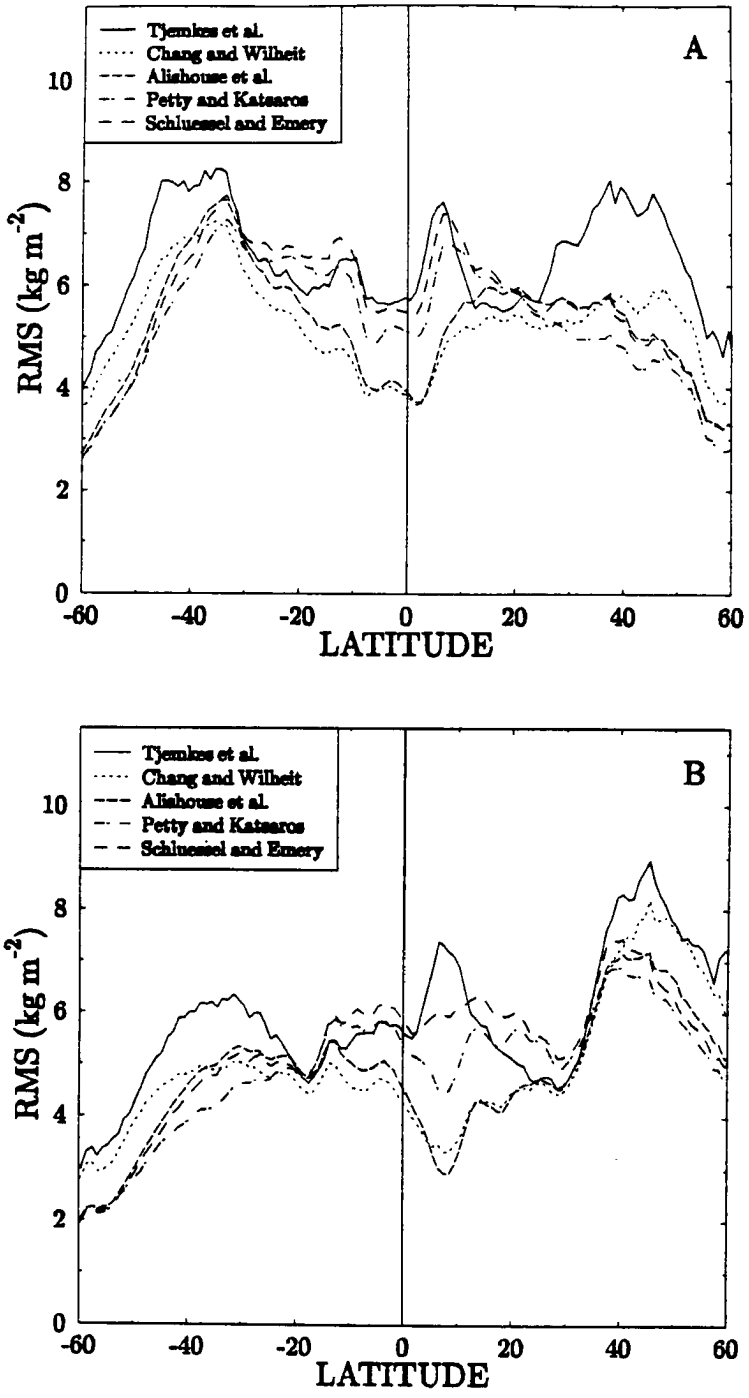

Figure 5.23: Zonal distribution of the deviation of daily PWC values from monthly mean PWC. (A) is for January 1989 and (B) is for July 1989.

Chapter 6

ANALYSIS OF TROPICAL PACIFIC DISTURBANCES USING SSM/I DERIVED PWC

This chapter examines the association of water vapor with the 1987 El Niño/1988 La Niña and westerly wind bursts during the fall of 1987. Both of these features were identified using the OLR, ECMWF zonal wind, and SST data discussed in Chapter 2 and analyzed using the PWC data retrieved from SSM/I data using Tjemkes' retrieval method. Following a brief background discussion on the composite El Niño, time/longitude (hovmoller) diagrams are used to show the development of the ENSO events along with the evolution of the PWC field. The relationship between the PWC and SST is explored for different regions in the tropical Pacific during this time period in order to better understand the oceanic effect on the water vapor variability and distribution in the tropical atmosphere. Following the large scale tropical discussion, two westerly wind bursts during the fall of 1987 are examined. PWC analysis is used to show water vapor convergence in the convective regions of the westerly wind bursts.

6.1 TROPICAL PACIFIC CLIMATOLOGY FOR 1986-1989

A climatological summary of the tropics was briefly explored in order to develop a background setting from which higher frequency motions can be analyzed. This section begins by discussing the current knowledge of the El Niño phenomena including brief discussions of the evolution of the SST, surface wind and precipitation fields and further discusses on how they are thought to be related. Following this background discussion, hovmoller diagrams of several data sets centered at the equator are presented to show the evolution of the 1987 El Niño and 1988 La Niña. Also, a relationship between PWC and SST is explored for several regions in the tropical Pacific beginning in 1988 and

ending January 1991. Eastern and western Pacific regions are found to exhibit different relationships and evidence of significant changes in PWC in the tropical Pacific during the La Niña of 1988 is demonstrated.

6.1.1 The Composite El Niño

Rasmusson and Carpenter (1982) conducted a study which explored the similar characteristics of several El Niño events from the time period beginning in the early 1950's and ending in the late 1970's. Their study produced a composite El Niño for the 30 year period, and the following paragraphs describe the evolution of the composite El Niño which was a result of their findings.

The beginning stages of El Niño are marked by positive SST anomalies developing at the International Date Line and along the South American coast in November and December before the El Niño year. Easterly trade winds in the anomalously warm SST regions relax during this time which results in less upwelling of cold water along the South American coast and along the equator. Precipitation in the central equatorial Pacific begins to increase the November before the El Niño year.

The following February, the eastern Pacific begins to experience greater than normal precipitation. Warm SSTs along the equator prohibit the northward shift of the ITCZ in the spring of the El Niño year so enhanced precipitation stretches all along the equator from the central to eastern Pacific. During the summer of the El Niño year, the central Pacific receives its peak precipitation amounts in part due to the southward shift of the ITCZ and the northeasterly shift of the SPCZ. The western Pacific shows smaller amplitude changes in SST anomalies and precipitation during El Niño; however, a reduction in precipitation and slight cooling of the SSTs can be detected. Even regions outside of the tropical belt have also experienced unusual weather; for instance, Australia experienced one of its worst draughts during the 1982/83 El Niño.

The 1980s witnessed two El Niño events of similar character; however, their evolution differed significantly from those events analyzed in Rasmusson and Carpenter (1982). The main difference centered around the initial stage of the events. The warm events of the 1980s primarily had only an eastward propagating positive SST anomaly from the western

Pacific with virtually no significant positive SST anomalies along the South American coast. The 1982/83 El Niño started several months earlier than the composite El Niño, was stronger than any of the composite El Niños analyzed in Rasmusson and Carpenter (1982), and lasted several months longer than the composite El Niño. The 1987 El Niño was similar to that of the 1982/83 El Niño except that its length in time was more similar to the composite El Niños and the amplitude of the anomaly fields were much smaller.

An important aspect of El Niño recently discussed in both Rasmusson and Carpenter (1982) and Yasunari (1987) is the misconception that the El Niño can only be explained as a standing oscillation. Their work demonstrated that convection was not a result of a stationary heat source which shifted off and on, rather the convection propagated eastward from the western Pacific. This propagating element is different from an opposing theory that the Southern Oscillation, which is observed to be a standing oscillation, modulates the El Niño phenomena. This point is essential in relating higher frequency motions, such as westerly bursts, to the ENSO phenomenon.

6.1.2 The 1987 El Niño/1988 La Niña

A brief analysis has been performed to help give an overview of the ENSO events during 1987 and 1988. The analysis consists of the producing anomaly fields of the OLR, ECMWF 850 mb zonal wind, SST and PWC data. The OLR anomalies were constructed by removing the 15 year mean (1973-1988) OLR from monthly mean data. Likewise, the wind data used a 10 year mean, the SST data used a 6 year mean (1985-90), and the PWC used a $3\frac{1}{2}$ year mean to produce the monthly anomaly fields. These different long term means were the longest records available to produce the anomaly fields.

The OLR field was used to examine the anomalous change in deep convection over the tropical Pacific during the 1987 El Niño. Figure 6.1 is a hovmoller diagram of the OLR anomaly field at the equator for the period from 1986 through 1988. Negative anomalies less than -25 Wm^{-2} begin west of the International Date Line in September of 1986 and propagate eastward into the central and eastern Pacific by January of 1987. The most distinct feature of this hovmoller diagram is the large region of negative anomalies that develops in the central Pacific in the fall of 1986 and extends into the eastern Pacific in

the summer and fall of 1987. Negative anomalies indicate regions of OLR less than the climatological mean which indicates regions of anomalously deep convection. Negative anomalies show a peak of -60 W m^{-2} in January of 1987 just east of the Date Line and a broad negative anomaly region extends from the central to the eastern Pacific during the entire boreal spring of 1987. The eastern Pacific anomalies dissipate by the fall of 1987 and the negative anomalies in the central Pacific disappear by January 1988.

The western Pacific shows a smaller region of positive anomalies beginning in February of 1987 indicating less convection than normal. Anomalies in the western Pacific are smaller in magnitude to the large anomalies in the eastern and central Pacific. This result was expected since the change in convection is typically much greater in the eastern Pacific than in the western Pacific (Rasmusson and Carpenter, 1982).

The La Niña of 1988 is also evident by the large swing from negative to positive anomalies in the eastern Pacific at the beginning of 1988. A broad region of positive anomalies propagates westward beginning in January of 1988 and values as large as 25 W m^{-2} occur in the central Pacific by September 1988. The gradient of these anomalies became quite large during the fall of 1988 across the western Pacific as intense convection occurred over Indonesia and the eastern Indian Ocean. The intensification of the Walker cell during this strong La Niña event is evident from this analysis.

The 850 mb zonal wind field anomalies were investigated to give evidence of the reversal of the easterly trades during the El Niño of 1987. Figure 6.2 shows the zonal wind field anomalies at 850 mb from January 1986 through 1988. Westerly wind anomalies propagate from the western to the central Pacific in September of 1986 and reaches a maximum in the central Pacific in April of 1987. The beginning of the westerly anomalies in September of 1986 correspond very well to negative OLR anomalies in the central Pacific found in Figure 6.1. These westerly anomalies suggest a reversal in the Walker circulation during the El Niño event which is a result of the weakening of the easterly trades. Westerly anomalies remained for over a year in the central and eastern Pacific and subsided to zero beginning in the eastern Pacific in November of 1987. The OLR anomalies in Figure 6.1 show a corresponding end to its negative anomalies in the central Pacific by January of

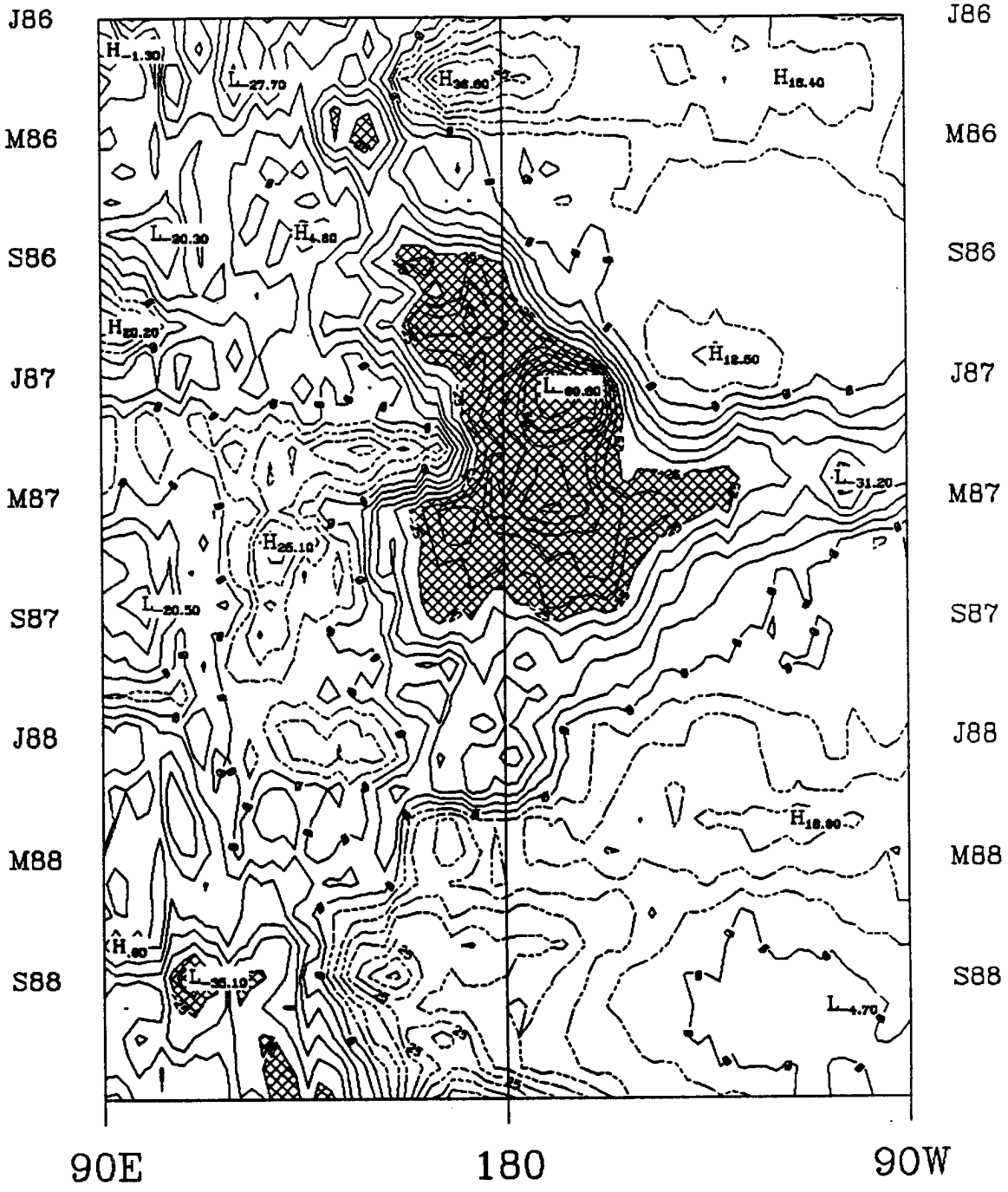

Figure 6.1: NOAA monthly mean OLR at the equator from January 1986 through 1988. Shaded region indicates OLR < -25 Wm^{-2}.

1988 as the tropical circulation changes to a strong easterly trade wind period. A strong negative wind anomaly develops in 1988 in association with the development of a strong La Niña event.

Time series of the sea surface temperatures were examined in the eastern and western Pacific. Figure 6.3 is a four year time series of the SST averaged over the eastern and western basins of the Pacific Ocean. The western basin shows both less interannual and intrannual variability over this period than the eastern basin. The El Niño of 1987 is clearly marked by the increased SST in the eastern basin while the La Niña of 1988 is displayed by the cold SSTs in the last 6 months of that year. Conversely, the western basin shows slight cooling in the summer and fall of 1987. However, the La Niña of 1988 shows no signal of warmer SSTs in the western basin.

While the SST time series can be useful in monitoring ENSO events, typically SST anomalies in the equatorial Pacific are used to identify ENSO events. Figure 6.4 shows the SST anomalies at the equator for this four year period in the Pacific. A six year mean for each month was used to remove the season variations from the anomaly field. A prominent feature in Figure 6.4 are the positive anomalies located in the central and eastern Pacific from May of 1986 through March 1988. Anomalously warm SSTs propagated from ~140E at the beginning of 1986 to the central Pacific by May 1986. These anomalously warm SSTs in the central Pacific precede the OLR and zonal wind anomalies shown in the previous figures by about 4 months. This time period, coincidently, is roughly the time required for an oceanic Kelvin wave from the western Pacific to propagate to the eastern Pacific (Cane, 1983). Peak anomalies reach 2.0°C in February 1987 while a corresponding weak negative anomaly region occurs in the western Pacific. The abrupt change from El Niño to La Niña is certainly evident during the first three months of 1988, and the ensuing summer and fall of 1988 shows large negative anomalies throughout the central and eastern Pacific with the peak anomaly reaching -3.0°C. The western Pacific, on the other hand, shows only weak positive anomalies during the La Niña which are similar in amplitude to the negative anomalies found during the El Niño. These results support the findings of Rasmusson and Carpenter (1982) which found the western Pacific to have less amplitude in the SST over several ENSO events.

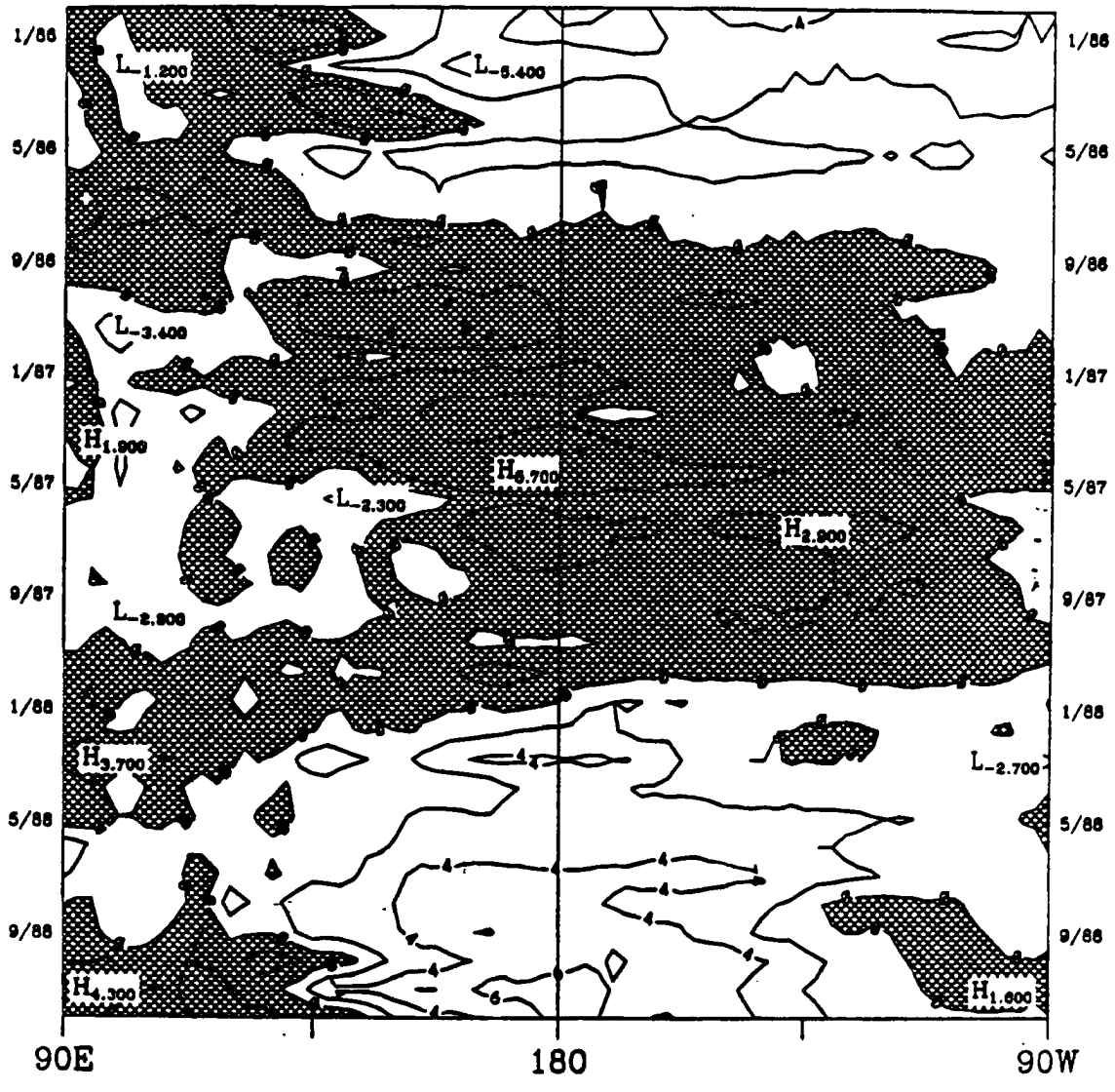

Figure 6.2: ECMWF 850 mb wind anomalies at the equator from January 1986 through 1988. (from J. Knaff, personal communication)

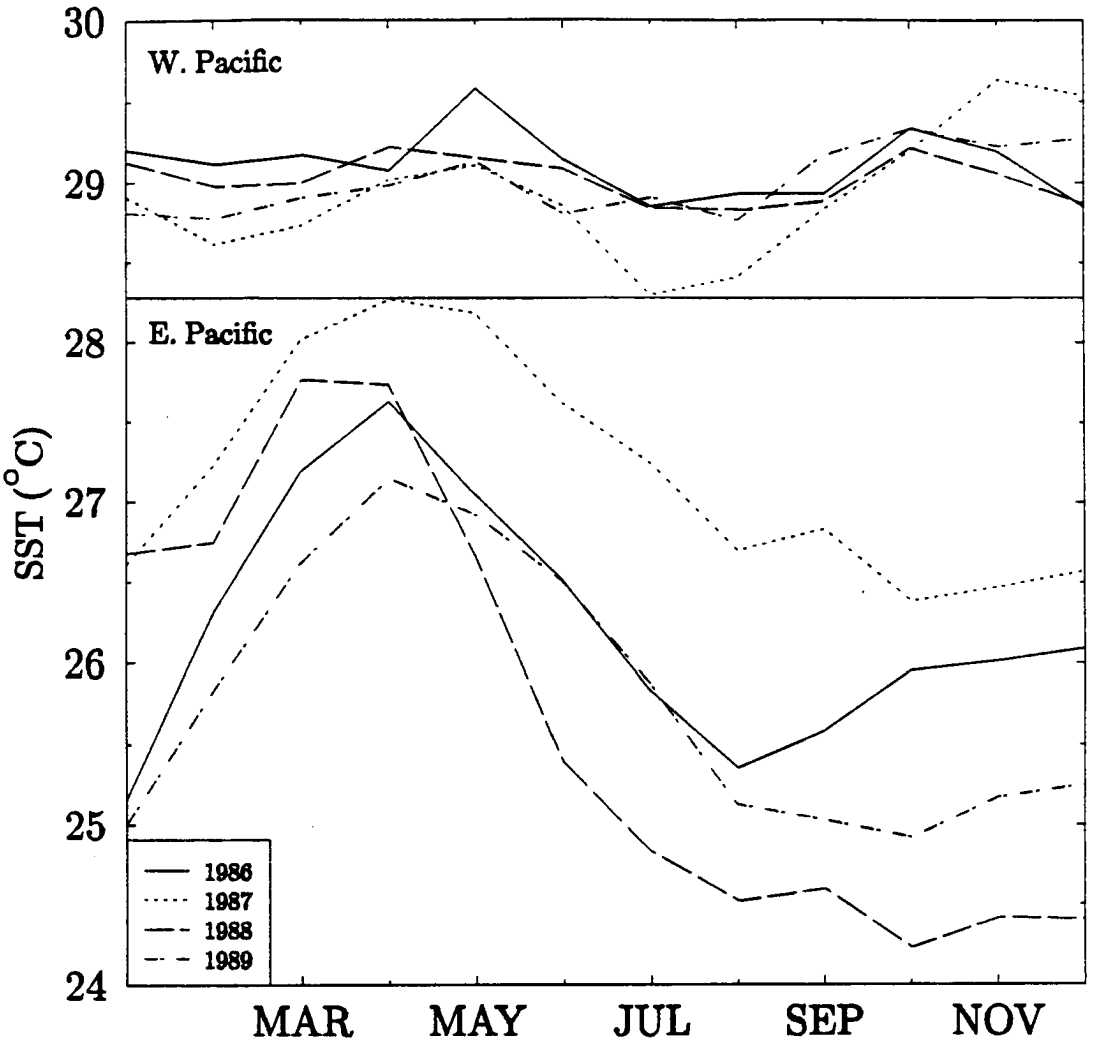

Figure 6.3: Time series of monthly mean SST temperatures averaged over two Pacific regions between 10N and 10S. Eastern basin is defined as 180 to 90W and the western basin is defined as 90E to 180.

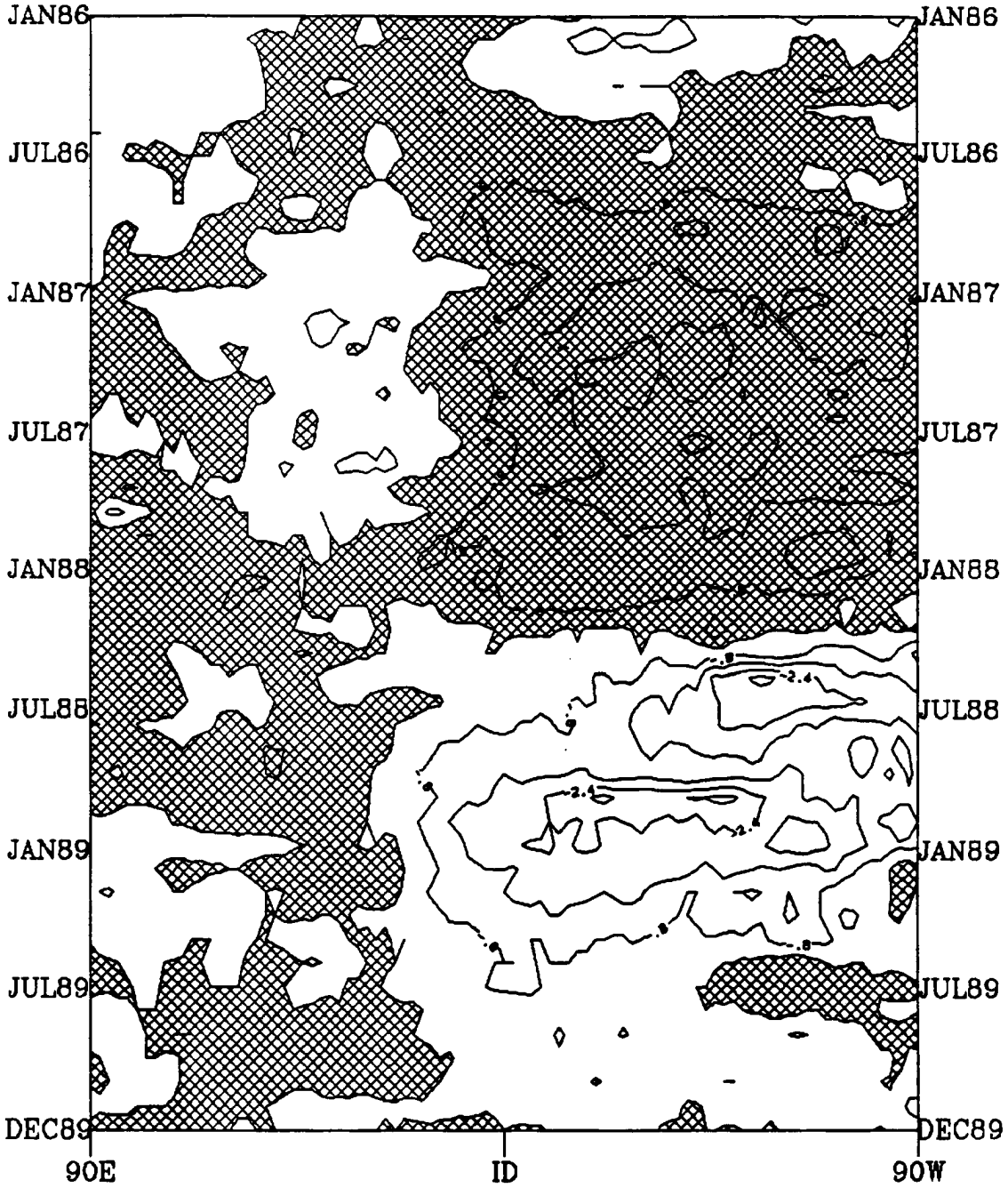

Figure 6.4: SST anomalies at the equator from 90E to 90W for a four year period from January 1986 through 1989 using a 6 year mean (1985-1990) for each month. Cross hatched regions indicate positive anomalies.

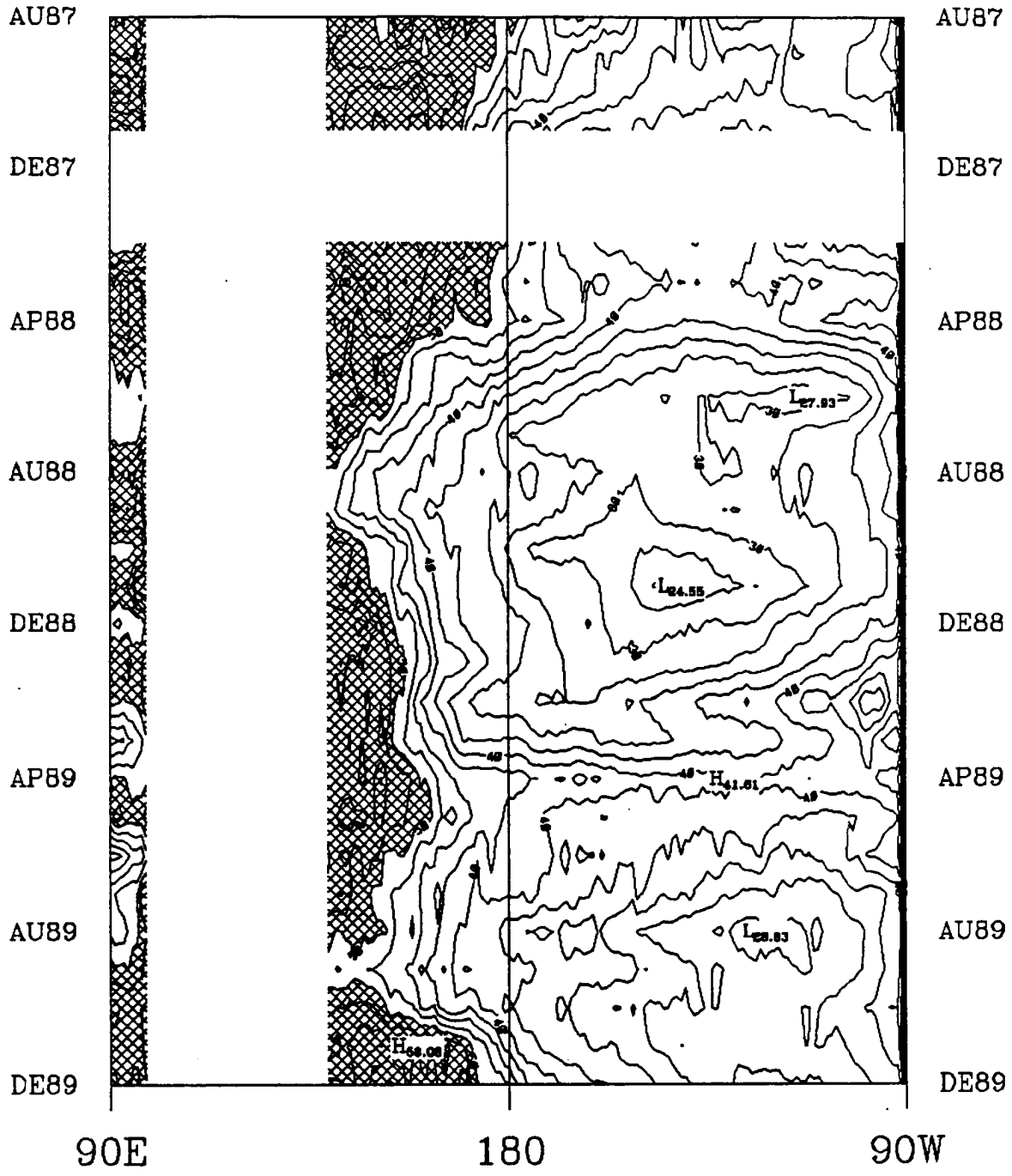

Figure 6.5: PWC (kg m^{-2}) along the equator from August 1987 to December 1989. Cross hatched regions indicate areas of PWC > 50 kg m^{-2}, and blank regions indicate areas of land mass or missing data.

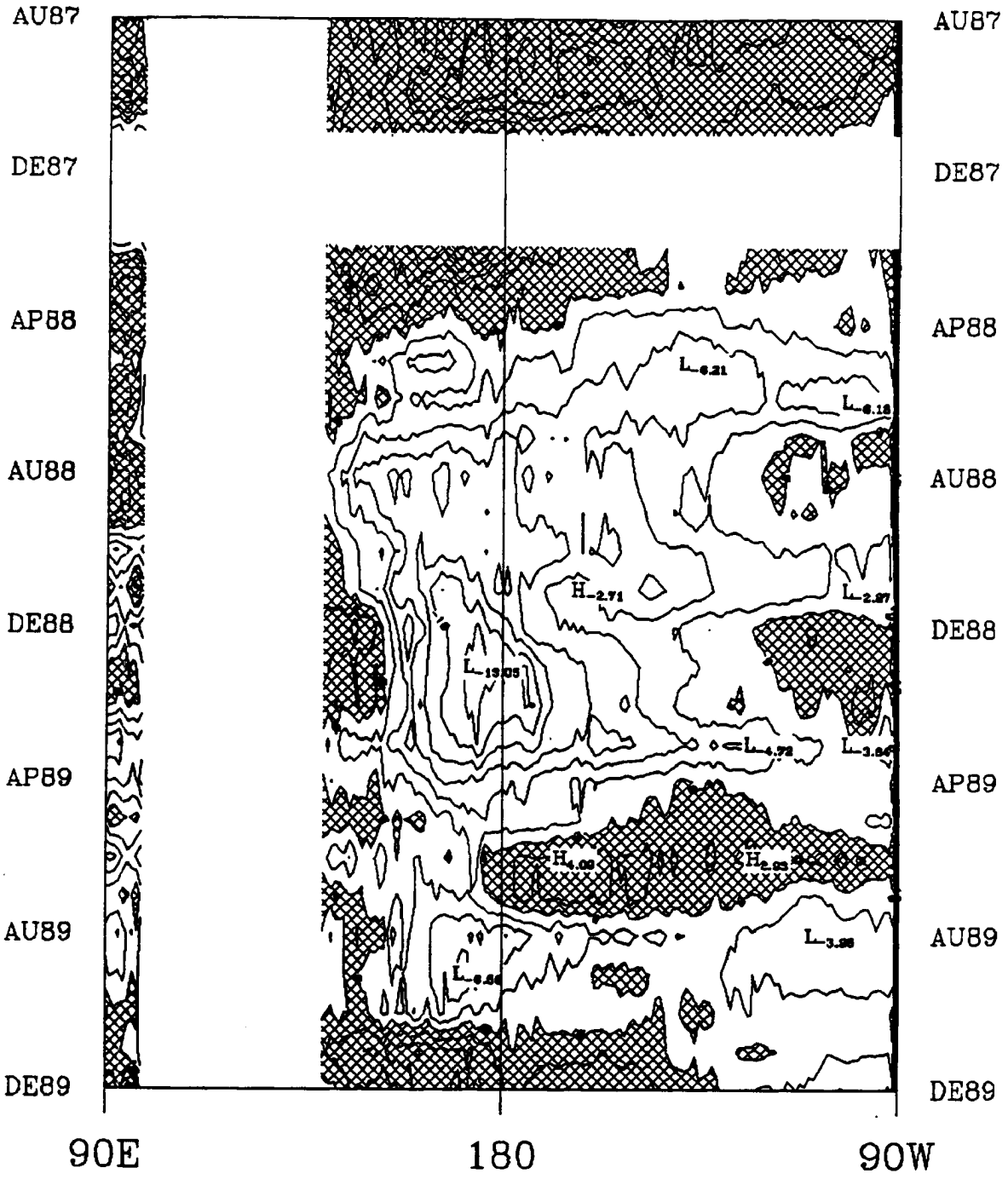

Figure 6.6: PWC (kg m^{-2}) anomalies along the equator from August 1987 to December 1989. Cross hatched regions indicate areas of positive anomalies, and blank regions indicate areas of land mass or missing data.

A hovmoller diagram of the PWC field at the equator was constructed for the time period beginning in August of 1987 and ending December 1989. Figure 6.5 shows the annual cycle of PWC has a maximum along the equator during April. PWC increases at all longitudes in the Pacific during this period. The western Pacific PWC increases due to the equatorial position of the monsoon trough as it progresses from the southern to northern hemisphere. The central and eastern Pacific shows increased PWC because the SSTs are maximum at the equator due to reduced upwelling from the relaxation of the easterly trades. The existence of the El Niño is evident when comparing PWC values in the western Pacific from August 1987 to those of the following two years. Distinct minimums in August 1988 and 1989 occur since the ITCZ is at its northernmost position; however, August 1987 shows a broad region of PWC greater than 50 kg m^{-2} in the western and central Pacific. Remnants of the deep convection along equator during the final stage of the 1987 El Niño shown in Figure 6.1 attribute to the increased PWC in that region.

PWC anomaly fields were constructed by subtracting the $3\frac{1}{2}$ year mean PWC from the field in Figure 6.5. Figure 6.6 shows the anomaly field with positive anomalies in cross hatched regions indicating regions of greater than normal PWC. A broad region of greater than normal PWC appear throughout the entire Pacific from August 1987 to March 1988. This broad region coincides very well with the positive SST anomalies which occurred during the El Niño of 1987. Most of 1988 shows less PWC than average throughout the central and eastern portions of the Pacific during the La Niña of 1988. A large minimum of -13.05 kg m^{-2} occurred at the Date Line in January of 1989 during the peak negative SST anomalies of the La Niña. The 1989 year shows generally negative anomalies before November except for a broad positive region in the eastern Pacific during the boreal summer.

The results of this climatological analysis shows a good correlation between OLR, SST, PWC and zonal winds in the tropical Pacific during the El Niño of 1987 and La Niña of 1988. These figures show the movement of convection to the central and eastern Pacific in association with warmer SSTs and weakening easterly trade winds during the fall of 1986. The strength of the El Niño appeared strongest during from January to

March 1987 and the existence of the El Niño gradually dissipated by January 1988. The easterly trades were weakest, the OLR anomalies were the most negative, and the SST anomalies were the warmest during that 3 month period. The La Niña of 1988 shows a dramatic change in all these fields and including the PWC field. The OLR, 850 zonal wind, and SST anomalies all change sign and achieve a higher amplitude during the fall of 1988. The PWC field shows good correspondence to the SST field in the eastern Pacific and dramatic interannual changes in the Pacific occur during the transition from the El Niño year to the La Niña year. PWC anomalies suggest that a general convergence of water vapor occurred in the anomalously more intense convective regions of the tropics.

6.1.3 Tropical Pacific PWC/SST Relationship

A closer look at the relationship between PWC and SST was made for the tropical Pacific. A three year analysis of the PWC and SST fields beginning in February of 1988 was made in order to investigate the variability of the mean and anomaly fields. The relationship between these fields can help explain changes in the hydrologic cycle during and after the La Niña of 1988. It was shown in the previous section that SST and PWC at the equator were closely related, and this section will develop this relationship even further for a broader region of the Pacific. Unfortunately, since the SSM/I data begins in July of 1987 and since December 1987 and January 1988 have big gaps of missing data, it was impossible to analyze the El Niño event of 1987.

Four regions in the tropical Pacific were investigated and are shown in Figure 6.7. Boxes 1 and 2 (western Pacific) are separated from 3 and 4 (eastern Pacific) by the International Date Line. The Date line was chosen as the cutoff because that longitude generally separates the convective region of western Pacific and relatively nonconvective regions of the central and eastern Pacific.

Figures 6.8a and 6.8b show the PWC and SSTs for all four regions given in Figure 6.7. Region 4 has a distinctive annual cycle for both the SST and PWC which has a maximum in March and April and minimum in October. This cycle tends to lag the solar cycle by about 3 to 4 months. The PWC show far greater annual amplitude changes in the eastern Pacific and reflects the greater SST changes in that region. PWC changes in the western

Pacific have a less annual periodicity while the SST temporal variations are coincident with the solar cycle in both hemispheres. PWC changes in region 1 does show an annual minimum in September of each year and a double maximum in January and March in 1989 and 1990. The maxima occur during the winter monsoonal period which typically brings precipitation to the western Pacific tropical regions south of the equator. Region 2 shows very little correlation between PWC and SST because the PWC time series shows no regular periodicity.

Variability of the western Pacific PWC shows monthly changes as large as the annual changes. The advection of moisture from the eastern Pacific and the convergence of moisture into the monsoonal troughs most likely reduces the correlation of PWC to SSTs in the western Pacific. These dynamical effects weaken the Clausius-Clapeyron relationship discussed in Chapter 5.

PWC anomalies were found by subtracting the 3 year average for each month from the PWC, and the SST anomalies were derived by subtracting a 10 year mean from the SST data. Figures 6.9a and 6.9b show negative PWC and SST anomalies (representing values less than the mean) occurring at the end of 1988 and first 5 months of 1989 for the western and eastern Pacific. The eastern Pacific shows an SST anomaly of -0.6 °C near January of 1989 which marks the peak of the strong La Niña event. The western Pacific also shows negative SST anomalies during period which peak in March 1989. The PWC field also reflects the cooling of the Pacific ocean as PWC anomalies in the eastern and western Pacific go below -3 kg m^{-2} in March of 1989.

Since La Niña events generally increases the convection in western Pacific, an anomalously low PWC in that region seemed intuitively incorrect. Further analysis (not shown) found the SST and PWC anomalies in Region 1 were negative during the La Niña while Region 2 had small positive SST anomalies (< 0.5 °C) and nearly zero PWC anomalies. Therefore, the negative anomalies were dominated by Region 1 in the western Pacific averages.

This section has shown that the eastern Pacific SSTs had a much closer relationship to the PWC than the western Pacific SSTs. Monthly changes in PWC in the western

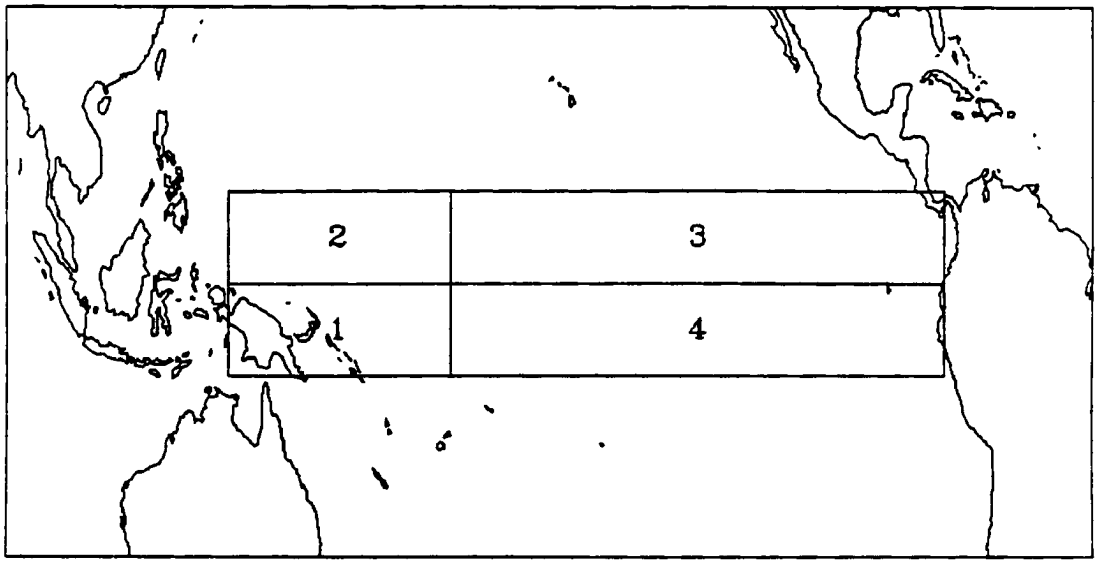

Figure 6.7: Map indicating 4 regions in the tropical Pacific used in analysis of PWC and SST.

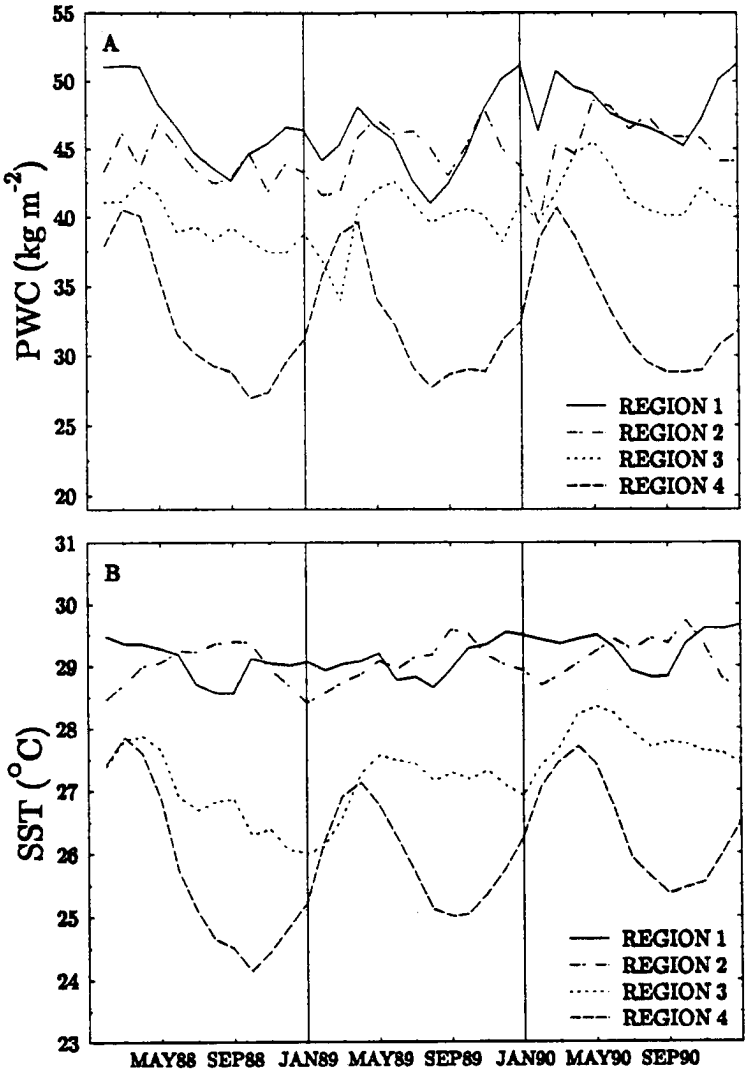

Figure 6.8: Time series of average PWC (A) and average SST (B) in the four regions shown in Figure 6.7

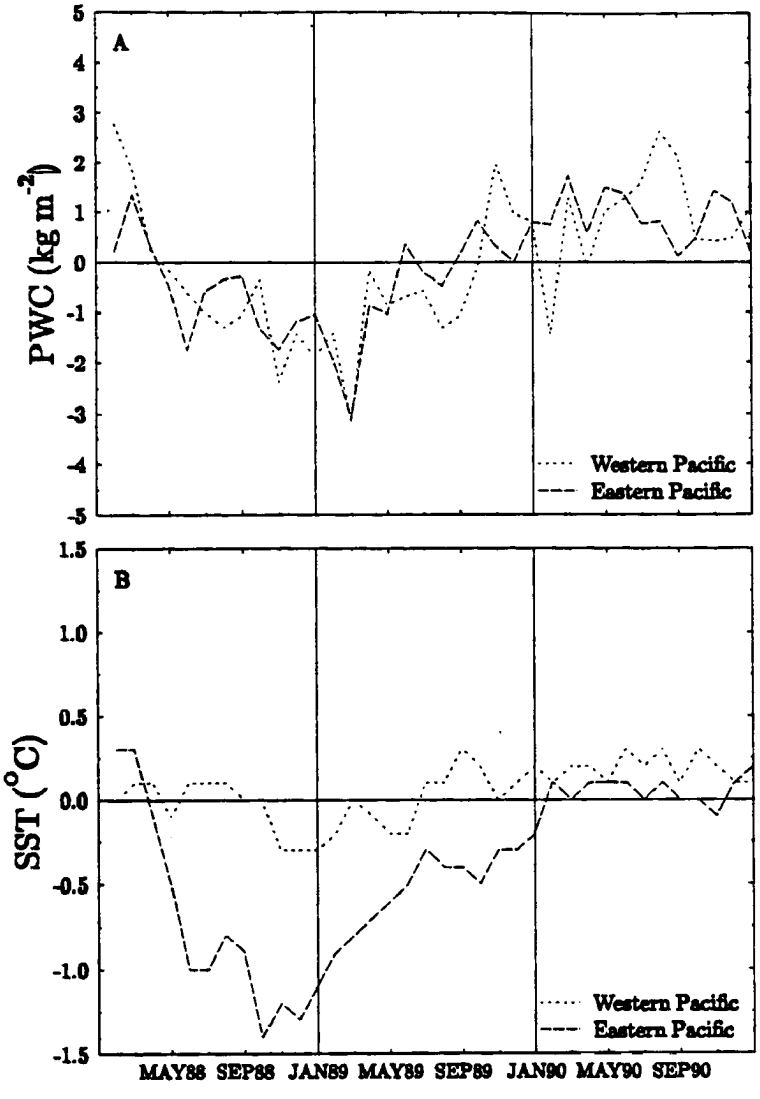

Figure 6.9: Time series of average PWC anomalies (A) and average SST anomalies (B) in the eastern Pacific (180-70W) and western Pacific (140E-180) in the tropical region between 10N and 10S.

Pacific are less correlated to SSTs because the small changes in monthly SST allow other processes in the hydrologic cycle which are associated with convection to dominate the variability of water vapor. PWC monthly variations in the eastern Pacific are more closely related to SST monthly variations because the general lack of convection in that region allow the large changes in SST to dominate the PWC variability. Also, the La Niña of 1988 coincided with the reduction of both the SST and the PWC in the tropical Pacific basin; therefore, the reduction of convection in the central and eastern Pacific was seen as a result of less available water vapor in this region.

6.2 THREE MONTH COMPARISON OF ALL FIELDS

An investigation of the relationship between OLR, PWC, and zonal winds for higher frequency variability was conducted for the tropical region of the Pacific and east Indian Ocean (10N-10S, 90E-90W) for September through November 1987. The purpose of this investigation was to gain a gross understanding of the correlation of the cloud, water vapor, and wind fields in the tropical Pacific region.

The data fields investigated were mapped onto a 2.5 degree grid since the OLR and ECMWF data sets were of that resolution. The other data sets were of various finer resolutions and were averaged onto a 2.5 degree grid using linear interpolation. Five day running means (1-2-3-2-1) were performed on all the daily data sets in order to remove some of the day-to-day variability found in the daily fields and remove some of the effects of liquid water contamination on the PWC field. Monthly means and seasonal means were also constructed for each data set using a standard average of the daily fields.

The data fields were also separated into different latitude and longitude zones. Zones from 90E to 180 and 180 to 90W were considered in order to separate regions of tropical deep convection from regions of climatological subsidence. Correlations at various latitudes and longitude regions will show large differences in the relationships between OLR, PWC, and zonal winds for convective and drier subsident regions of the tropical atmosphere.

Figures 6.10 and 6.11 show the east Pacific (180-90W) has far greater correlation between the PWC and OLR fields than the west Pacific/east Indian Ocean region (90E-180) at the equator. Since the east Pacific is typically a region with sparse deep convection,

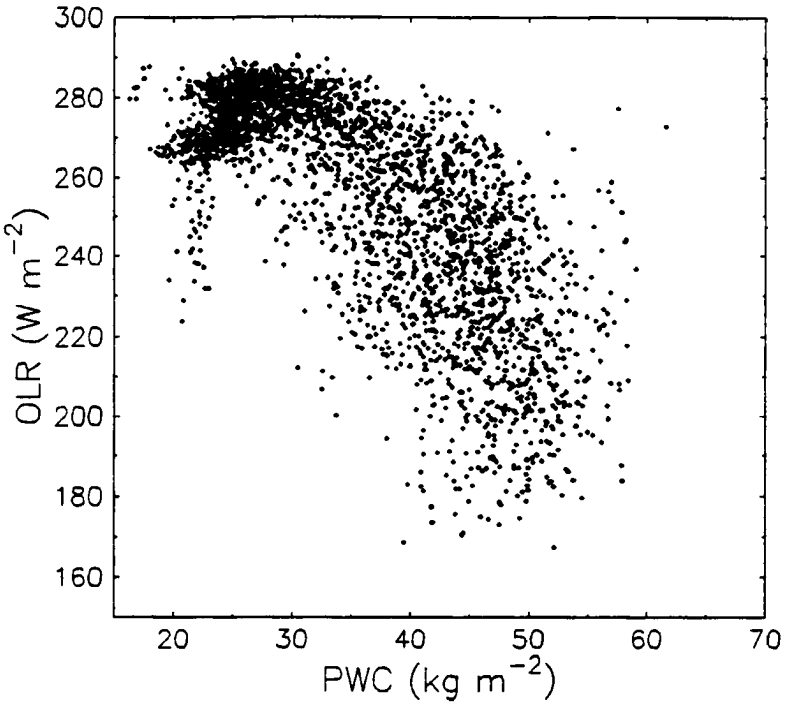

Figure 6.10: Scatter diagram of OLR and PWC in SON 1987 at the equator for the longitudinal region in the eastern Pacific from the 180W to 90W.

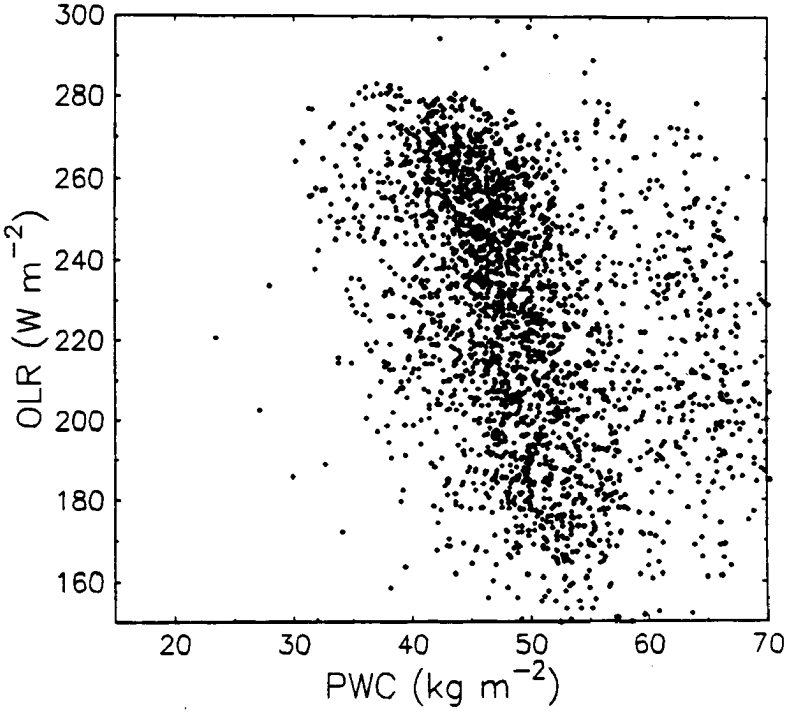

Figure 6.11: Same as Figure 6.10 except that the longitudinal region is from 90E to 180E.

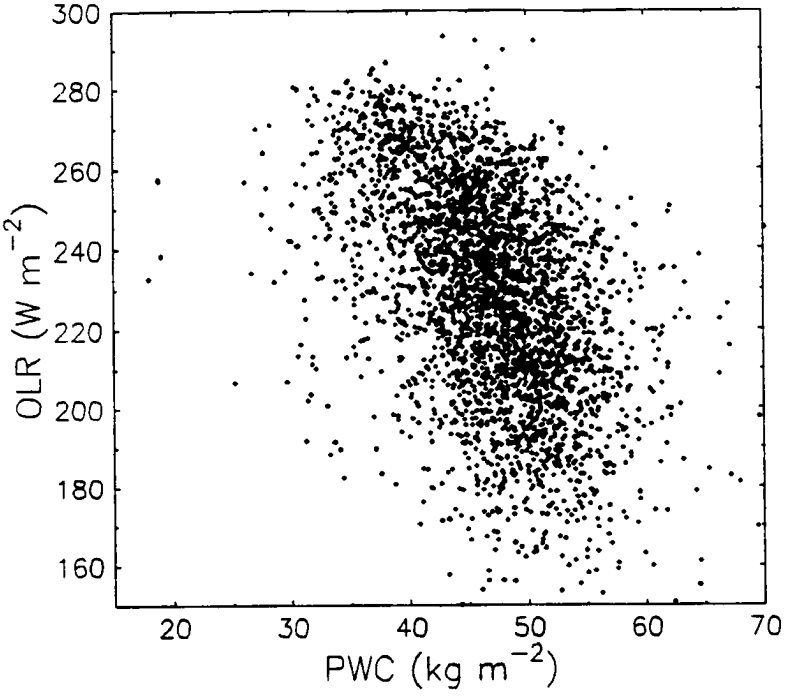

Figure 6.12: Scatter diagram of OLR and PWC in SON 1987 at 10N for the longitudinal region in the eastern Pacific from the 90E to 90W.

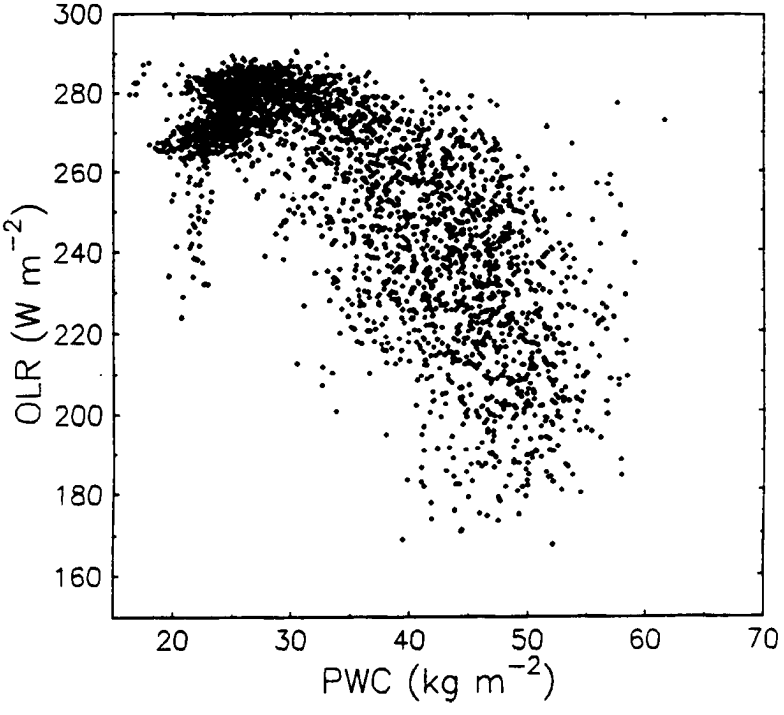

Figure 6.13: Same as Figure 6.10 except the latitude is 10S.

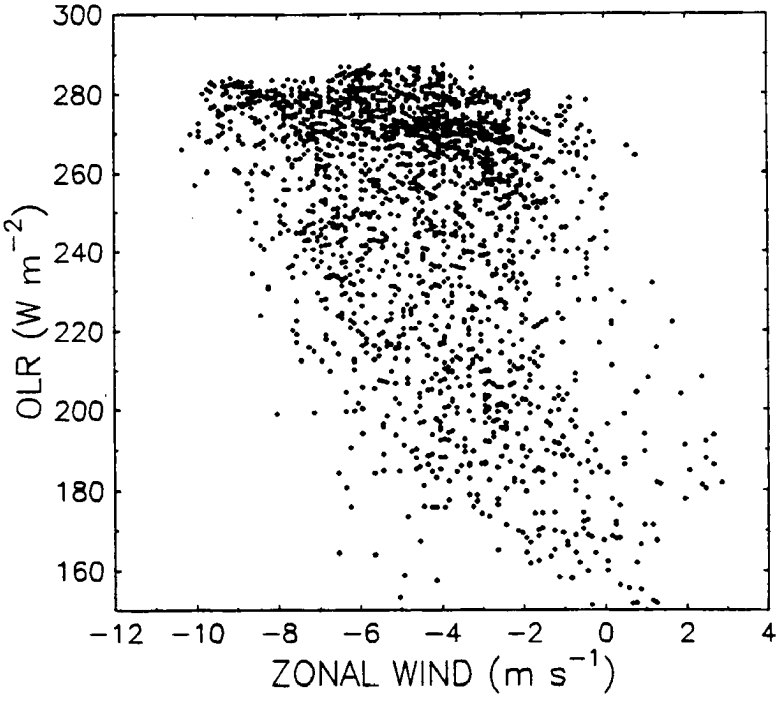

Figure 6.14: Scatter diagram of OLR and zonal winds in September 1987 at the equator in the longitudinal region from 90E to 90W.

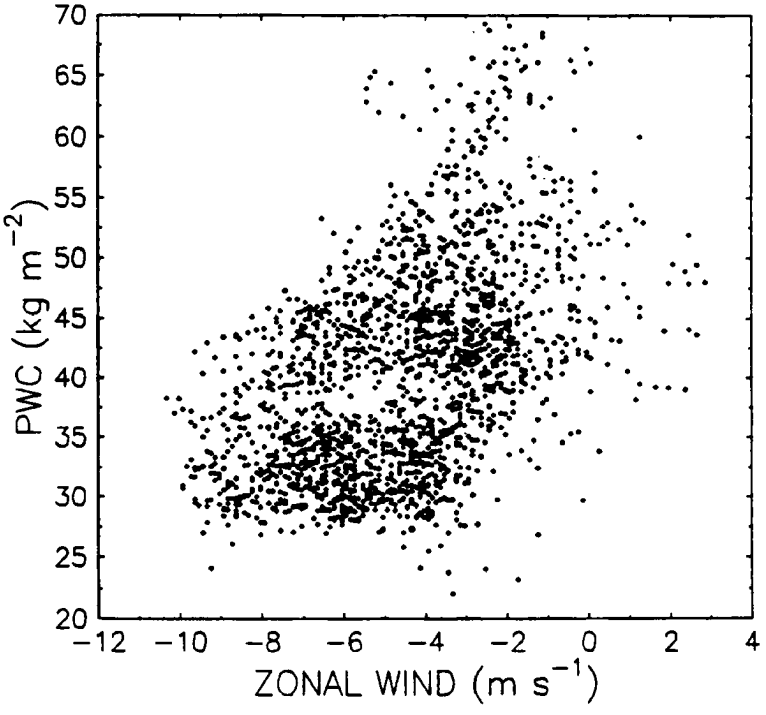

Figure 6.15: Scatter diagram of PWC and zonal winds in September 1987 at the equator in the longitudinal region from 90E to 90W.

OLR is generally greater than 260 Wm^{-2} while the more convective west Pacific has a wide range of OLR values from 280 Wm^{-2} to 150 Wm^{-2}. Figure 6.10 shows a good correlation between OLR and PWC in the east Pacific and demonstrates that PWC is generally greater in areas of lower OLR where clouds exist. Figure 6.11 shows less correlation between the OLR and PWC in the western Pacific. Virtually no PWC values are less than 40 kg m^{-2} because of the warm SSTs in that region. A general trend which slopes steeply from high OLR and low PWC to low OLR and high PWC exists; however, many points in wet regions (PWC > 60 kg m^{-2}) exist at both high and low OLR values. This result could be, in part, a problem in the PWC retrieval since cloud liquid water and precipitation is known to contaminate the PWC values in thick cloud regions; however, that would not explain the low PWC values (>40 m^{-2}) in OLR regions less than 200 Wm^{-2}. Problems also could exist because the data are from two different satellites which take samples at different overpass times.

Scatter diagrams at other latitudes tend to demonstrate that convective regions show less of correlation between OLR and PWC than nonconvective regions. Figure 6.12 at 10N shows significant scatter on both sides of the Pacific because the cloudiness associated with the ITCZ stretches across the entire Pacific at this latitude. A general trend can be seen like Figure 6.11 which puts the higher PWC values in regions of low OLR or deeper convection. Figure 6.13 at 10S from 180 to 90W shows a good correlation due to the lack of convective activity in this cold SST region of the Pacific.

Scatter plots relating the 850 mb zonal wind field to PWC and OLR were constructed to examine how the distribution of zonal winds correlated with these fields. Figure 6.14 shows an interesting correlation between the zonal wind and OLR at the equator. High OLR values near 280 Wm^{-2} show very little correlation with the zonal wind; however, in regions of westerly winds almost of values are less than 240 Wm^{-2}. Figure 6.15 shows that PWC correlates with zonal wind such that regions of less than 40 kg m^{-2} were only found with easterly flow while more moist regions were found in regions of easterly flow less than 5 ms^{-1}. These results show that the weak easterlies and westerly wind flows are more generally in convective regions, and that these more convective regions are where greater amounts of water vapor exists.

6.3 WESTERLY BURSTS ANALYSIS

Two westerly bursts were analyzed during the mature stage of the 1987 El Niño from September through November of 1987. The choice of this period was primarily due to the enhanced convection in the central Pacific (ie. Figure 6.1) during this period and the knowledge that westerly bursts occur most frequently in the central Pacific during the mature stages of El Niño (Murakami and Sumathipala, 1989).

This section begins by defining westerly wind burst. Following its definition, the zonal wind distribution at 850 mb and 200 mb for particular latitudes and longitudes is analyzed to show regions of more frequent westerly wind occurrences and to show the basic motion of the tropical atmosphere during this period. Follow this discussion, hovmoller diagrams are used to identify westerly wind bursts at the equator, and PWC anomalies are used to show moisture convergence in these systems.

6.3.1 Definition

Westerly bursts are an episodic event found primarily in the western Pacific where anomalously westerly flow occurs in a small region along or near the equator. The general definition for westerly bursts depends on the author, so the following list was made to define the westerly burst for this thesis.

1. The wind abruptly shifts to an anomalously westerly direction,
2. The wind shift lasts for at least 2 days but not longer than 2 weeks,
3. Associated with convection,
4. Located on or near the equator.

Wind speed is often defined in studies concerning westerly bursts; however, this definition was neglected for this study. The westerly burst, by strict definition, does not necessarily mean a westerly wind but refers to a relaxation in the climatological easterly flow.

6.3.2 Seasonal Wind Structure

The initial step in analyzing westerly bursts was to consider the 850 mb zonal wind distribution in the Pacific basin (90E to 90W) for various longitudes and latitudes using the ECMWF wind data. The purpose of this analysis was observe the 850 mb and 200 mb wind stucture of the tropical Pacific for SON of 1987, identify regions with a higher frequency for low level westerly winds, and explain the basic circulation pattern of tropical Pacific.

Figure 6.16 shows the 850 mb zonal wind distribution at different latitude bands and longitude regions in the tropics. The latitudes north of the equator show far greater occurrences of westerly winds particularly west of the International Date Line, while the longitude regions east of the Date Line show virtually no change in its distribution from 10N to 10S. This distribution shows the distinctive characters of west and east Pacific during the boreal fall. The ITCZ in September begins its progression southward from its most northern position near 10N. Along this convergence zone, westerly winds develop in association with monsoon trough where southerly winds bend eastward due to the Coriolis effect. Furthermore, regions near the equator develop westerly winds in association with dynamical response convective systems create along the equator. South of the equator, easterly trades are the dominant feature in their springtime flow in the tropics.

Figure 6.17 shows the 200 mb zonal wind distribution over the same range of longitudes and latitudes as Figure 6.16. The results show a general shift in the zonal wind from easterly in the northern hemisphere to westerly in the southern hemisphere. The equator shows predominately easterly flow west of the Date Line while a significant number of westerly wind occurrences east of the Date Line. This result substantiates the existence of convection in the central Pacific during this period since a divergent flow aloft forces easterlies in the western Pacific and westerlies in the eastern Pacific. The southern hemisphere shows increasing occurrences of westerly winds as the upper part of the southward flowing Hadley circulation bends to the east due to the Coriolis effect.

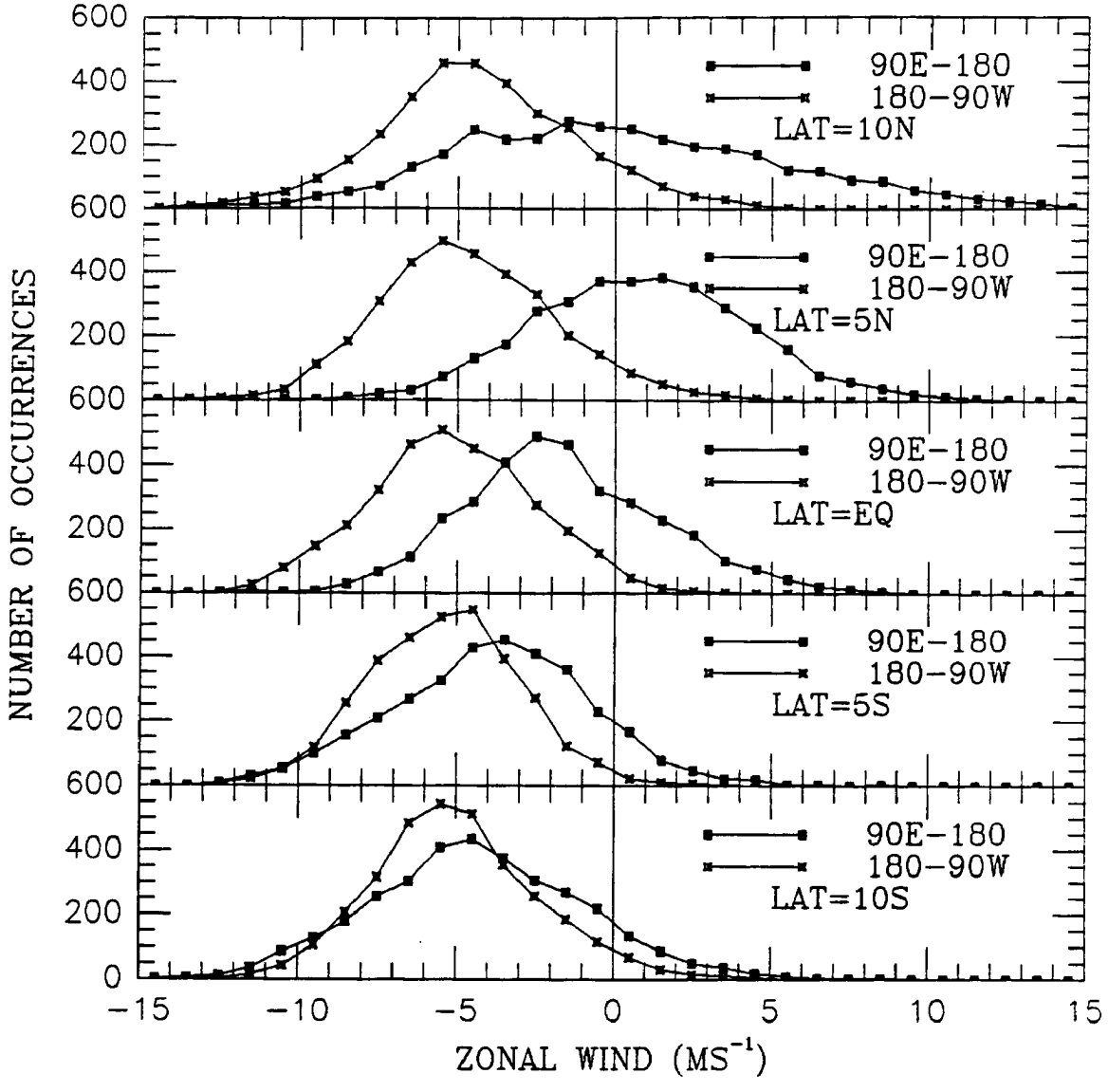

Figure 6.16: 850 mb zonal wind speed occurrences for various latitude bands between 90E and 90W in the Pacific basin. This composite spans over the time period from September 1987 through November 1987. Positive values are westerly winds.

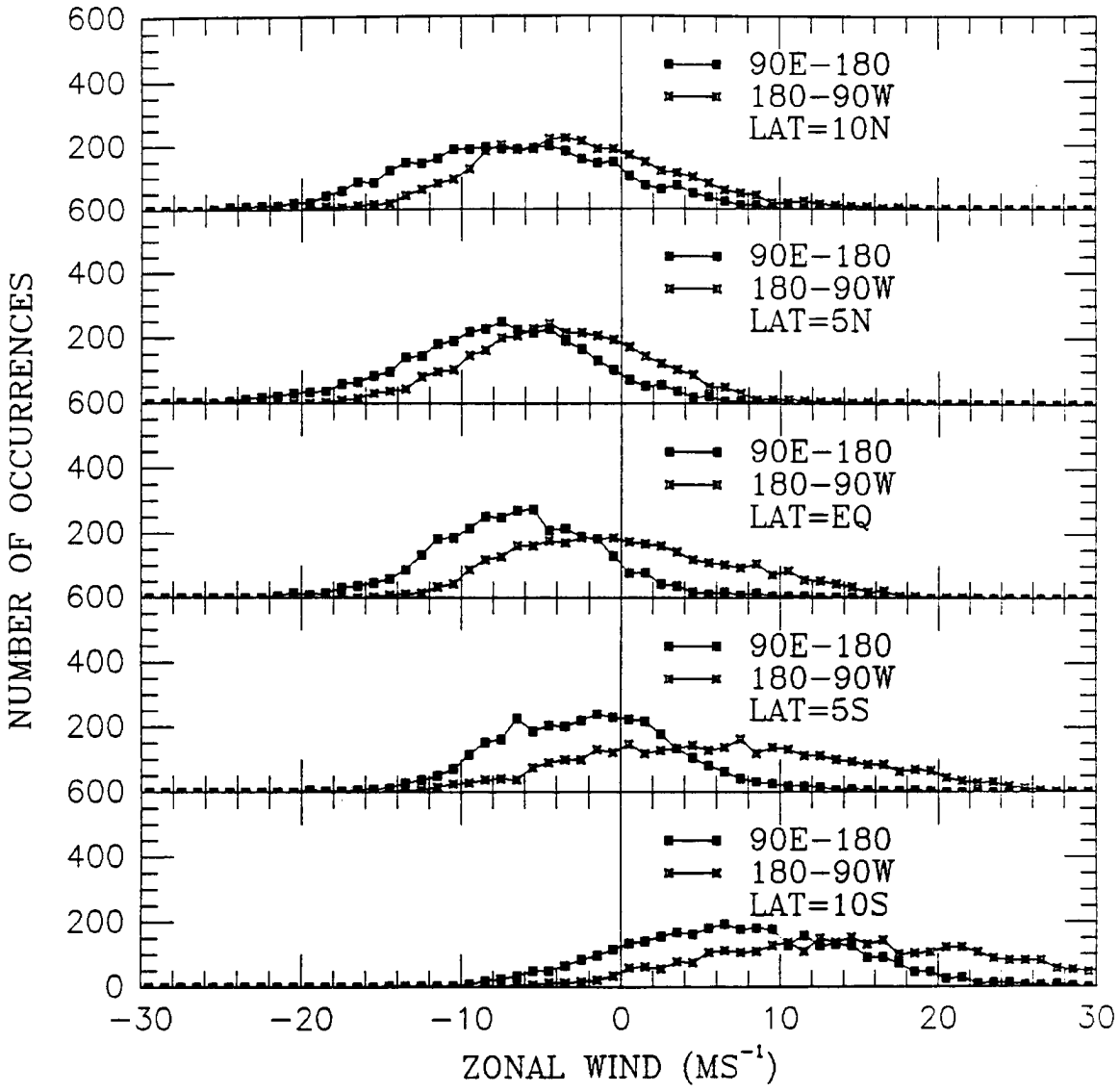

Figure 6.17: Same as Figure 6.15 except distributions are for the 200 mb zonal wind field.

6.3.3 Westerly Bursts: Fall of 1987

This analysis will consist of using hovmoller diagrams to show the time evolution and spatial movement of westerly wind bursts for the fall of 1987. The PWC anomaly field will also be analyzed to show regions where moisture convergence and divergence occur in the westerly burst.

Regional plots of the OLR anomaly fields in the tropical Pacific were constructed for September, October and November of 1987. Figures 6.18, 6.19 and 6.20 show large areas of negative anomalies centered at the Date line and just south of the equator along with negative anomalies north of equator in the eastern Pacific. These anomalies indicate deep convection in the central Pacific along the equator and deeper than normal convection along the ITCZ north of the equator. These results support the results in Rasmusson and Carpenter (1982) who found westward propagation of the largest areas of convection from the eastern Pacific to the central Pacific towards the end of the mature stage of the composite El Niño. By November, the negative anomaly field in the central Pacific moves north of the equator and reduces in magnitude while the eastern Pacific shows a growing area of positive anomalies as El Niño reaches its end. Since westerly wind bursts are typically associated with convection along the equator, this three month time period was considered as an ideal time to investigate westerly bursts along the equator.

Westerly bursts were first identified using producing hovmoller diagrams of a 5 day running mean (1-2-3-2-1) 850 mb zonal wind field. Figure 6.21 shows a series of westerly bursts in October of 1987 which propagate eastward throughout the month, and a broader region of westerly winds in the middle of November. Both originate in the Indonesia region (120E-130E) and propagate eastward to the International Date Line. This eastward propagation is not unlike the propagation of tropical 'supercell' convective systems which have been found in several studies (Sui and Lau, 1989, Lau *et al.*, 1989) to be associated with the 30 to 60 day oscillation. Wiekmann and Khalsa (1990) performed a case study which diagnosed these eastward propagating systems and found westerly winds to the associated on the western side of the convection.

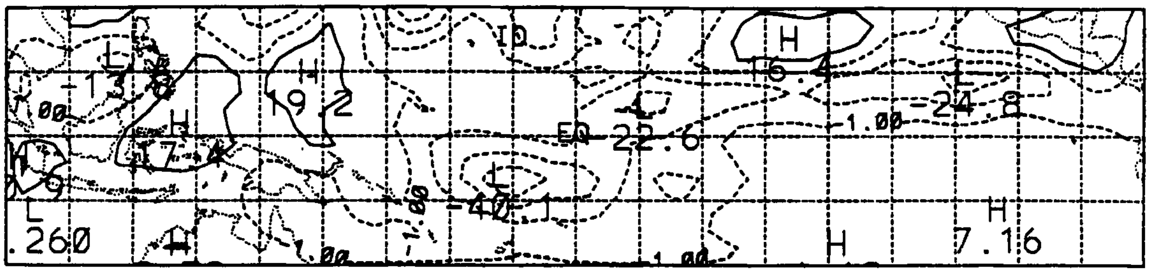

Figure 6.18: OLR anomalies (Wm^{-2}) for tropical Pacific region for September 1987.

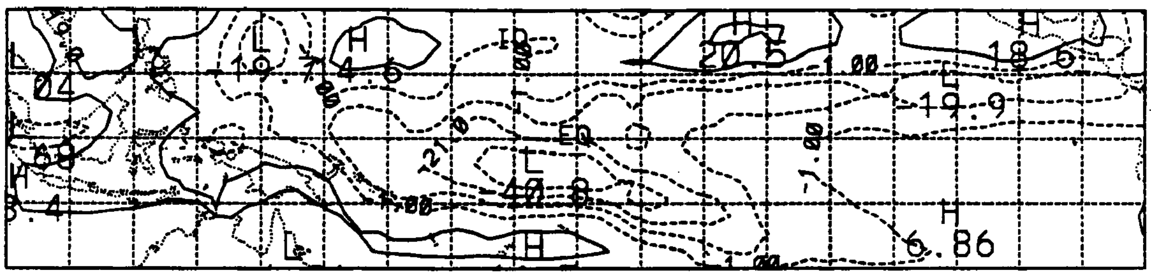

Figure 6.19: Same as Figure 6.18 except for October 1987.

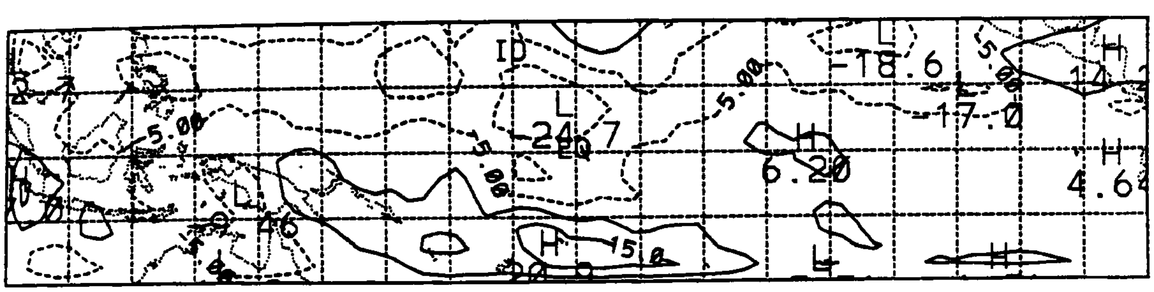

Figure 6.20: Same as Figure 6.18 except for November 1987.

The 200 mb zonal wind field shown in figure 6.22 shows strong easterly winds just to the west of the low level westerly bursts. The tropical upper troposphere responds to the westerly bursts and low level convergence by producing a divergent flow aloft which are evident by the strengthening of the easterly flow at 200 mb. The strongest easterly winds in the western Pacific are in phase with the westerly bursts showing the coupled flow between the lower and upper troposphere.

Figure 6.23 shows the pentad OLR for the same time period and region used in the wind data. The hatched regions of OLR less than 240 W m^{-2} was chosen because this is a commonly used threshold to determine regions of deep convective activity and precipitation. A broad region from 90E to 110E shows deep convection throughout the entire three month period with the exception of a small period in the middle of November. This convective activity is associated with the southward progression of the monsoon trough during the boreal fall. Two regions of deep convection are evident in the western Pacific throughout the three month period and each system propagates eastward to the Date Line where they diminish. The eastern Pacific shows no deep convective activity during this time.

A hovmoller diagram of the PWC field in Figure 6.24 was constructed to see the relationship between the water vapor field and westerly wind bursts. Regions larger than 52 kg m^{-2} are hatched to indicate regions of relatively high PWC. The rectangular region with no contours is a region of missing data due to the Indonesian islands. Results show a broad region of high PWC within the regions of westerly winds and deep convection. Low OLR corresponds quite well with higher regions of PWC and low level westerly wind flow.

The convergence of water vapor was investigated by calculating a PWC anomalies field. The mean was determined by using the 3 month relationship between PWC and SST (August-November 1987) and constructing a best fit to that relationship to determine the seasonal climatology. PWC anomalies were the difference between the 5 day mean PWC and this seasonal climatology. Positive anomalies indicate a wetter than normal atmosphere. Figure 6.25 shows positive anomalies (marked by cross hatch) in the convective regions in the western Pacific with breaks in the convection marked distinctly by

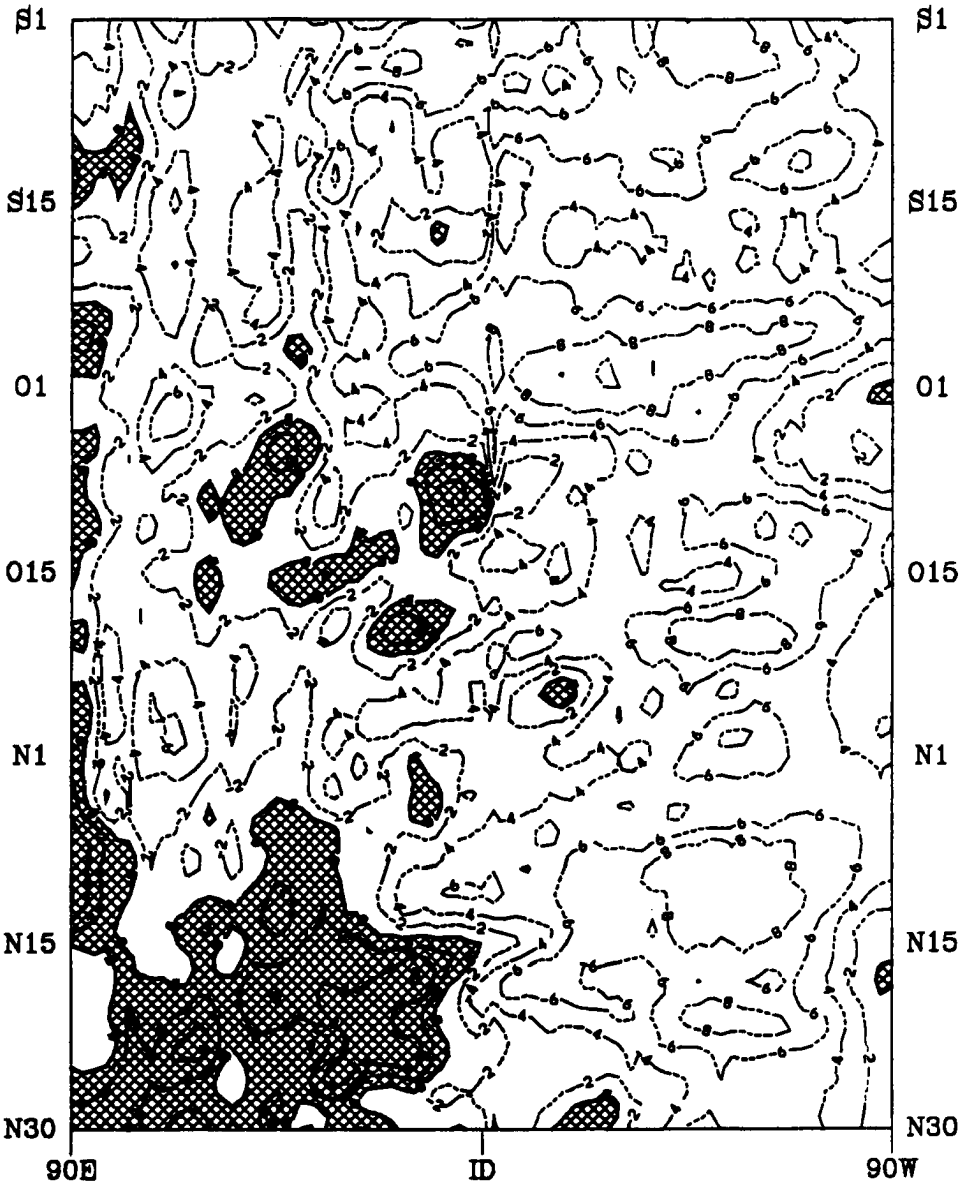

Figure 6.21: Hovmoller plot of the 850 mb 5 day mean zonal wind at the equator. Time series begins in September 1987 and ends in November 1987. Cross hatched regions indicate westerly winds.

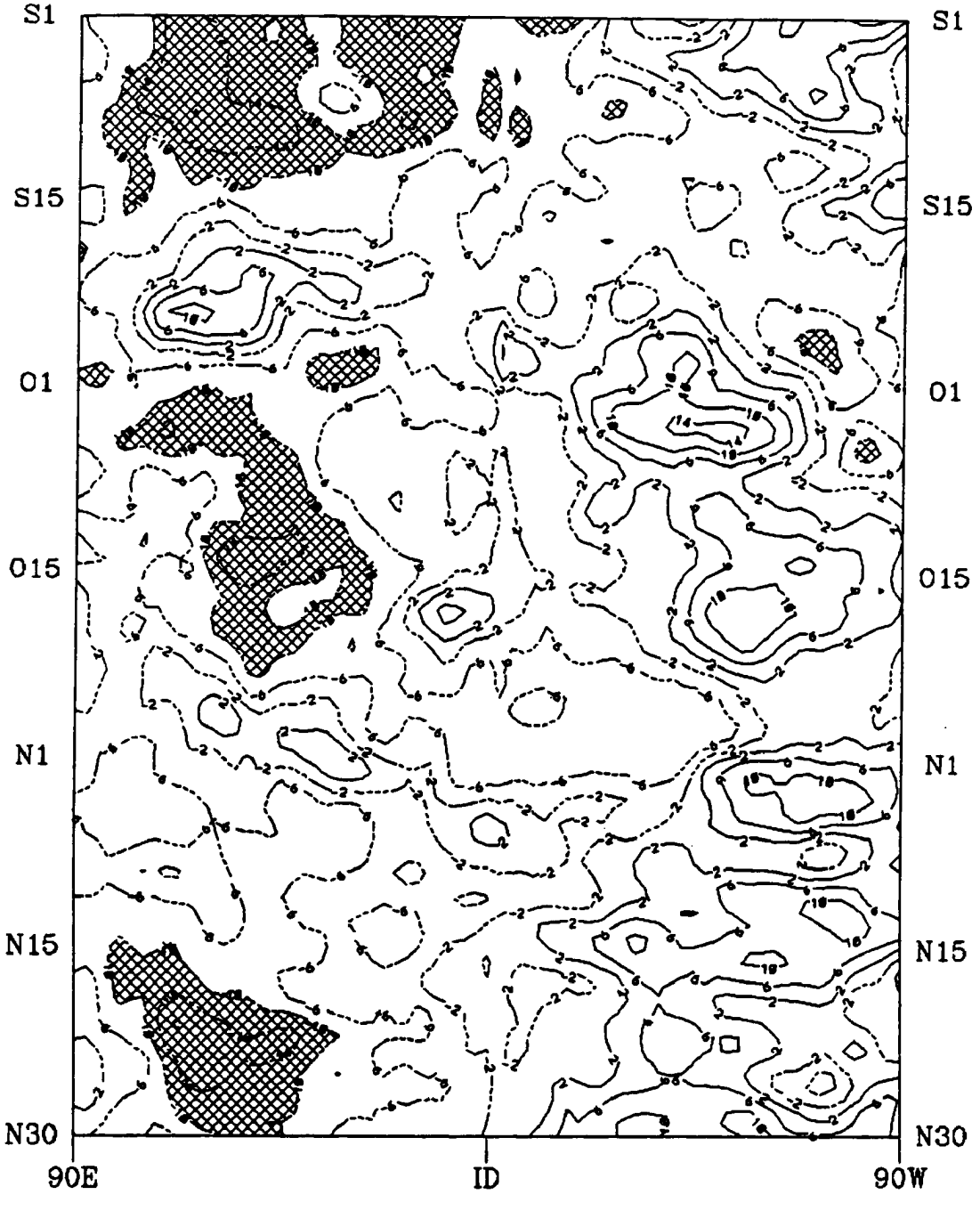

Figure 6.22: Same as 6.21 except the wind is at the 200 mb level and the cross hatched region indicates easterly winds exceeding 10 ms^{-1}.

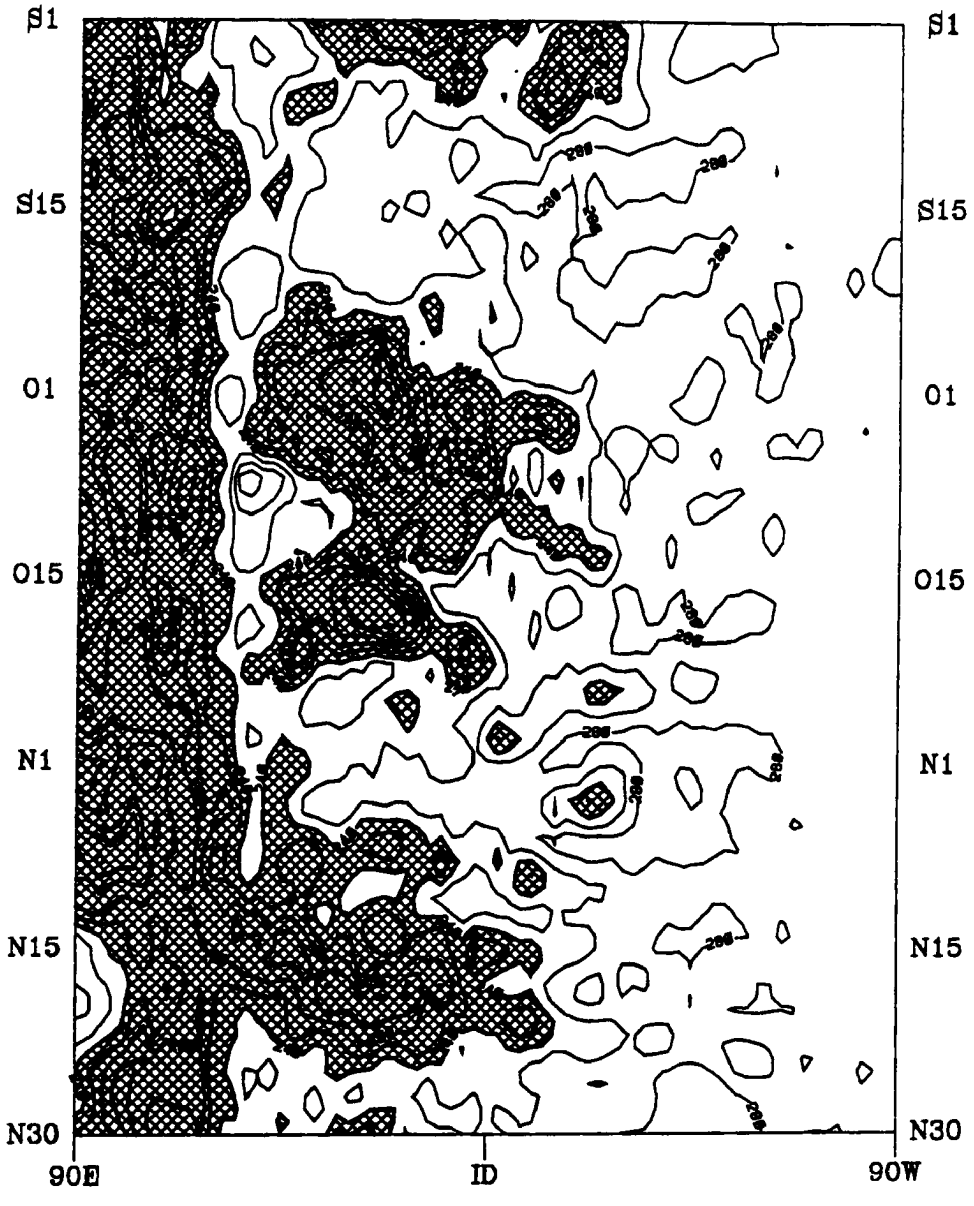

Figure 6.23: Hovmoller plot of OLR averaged over a 5 day running mean at the equator. Cross hatched regions indicate regions of OLR < 240 Wm^{-2}.

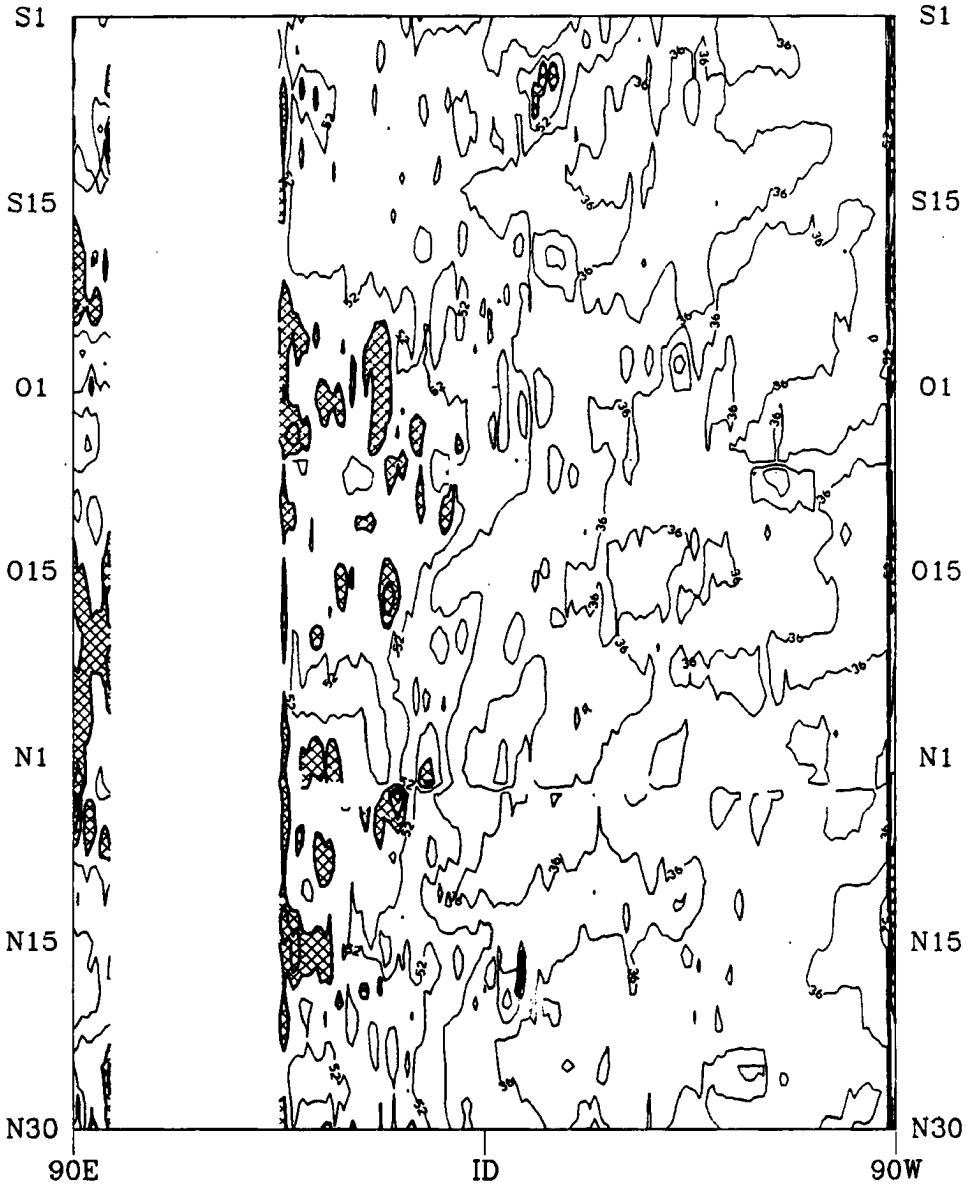

Figure 6.24: Hovmoller plot of PWC averaged with 5 day running mean at the equator for September 1987 through November 1987. Cross hatched regions are PWC > 52 kg m^{-2}.

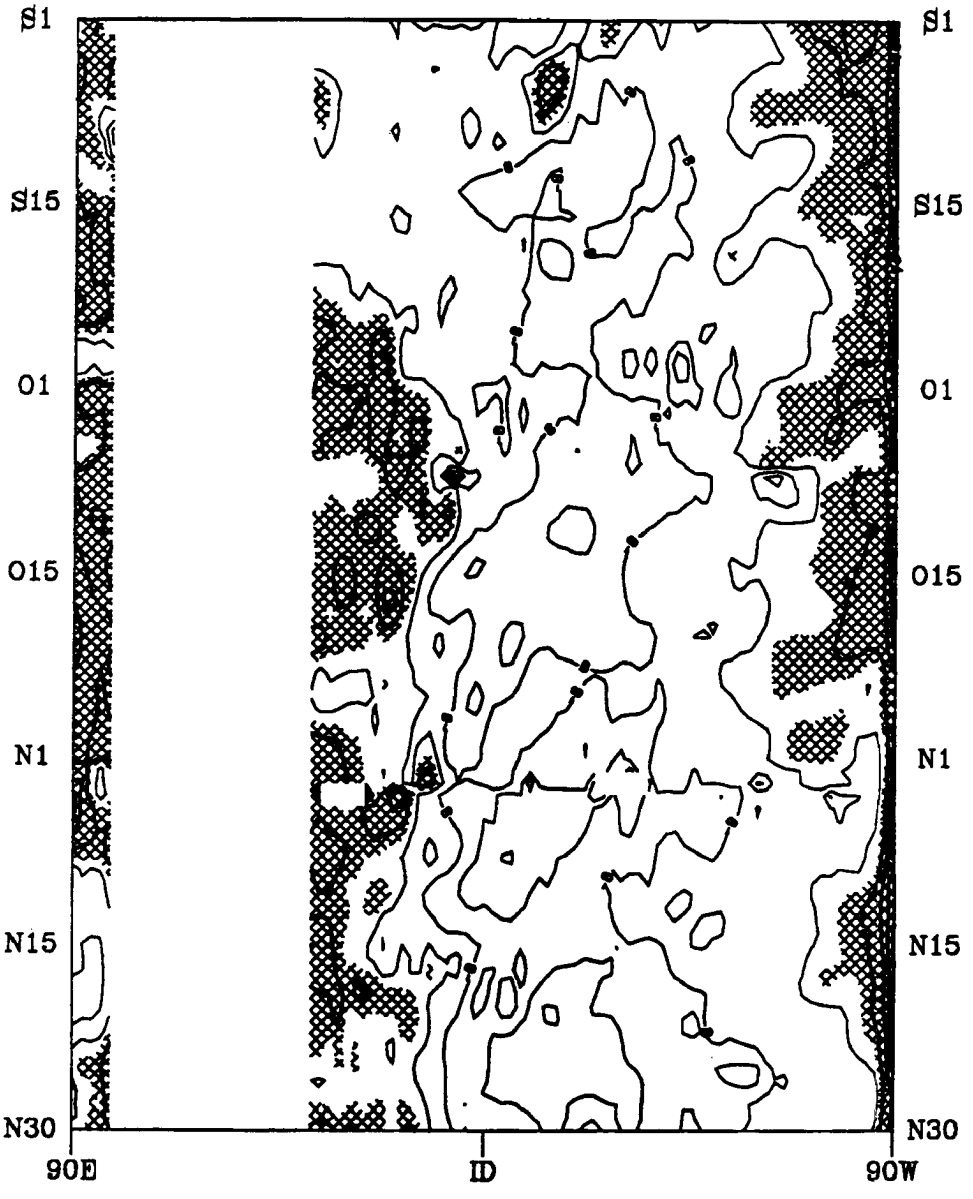

Figure 6.25: Hovmoller plot of PWC anomalies at the equator for the time period of September 1987 through November 1987. Cross hatched regions indicate positive anomalies (PWC greater than climatology).

the PWC fields. Positive anomalies near the South American coast can be attributed to moisture advection from the Caribbean which was discussed in Stephens (1990). These results indicate that a broad region of water vapor convergence occurred in the westerly burst regions.

6.4 SUMMARY

This chapter has shown the relationship of PWC to both low and high frequency motions in the tropical Pacific basin. The La Niña of 1988 was found to profoundly change the PWC throughout the tropical Pacific basin with anomalously low PWC occurring in regions of anomalously high OLR and low SST. Therefore, the distribution of PWC over interannual time scales is significantly influenced by clouds and SST. Higher frequency phenomena were also found to influence the PWC in the tropical atmosphere. Evidence of water vapor convergence in regions of westerly wind bursts was found. These results show that water vapor convergence plays an important role in enhancing convection for both large and small scale tropical motions, and these results show the potential capabilities of SSM/I data for analyzing various scales of atmospheric motions.

Chapter 7

CONCLUSIONS

Analysis of the global and tropical PWC derived from the method presented in Tjemkes *et al.* (1991) was performed over interannual, seasonal and daily time scales for the globe and tropical Pacific. Comparisons among several other retrieval methods found Tjemkes' method to have consistently larger values of PWC than radiosonde observations in relatively dry regions (PWC < 20 kg m^{-2}). However, results in wetter regions with higher PWC (PWC > 40 kg m^{-2}) using Tjemkes *et al.* (1991) method were found to produce much better results than the physical method of Chang and Wilheit (1979), and the results were as good or better than the three statistical methods. Global PWC comparisons showed the Tjemkes' method to be more variant in persistent cloud regions and comparable in total global water vapor content to all the retrieval methods. In the tropical regions, low frequency motions such as El Niño were found to significantly change the PWC for the globe, and the distribution of PWC in the tropical Pacific was found to be well correlated to the SSTs. Higher frequency motions such westerly wind bursts were also found to produce anomalously high PWC in regions of low level wind convergence. These results show the effectiveness of using the high resolution SSM/I data for many scales of atmospheric motion.

7.1 RADIOSONDE VALIDATION RESULTS

In order to justify using the Tjemkes' PWC retrieval method, a comparison with four other physical and statistically based retrieval methods was conducted. The validation of these five retrieval methods was performed using radiosonde data from an archive of NMC radiosonde data and the BASICS radiosonde data. Tjemkes' retrieval method proved to represent the daily temporal changes of PWC in the moist region of the western

Pacific much better than the physical retrieval method of Chang and Wilheit. While an adjustment to the absorption coefficient at 19 GHz was used to improve the results in the PWC regions of the tropics, this adjustment created a slight positive bias at the higher latitudes. This bias was thought to be related to cloud liquid water contamination in the dense cloud regions of the higher latitudes. Statistical methods were found to have good agreement with the NMC radiosonde data except at the highest PWC where overestimation by the retrieval methods occurred. Good agreement was expected for the Alishouse and Petty and Katsaros methods since the coefficients used in the regression formulas were derived from NMC radiosonde data. It was found that Tjemkes' method displayed PWC daily variability that agreed well with the results found from Petty and Katsaros' and Schluessel and Emery's methods, and the time series of PWC in the western tropical Pacific was not smoothed like that found in Alishouse's statistical method. One problem with the Tjemkes' method was its greater sensitivity to precipitation. Current work found in Greenwald *et al.* (1992) will account for liquid water and take measures to remove precipitation effects.

7.2 GLOBAL PWC RESULTS

Global analysis of three years of coincident PWC and SST data starting in February 1988 was performed and results were presented analogous to the results given in Stephens (1990). The results from this study showed the Clausius-Clapeyron relationship defined in Chapter 5 (Eqn. 5.2) produced a similar PWC/SST relationship to the results presented in Stephens (1990). Seasonal changes of this relationship were found to be negligible for SST $>$ 20°C; however, the seasonal changes were found to be significant for SST $<$ 20°C. It was found that large areas of water vapor convergence in the northern Pacific during the boreal summer attributed to this seasonal variability. Interannual changes of PWC and SST produced by ENSO were found to produce well correlated changes in both fields. Three year time series of the hemispheric means were found to be well correlated and trends in seasonal changes of these fields matched those found in Stephens (1990). Time series of the global means were found to differ between this study and Stephens

(1990) primarily because the magnitude of the SSTs in Stephens (1990) were found to be erroneously too low.

Global mean PWC values for during the year of 1989 showed similar trends but a systematic bias between all five retrieval methods. Zonally averaged annual mean PWC for each retrieval method revealed the positive bias in the Tjemkes' method at the higher latitudes. The monthly movement of water vapor shows a seasonal cycle of maximum PWC from the southern hemisphere in January to 10N in August. This zonal movement of PWC reflects the seasonal changes in SST and the seasonal movement of the ITCZ. Standard deviations of monthly mean PWC show the greatest PWC variability in the ITCZ, SPCZ and storm track regions where convection is the greatest. The largest deviations occurred in Tjemkes' retrieval method in the tropics and midlatitudes where the ITCZ and storm track regions enhance the daily variability of water vapor. Minimum deviations found in the tropics for the Alishouse and Petty and Katsaros retrieval methods showed the weakness of statistical methods in representing the daily variation in PWC.

7.3 PWC ANALYSIS OF TROPICAL DISTURBANCES RESULTS

Following the examination of these five retrieval methods, an examination of the association of water vapor with tropical disturbances for both low and high frequency motions was performed for the tropical Pacific. It was shown during the end of the 1987 El Niño and through the 1988 La Niña that positive (negative) anomalies in SST at the equator produced similar positive (negative) anomalies in the PWC. Local negative SST anomalies in the eastern Pacific occur simultaneously with negative PWC anomalies. These results indicate that SST changes profoundly effects the distribution of PWC in the tropical Pacific.

While for monthly means, the SST/PWC correlation is very good, daily comparisons of PWC, OLR and zonal wind show that the correlation is dependent on location. Examination of daily values for SON 1987 show the relationship is strongest between OLR and SST in the generally nonconvective regions of the eastern Pacific along the equator to 10S. Convective regions show generally increased PWC with decreased OLR; however,

the scatter of points is much greater due to precipitation contamination. These results indicate that more PWC exists in regions of cloudiness, presumably because convergence of water vapor occurs in cloudy regions. Scatter diagrams of zonal wind show the most moist regions occur in weak easterlies and westerly winds along the equator. Water vapor convergence in these areas, therefore, help supply the dynamically forced vertical motions with increased water vapor for cloud development.

The 3 year relationship of PWC and SST in the tropical Pacific shows the tropical Pacific, as a whole, dried out in response to the SST changes during the 1988 La Niña. PWC and SST anomalies were negative on both sides of the Pacific during the La Niña which indicates a reduction of total water vapor from the tropics. Therefore, the large scale low frequency motions of the tropical atmosphere act change the distribution of water vapor such that it reduces total integrated water vapor in the generally nonconvective regions of the Pacific.

Higher frequency motions indicate that the spatial and temporal variability of PWC changes quite dramatically on time scales of 5 days. Two westerly burst regions identified along the equator during the mature stages of the 1987 El Niño show that higher PWC than climatology occurred in these regions. Moisture convergence in these regions helps explain the increased convection associated with westerly bursts.

7.4 SUGGESTED IMPROVEMENTS AND FURTHER RESEARCH

Improvements in the water vapor retrieval are necessary to better understand how the earth's radiation budget is effected by changes in the hydrologic cycle. Physical retrieval methods like Tjemkes' method are advantageous because they give insight into the physics of the PWC retrieval and give a basis for tuning parameters which have no known value. Certainly, problems such as precipitation and cloud water contamination need to be resolved in order to improve the Tjemkes' method. Currently, Greenwald *et al.* (1992) will present a refinement to the Tjemkes' method where the cloud liquid water and PWC will be solved simultaneously, and precipitation effects will be considered.

While integrated water vapor studies are important, a comprehensive description of the vertical distribution of water vapor is essential for understanding radiative and diabatic

processes by water vapor in the atmosphere. Observational studies using radiosonde data in the western Pacific (Gray *et al.*, 1975) show the relative humidity in both tropical cloud clusters and in the clear sky regions have their greatest changes in the middle troposphere. Investigating the interannual, annual, and season changes in the vertical distribution of water vapor can better address issues concerning the earth radiation budget and the advection of water vapor. While data sets such as TOVS give a gross description of the vertical distribution of water vapor, the strong bias of this data set to climatology and to clear sky regions limit the use of this data for studies concerning higher frequency oscillations and climate. Future programs should begin by developing a climatology of the vertical distribution of water vapor from radiosonde data and continue the development of microwave retrieval methods for the retrieval of the vertical distribution of water vapor.

Another problem with microwave retrieval methods of water vapor is the inability to retrieve water vapor over land. New satellite information at higher frequency microwave channels such as the 183 GHz channel found on the Special Sensor Microwave Temperature Sounder (SSM/T2) should allow us to investigate PWC over land. However, many problems with land retrieval need to be addressed which include the development of a climatology of the surface emission properties of land surfaces over the globe. Merging PWC observations over land and ocean will help give the complete picture of global water vapor and help us understand how the hydrologic cycle differs and interacts between land and ocean. Programs such as The Global Energy and Water Cycle Experiment (GEWEX) will hopefully address these issues which are vital for understanding the hydrologic cycle of the earth-atmosphere system.

REFERENCES

Alishouse, J.C., S.A. Snyder, J. Vongsathorn, and R.R. Ferraro, 1990: Determination of oceanic total precipitable water from the SSM/I. *IEEE Trans. Geosci. Remote Sensing*, **28**, 811-816.

Barnett, T.P., M. Latif, E. Kirk, and E. Roeckner, 1991: On ENSO physics. *J. Climate*, **4**, 487-514.

Bates, J.J., 1991: High frequency variability of special sensor microwave/imager derived wind speed and moisture during an intraseasonal oscillation. *J. Geophys. Res.*, **96**, 3441-3423.

Benton, G.S., and M.A. Estoque, 1954: Water-vapor transfer over the North American continent. *J. Meteorol.*, **11**, 462-477.

Berlage, H.P., 1957: Fluctuations in the general atmospheric circulation of more than one year, their nature and prognostic value. *K. Ned. Meteorol. Inst., Meded. Verh.*, **88**, 152 pp.

Bjerknes, J., 1966: A possible response of the atmospheric Hadley circulation to equatorial anomalies of ocean temperature. *Tellus*, **18**, 820-829.

Bjerknes, J., 1969: Atmospheric teleconnections from the equatorial Pacific. *Mon. Wea. Rev.*, **97**, 163-172.

Cane, M., 1983: Oceangraphic events during El Niño. *Science*, **222**, 1180-1195.

Chang, A.T.C., and T.T. Wilheit, 1979: Remote sensing of atmospheric water vapor, liquid water, and wind speed at the ocean surface by passive microwave techniques from the Nimbus 5 satellite. *Radio Science*, **14**, 793-802.

Chu, P.-S., 1988: Extratropical forcing of the burst of equatorial westerlies in the western Pacific: a synoptic study. *J. Meteor. Soc. Japan*, **66**, 549-564.

Chu, P.-S., J. Frederick, and A.J. Nash, 1991: Exploritory analysis of surface winds in the equatorial western Pacific and El Niño. *J. Climate*, **4**, 1087-1102.

Doberitz, R., 1968: Cross spectrum analysis of rainfall and sea temperature of the equatorial Pacific Ocean. *Bonner Meteor. Abhand.*, **8**, 61 pp.

Gill, A.E., 1982: Studies of moisture effects in simple atmospheric models: the stable case. *Geophys. Astrophys. Fluid Dynamics*, **19**, 119-152.

Gray, W.M., E. Ruprecht, and R. Phelps, 1975: Relative humidity in tropical weather systems. *Mon. Wea. Rev.*, **103**, 685-690.

Greenwald, T.J., and G.L. Stephens, 1991: The earth's radiation budget and its relation to atmospheric hydrology 2. Observations of cloud effects. *Journ. Geophys. Res.*, **96**, 15,325-15,340.

Greenwald, T.J., G.L. Stephens, T.H. Vonder Haar, and D.L. Jackson, 1992: A physical retrieval method of liquid water over the global oceans using SSM/I observations. in preparation.

Gruber, A., and J.S. Winston, 1978: Earth-atmosphere radiative heating based on NOAA scanning of radiometer measurements. *Bull. Amer. Meteor. Soc.*, **59**, 1570-1573.

Gruber, A., and A.F. Krueger, 1984: The status of the NOAA outgoing longwave radiation data set. *Bull. Amer. Meteor. Soc.*, **65**, 958-962.

Harrison, D.E., and D.S. Luther, 1990: Surface winds from tropical Pacific islands-climatological statistics. *J. Climate*, **3**, 251-271.

Hillger, D.W., and T.H. Vonder Haar, 1981: Retrieval and of high resolution moisture and stability fields from Nimbus 6 HIRS radiances in pre-convective situations. *Mon. Wea. Rev.*, **109**, 1788-1806.

Hollinger, J., R. Lo, G. Poe, R. Savage, and J. Pierce, 1987: Special sensor microwave/imager user's guide, report, Nav. Res. Lab., Washington, D.C.

Knutson, T.R., and K.M. Weikmann, 1987: 30-60 day atmospheric oscillations: composite life cycles of convection and circulation anomalies. *Mon. Wea. Rev.*, **115**, 1407-1436.

Kornfield, J., and A.F. Hasler, 1969: A photographic summary of the Earth's Cloud Cover for the Year 1967. *J. Appl. Meteor.*, **8**, 687-700.

Lau, K.-M., L. Peng, C.H. Sui, and T. Nakazawa, 1989: Dynamics of super clusters, westerly wind bursts, 30-60 day oscillation and ENSO: an unified view. *J. Meteor. Soc. Japan*, **67**, 205-219.

Liebe, H.J., 1981: Modeling attenuation and phase of radio waves in air at frequencies below 1000 GHz. *Radio Science*, **16**, 1183-1199.

Lorenc, A.C., 1981: A global three-dimensional multivariate statistical interpolation scheme. *Mon. Wea. Rev.*, **109**, 701-721.

Luther, D.S., D.E. Harrison, and R.A. Knox, 1983: Zonal winds in the central equatorial Pacific and El Niño. *Science*, **222**, 327-330.

Madden, R.A., and P.R. Julian, 1972: Description of global scale circulation cells in the tropics with a 40-50 day period. *J. Atmos. Sci.*, **29**, 1109-1123.

McClain, E.P., W.G. Pichel, and C.C. Walton, 1985: Comparative performance of AVHRR-based multichannel sea surface temperature. *J. Geophys. Res.*, **90**, 11,587-11,601.

Murakami, T., and W.L. Sumathipala, 1989: Westerly bursts during the 1982/83 ENSO. *J. Climate*, **2**, 71-85.

Oort, A.H., and E.M. Rasmussen, 1971: Atmospheric Circulation Statistics. NOAA Professional Paper No. 5, 323 pp. [Available from US Government Printing Office, Washington, DC, 20402, Stock No. 0317-0045.]

Pandey, P.C., and R.K. Kakar, 1982: An empirical microwave emissivity model for a foam covered sea. *IEEE J. Oceanic Eng.*, **OE-7(3)**, 135-140.

Peixoto, J.P., D.A. Salstein, and R.D. Rosen, 1981: Intra-annual variation in large scale moisture fields. *J. Geophys. Res.*, **86**, 1255-1264.

Peixoto, J.P., and A.H. Oort, 1983: The atmospheric branch of the hydrological cycle and climate. in *Variations on the Global Water Budget*, D. Reidel, Norwell, Mass., 5-65.

Petty, G.W., and K.B. Katsaros, 1990: New geophysical algorithm for the special sensor microwave imager. *5th Conf. on Satellite Met. and Oceanog.*, Sept. 3-7, 1990, London, England.

Prabhakara, C., H.D. Chang, and A.T.C. Chang, 1982: Remote sensing of precipitable water over the oceans from Nimbus 7 microwave measurements. *J. Appl. Meteor.*, **21**, 59-68.

Rasmussen, E.M., and T.H. Carpenter, 1982: Variations in tropical sea surface temperature and surface wind fields associated with the southern oscillation/El Niño. *Mon. Wea. Rev.*, **110**, 354-384.

Reynolds, R.W., 1987: A real-time global sea surface temperature analysis. *J. Climate*, **1**, 75-86.

Rosen, R.D., D.A. Salstein, and J.P. Peixoto, 1979: Variability in the annual fields of large-scale atmospheric water vapor transport. *Mon. Wea. Rev.*, **107**, 26-37.

Rosenkrantz, P.W., D.H. Staelin, and N.C. Grody, 1978: Typhoon June (1975) viewed by a scanning microwave spcatrometer. *J. Geophys. Res.*, **83**, 1857-1868.

Saha, K.R., 1973: Global distribution of double cloud bands over tropical oceans. *Quart. J.R. Met. Soc.*, **99**, 551-555.

Schluessel, P., and W.J. Emery, 1990: Atmospheric water vapour over oceans from SSM/I measurements. *Int. J. Remote Sensing*, **11**, 753-766.

Sellers, W.D., 1965: *Physical Climatology.* The University of Chicago Press, 272 pp.

Starr, V.P., Peixoto, J.P., and R.G. McKean, 1969: Pole-to-pole moisture conditions for the IGY. *Pure Appl. Geophys.*, **75**, 300-331.

Steiner, E.J., 1987: The relationship of low-level winds and moisture to convection in the tropical Pacific. *Mon. Wea. Rev.*, **115**, 744-749.

Stephens, G.L., 1990: On the relationship between water vapor over the oceans and sea surface termperature. *J. Climate*, **3**, 634-645.

Sui, C.-H., and K.-M. Lau, 1989: Origin of low-frequency (intraseasonal) oscillations in the tropical atmosphere. Part II: Structure and propagation of mobile wave-CISK modes and their modification by lower boundary forcings. *J. Atmos. Sci.*, **46**, 37-56.

Teten, O., 1930: "Uber einige meteorologische begriffe." *Z. Geophys.*, **6**, 297-309.

Tjemkes, S.A., G.L. Stephens, and D.L. Jackson, 1991: Spaceborne observation of columnar water vapor: SSMI observations and algorithm. *J. Geophys. Res.*, **96**, 10,941-10,954.

Ulaby, F.T., R.K. Moore, and A.K. Feng, 1982: *Microwave Remote Sensing, Vol. II.* Add-Wesley.

Walker, G.T., 1923: Correlation in seasonal variations of weather, VIII: A preliminary study of world weather. *Mem. Indian Meteor. Dep.*, **24**, 75-131.

Walker, G.T., 1924: Correlation in seasonal variations of weather, IX: A further study of world weather. *Mem. Indian Meteor. Dep.*, **24**, 275-332.

Walker, G.T., 1928: World Weather III. *Mem. Roy. Meteor. Soc.*, **2**, 97-106.

Weickmann, K.M., and S.J.S. Khalsa, 1990: The shift of convection from the Indian Ocean to the western Pacific ocean during a 30-60 day oscillation. *Mon. Wea. Rev.*, **118**, 964-978.

Wentz, F.J., 1988: User's manual SSM/I Ocean Products Tapes. Remote Sensing Systems Tech. Report 033088. Remote Sensing Systems, Inc., Santa Rosa, CA 95404.

Wittmeyer, I.L., 1990: Satellite based estimates of global precipitable water and poleward latent heat transport. M.S. thesis, Colorado State University, Ft. Collins, 76 pp.

Yasunari, T., 1987: Global structure of the El Niño/ southern oscillation Part I. El Niño composites. *J. Meteor. Soc. Japan*, **65**, 67-80.

Yasunari, T., 1987: Global structure of the El Niño/ southern oscillation Part II. time evolution. *J. Meteor. Soc. Japan*, **65**, 81-102.

Zebiak, S.E., and M. A. Cane, 1987: A model El Niño-southern oscillation. *Mon. Wea. Rev.*, **115**, 2262-2278.